# 4 Motions in Planetary Atmospheres

Atmospheric motions are an inevitable response to a planet's rotation, gravity, differential stellar heating, and other forces. *Dynamics* are the relationships between the heating, the forces, and the winds that they drive.

Dynamics are important for climate for many reasons and so affect a planet's climate evolution and habitability. Winds transport heat, e.g., from warm tropics to cold poles. Furthermore, winds can affect atmospheric chemistry. Air movement carries condensable species responsible for clouds, such as water on Earth and Mars, ammonia on Jupiter, or methane on Titan. The albedo of clouds is so important to the radiation balance that the presence of clouds and their net global cooling effect makes the Earth habitable (e.g., Goldblatt *et al.*, 2013). Dynamics also strongly affects the distribution of non-condensable trace gases such as ozone in Earth's stratosphere. Furthermore, winds can modify a surface, such as long-term erosion or deposition of solid material on Mars.

Of course, winds are highly variable in time, changing hourly and daily, and in this chapter we concentrate on winds averaged over days or months and over large areas, often of continental scale for Earth. Generally, winds have a preferred direction that either persists throughout a year or season. Such average winds are the *general circulation* of a planetary atmosphere.

We note that winds can drive secondary circulations, in particular, ocean currents on Earth, which strongly affect climate by transporting heat and mass. However, to limit the scope of this chapter, we restrict ourselves to atmospheric dynamics. For ocean dynamics, the reader is referred to textbooks by Marshall and Plumb (2008) and Williams and Follows (2011).

This chapter was originally going to be contributed as a guest chapter by Conway Leovy (1933–2011). His rough draft, which has been expanded and developed, provided essential guidance and insight.

The role of atmospheric dynamics in the long-term evolution of atmospheres and planetary habitability remains relatively unexplored. There are a few examples of the influence of dynamics on the Earth's Precambrian climate and the habitability of exoplanets that have been identified, which we mention as we go along. But this chapter is merely a point of departure to introduce some key concepts of the dynamics of planetary atmospheres. We anticipate much more research in this area in the future.

## 4.1 Introductory Concepts

### 4.1.1 Forces, Apparent Forces, and the Equation of Motion

At the heart of fluid dynamics are forms of Newton's second law expressed per unit mass. The second law gives acceleration in a particular direction as:

$$a_i = \frac{\sum F}{m} \tag{4.1}$$

Here, $\Sigma F$ is a sum of forces, $m$ is the mass, and $a_i$ is the acceleration of a parcel of air in an *inertial* coordinate system, which is that fixed in space outside the planet–atmosphere system.

In dynamics, various forces $F$ cause air to flow, including *real forces*, such as gravity, and *apparent forces* that arise because we conventionally use a *non-inertial* frame of reference that co-rotates with the planet and is therefore accelerated. An everyday example of real and apparent forces occurs in an upwardly accelerating elevator, where scales would measure your weight (a force) in excess of your true weight. Upward acceleration of the frame of reference results in an apparent force in the *opposite* direction of a real acceleration that, if neglected, gives an incorrect weight in applying Newton's second law. The real forces in atmospheric dynamics are pressure gradients, friction and gravity, while the apparent forces

that arise from choosing a co-rotating frame of reference are centrifugal and Coriolis forces.

#### 4.1.1.1 *The Pressure Gradient Force*

In Sec 1.1.2.3, we discussed hydrostatic balance, where gravitational acceleration $g$ balances a pressure ($p$) gradient force per unit mass over vertical distance $z$ of $-1/\rho\ (\partial p/\partial z)$, where $\rho$ is air density. In this chapter, the large-scale motions we consider will always be close to hydrostatic equilibrium, so that the vertical equation of motion simplifies to the hydrostatic equation (eq. (1.8)). Later, in Sec. 5.10, we will consider a special non-hydrostatic case of hydrodynamic escape.

The pressure gradient forces $F_{PG}$ per unit mass in horizontal directions are analogous. Defining local $x$- and $y$-axes pointing in the local horizontal eastward and horizontal northward directions, we have:

$$\frac{F_{x,\,PG}}{m} = -\frac{1}{\rho}\frac{\partial p}{\partial x},\quad \frac{F_{y,\,PG}}{m} = -\frac{1}{\rho}\frac{\partial p}{\partial y},\quad \text{or in 3-D, } \frac{\mathbf{F}_{PG}}{m} = -\frac{1}{\rho}\nabla p \tag{4.2}$$

Here, the minus sign indicates that the force acts from high to low pressure. As an example, a pressure gradient of 2.5 hPa over 100 km horizontal distance in terrestrial midlatitudes exerts a force per unit mass of $(-1/(1.2\ \text{kg m}^{-3})) \times (250\ \text{Pa}/10^5\ \text{m}) = -2.1 \times 10^{-3}\ \text{m s}^{-2}$, and would produce gale-force winds of ~20 m s$^{-1}$.

#### 4.1.1.2 *Centrifugal and Coriolis Forces*

When dealing with planetary atmospheres, our coordinate system is fixed with respect to the planet's surface. A planet rotates with an angular rate of magnitude $\Omega = 2\pi/\tau_d$, where $\tau_d$ is the rotation period (or sidereal day). For Earth, $\Omega = 2\pi/(86\ 164\ \text{s}) = 7.29 \times 10^{-5}$ rad s$^{-1}$. The apparent forces per unit mass that arise for an observer in the rotating frame are as follows.

(1) A *Coriolis force*, which is perpendicular to both the velocity vector **v** in the rotating frame and to the rotation vector $\boldsymbol{\Omega}$.

(2) A *centrifugal force*, which has magnitude $\Omega^2 R$, where $R$ is the distance from the point with position vector **r** to the rotation axis, directed perpendicularly away from the rotation axis. Usually, this force is merely regarded as a correction to gravity $g$, which we have already discussed in Sec. 1.1.2.3.

A pedagogical illustration (from McIlveen (1992, p. 187)) of how apparent forces arise is a toy train with an imaginary toy passenger going around a circular track at train speed $V$ on a turntable that has angular rotation $\Omega$ and tangential speed $V_t = \Omega R$. The train speed is $V_{total} = V + V_t$, as viewed externally (Fig. 4.1). If the train is stationary ($V = 0$), the passenger on the train measures no centripetal acceleration. The difference of his measurement and the actual radially inward centripetal acceleration of the track is $0 - V_t^2/R = -\Omega^2 R$. The net result is that the passenger experiences a *force* per unit mass in the direction *opposite* to the real inward centripetal acceleration, which is a centrifugal force of magnitude $\Omega^2 R$ acting radially outwards. If the train moves at speed $V$, the centripetal acceleration is $V_{total}^2/R = (V + \Omega R)^2/R$ as viewed from the exterior, but the co-rotating passenger sees only $V^2/R$. The difference in accelerations is now $V^2/R - (V^2/R + 2\Omega V + \Omega^2 R) = -\Omega^2 R - 2\Omega V$. The passenger not only experiences a centrifugal force ($-\Omega^2 R$) but also a Coriolis *force* of magnitude $2\Omega V$, which acts to the right of velocity vector, as shown in Fig. 4.1.

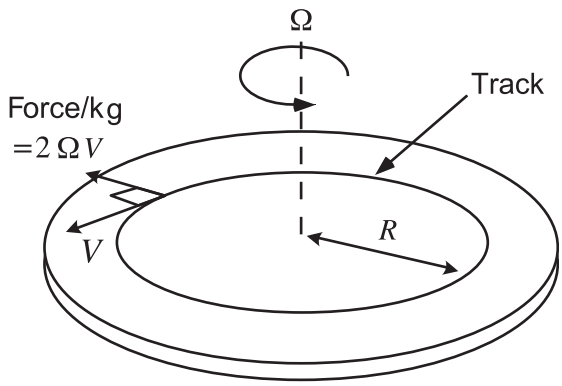


**Figure 4.1** Circular motion on a rotating turntable illustrates the origin of the Coriolis force. Accelerations lost from measurements made in the co-rotating frame create equal and opposite apparent accelerations (see text).

A planet is a rotating sphere, not a disk. For a sphere, the Coriolis acceleration is $2\Omega V$ in magnitude only at the poles, where the planet's angular rotation vector $\boldsymbol{\Omega}$, is vertical. Elsewhere, the Coriolis acceleration depends on the latitude because the vector $\boldsymbol{\Omega}$ is no longer perpendicular to the local surface. To see how the scaling operates, we have to consider a spherical coordinate system.

#### 4.1.1.3 *The Spherical Coordinate System*

Atmospheric dynamics is commonly described with local Cartesian coordinates on a spherical planet (Fig. 4.2(a)). The $x$-, $y$- and $z$-axes point in the horizontal eastward, horizontal northward, and vertical directions, respectively, while the winds in these directions are the *zonal wind u* in the west-to-east or "zonal" direction, the *meridional wind v* along a meridian in the south-to-north direction, and the

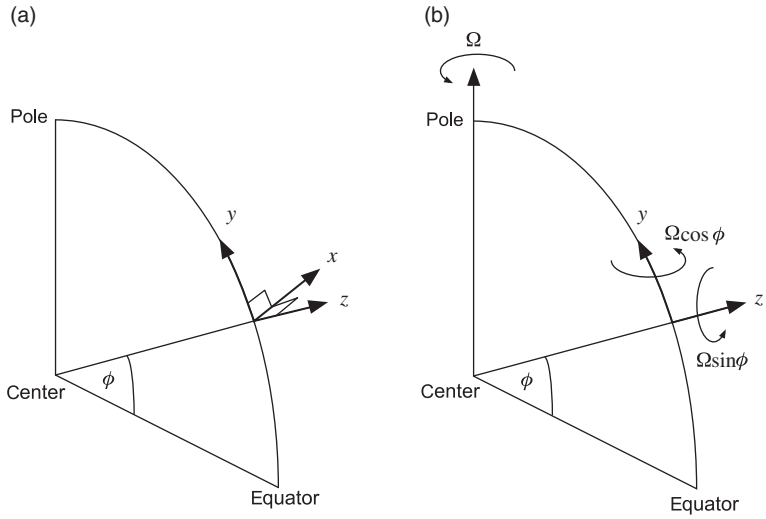


**Figure 4.2** (a) Local Cartesian system at a point on a planet at latitude $\phi$. The $x$ distance is along a line of latitude, the $y$ distance is along a meridian, and $z$ is altitude. (b) Components of the planetary rotation about local vertical and meridional axes. Here, $\Omega$ is the angular rotation rate of the planet's spin.

*vertical wind w* upwards. The $z = 0$ level is sea level on Earth. On other planets, a mean pressure level or a geopotential surface serves as a reference surface.

Here and later, we also use the word *prograde* to mean in the same direction as planetary rotation. Although we use prograde interchangeably with "eastward" for the Earth, prograde is more general and applies to any spin direction. *Retrograde* is the opposite direction to planetary rotation. Specifying "prograde" or "retrograde" for winds is useful because there are two conventions for which pole of a planet is the North Pole. NASA often defines the North Pole of a planet with a right-hand rule: If curled fingers represent the direction of rotation, the thumb points north. Using this definition, Venus has an obliquity of 177.4° and is upside down and rotating in a conventional counter-clockwise direction when viewed from above its North Pole. Similarly, Uranus is tilted at 97.9° degrees with respect to its orbital axis. In contrast, the International Astronomical Union (IAU) has the convention that the North Pole of a planet points upwards from the plane defined by the counter-clockwise orbital motion of the planet. With this definition, Venus and Uranus have obliquities of 2.6° and 82.1°, respectively, to their orbits, and both planets spin "backwards" (to the west) when viewed from above the orbital plane.

In our $x$–$y$–$z$ coordinate system, we define a wind vector (m s$^{-1}$) as:

$$\mathbf{v} = u\mathbf{i} + v\mathbf{j} + w\mathbf{k} \quad \text{3-D wind vector} \tag{4.3}$$

where **i**, **j**, and **k** are orthogonal unit vectors. Because the vertical wind is generally much smaller than horizontal winds, often we neglect $w$ and work with a horizontal wind vector:

$$\mathbf{v}_h = u\mathbf{i} + v\mathbf{j} \quad \text{2-D horizontal wind vector} \tag{4.4}$$

At any latitude $\phi$, a planet's angular velocity vector $\mathbf{\Omega}$ (rad s$^{-1}$) can be resolved into two orthogonal components along the local $y$-axis and vertical, as shown in Fig. 4.2(b):

$$\mathbf{\Omega} = \mathbf{j}(\Omega\cos\phi) + \mathbf{k}(\Omega\sin\phi) \tag{4.5}$$

Given $\mathbf{\Omega}$, we can calculate the Coriolis force per unit mass with vector algebra as:

$$\begin{aligned}\frac{-\mathbf{F}_{\text{Coriolis}}}{m} &= -2\mathbf{\Omega}\times\mathbf{v} = -2\Omega\begin{vmatrix}\mathbf{i} & \mathbf{j} & \mathbf{k}\\ 0 & \cos\phi & \sin\phi\\ u & v & w\end{vmatrix}\\ &= \mathbf{i}(-2\Omega(w\cos\phi - v\sin\phi)) - \mathbf{j}(2\Omega u\sin\phi)\\ &\quad +\mathbf{k}(2\Omega u\cos\phi)\end{aligned} \tag{4.6}$$

(For a readable derivation of the vector form of forces in a rotating frame, see Taylor (2005).) Here the negative sign is because the Coriolis acceleration would be positive in the inertial frame, so in the co-rotating frame it is subtracted, analogous to outward centrifugal versus inward centripetal force in circular motion. If we consider a southward wind $v$ in the northern hemisphere (i.e., positive latitude $\phi$, and no zonal or vertical wind so $u = w = 0$), then the Coriolis acceleration vector is $\mathbf{i}(2\Omega v\sin\phi)$. With negative $v$, the acceleration is in the negative $x$-direction (westward), so the southward moving parcel of air experiences acceleration to the right of motion. This is the origin of terrestrial trade winds. Air traveling towards the equator in the northern tropics is deflected westward, so that the resultant winds blow from the northeast to the southwest (Sec. 4.2.2).

We can simplify eq. (4.6) by neglecting terms in $w$ because vertical wind speeds are usually much smaller

than horizontal ones. Also the vertical component term in **k** of the Coriolis acceleration is often much smaller than the vertical acceleration of gravity. Then, the Coriolis force per unit mass is

$$= \mathbf{i}(-2\Omega(\cancel{w\cos\phi} - v\sin\phi)) - \mathbf{j}(2\Omega u\sin\phi) + \mathbf{k}(\cancel{2\Omega u\cos\phi}) \approx \mathbf{i}(2\Omega v\sin\phi) + \mathbf{j}(-2\Omega u\sin\phi)$$
$$= \mathbf{i}(fv) + \mathbf{j}(-fu) \tag{4.7}$$

Here, we have introduced a new variable,

$$\text{the Coriolis parameter, } f = 2\Omega\sin\phi \tag{4.8}$$

Given a typical zonal wind speed of $u$ = 10 m s$^{-1}$ on Earth, the magnitude of the Coriolis force per unit mass in mid-latitudes (e.g., $\phi$ = 45°) is $fu = 10^{-3}$ m s$^{-2}$, which is similar in magnitude to the pressure gradient acceleration we estimated in Sec. 4.1.1.1. This is no coincidence. The pressure gradient acceleration often approximately balances the Coriolis acceleration on rapidly rotating planets, such as Earth (Sec. 4.1.2.1).

### 4.1.1.4 *The Equations of Motion and the Role of Advection*

Considering all the forces gives a vector form of Newton's second law for fluid flow, specifying the acceleration of a unit mass of air in a frame co-rotating with the planet:

$$\underbrace{\frac{d\mathbf{v}}{dt}}_{\text{acceleration in co-rotating frame}} + \underbrace{(2\boldsymbol{\Omega}\times\mathbf{v})}_{\text{Coriolis acceleration}} + \underbrace{[\boldsymbol{\Omega}\times(\boldsymbol{\Omega}\times\mathbf{r})]}_{\text{centripetal acceleration}} = \underbrace{\frac{\mathbf{F}_g}{m}}_{\text{force of gravity}} + \underbrace{\frac{\mathbf{F}}{m}}_{\text{all other forces}} \tag{4.9}$$

Here, the last term includes pressure gradient forces, frictional or viscous forces, and external tidal forces (from the Sun or parent star, from a moon, or from a planet being orbited if we're considering the atmosphere of a large moon). Viscous forces are usually small and neglected, but they necessitate a constant resupply of angular momentum to the equatorial jets of Jupiter, Saturn, Venus, and Titan (Hide, 1969) as well as the eastward phase of a stratospheric circulation on Earth known as the quasi-biennial oscillation. External torques are also small and conventionally neglected. However, some authors have suggested that these forces give rise to torques that balance the viscous torques in deep atmospheres. For example, solar gravitational torques acting on an atmospheric mass distribution that is non-uniform in longitude because of solar heating has been proposed as the cause of a *superrotation* in the upper atmosphere of Venus (Gold and Soter, 1971). Superrotation is where the equatorial atmosphere rotates faster than the solid planet below (defined more precisely in Sec. 4.5). The deep atmospheres in the Solar System all exhibit superrotation or strong differential rotation, and the dynamical effects of external tidal torques remains to be fully investigated.

If the centripetal acceleration is taken to the right-hand side of eq. (4.9), by convention it is treated as centrifugal force per kg, which we can lump in with gravity (because both are the gradient of a potential) to form an effective gravity $g$ that we measure. An effective gravity applies because planets deform and become oblate (Sec. 1.1.2.3). Thus, neglecting tidal torques, we can re-write eq. (4.9) as:

$$\frac{d\mathbf{v}}{dt} = \underbrace{-\frac{1}{\rho}\nabla p}_{\text{pressure gradient force/kg}} - \underbrace{(2\boldsymbol{\Omega}\times\mathbf{v})}_{\text{Coriolis force/kg}} - g\mathbf{k} + \mathbf{F}_{\text{visc}} \tag{4.10}$$

Here, $\mathbf{F}_{\text{visc}}$ is the frictional or viscous force per unit mass. Eq. (4.10) is the conventional basic equation of dynamics called the *momentum equation*.

For practical use, we expand the above equation into three components of acceleration in the $x$, $y$, and $z$ directions of eastward, northward and upward. We will not go through the derivation because the dedicated reader can find it in various textbooks, e.g., a vector form in Appendix B of Andrews (2010), a geometric derivation in Ch. 2 of Holton and Hakim (2013), and another derivation in Ch. 4 of Jacobson (2005). Suffice it to say that scaling theory allows one to drop small terms so that large-scale motions simplify to the following equations when we neglect vertical motions and friction:

$$\text{Vertical (eq.(1.8))}: \quad \frac{\partial p}{\partial z} = -g\rho \tag{4.11}$$

$$\text{Zonal}: \quad \frac{du}{dt} - \underbrace{\left(f + \frac{u\tan\phi}{a}\right)}_{\text{Coriolis term}\quad\text{Centrifugal term}} v = -\frac{1}{\rho}\frac{\partial p}{\partial x} \tag{4.12}$$

$$\text{Meridional}: \quad \frac{dv}{dt} + \underbrace{\left(f + \frac{u\tan\phi}{a}\right)}_{\text{Coriolis term}\quad\text{Centrifugal term}} u = -\frac{1}{\rho}\frac{\partial p}{\partial y} \tag{4.13}$$

Here, $a$ is the planetary radius at the origin of the $x$, $y$, $z$ surface coordinates and $f$ is the Coriolis parameter (eq. (4.8)). Terms $fv$ and $-fu$ are the $x$ and $y$ components of the Coriolis acceleration discussed earlier. The Coriolis force is perpendicular to the wind vector, to the right in Earth's northern hemisphere and to the left of the wind vector in Earth's southern hemisphere. So-called "metric terms" $(u\tan\phi/a)v$ and $-(u\tan\phi/a)u$ are the $x$ and $y$ components of *cyclostrophic* acceleration, which is the acceleration arising from the excess or deficit of centrifugal acceleration due to motion relative to the planetary rotation. Equations (4.12) and (4.13) are often called *the momentum equations*.

Another key concept in fluid dynamics is advection. The *substantial*, *total*, *material* or *Stokes derivative* of the form $dX/dt$ (written $DX/Dt$ in some textbooks) represents the rate of change of some quantity $X$ with respect to time *following* a fluid parcel, unlike $\partial X/\partial t$, the change with respect to time at a *fixed point*. The relationship between these derivatives of any flow-field quantity that is a function of $x$, $y$, $z$ and $t$ is:

$$\underbrace{\frac{d(\,)}{dt}}_{\text{substantial derivative}} \equiv \underbrace{\frac{\partial(\,)}{\partial t}}_{\text{local derivative}} + \underbrace{u\frac{\partial(\,)}{\partial x} + v\frac{\partial(\,)}{\partial y} + w\frac{\partial(\,)}{\partial z}}_{\text{advective terms}} = \frac{\partial(\,)}{\partial t} + \mathbf{v}\cdot\nabla(\,) \qquad (4.14)$$

Here, $\mathbf{v}$ is the 3-D velocity vector (eq. (4.3)), and we have used $\mathbf{a}\cdot\mathbf{b} = a_1b_1 + a_2b_2 + a_3b_3$, along with the gradient operator, $\nabla = \partial/\partial x + \partial/\partial y + \partial/\partial z$. Box 4.1 illustrates a physical interpretation of advective terms. When the quantity in the dot product is $\mathbf{v}$, i.e., $\mathbf{v}\cdot\nabla\mathbf{v}$, the nonlinearity makes atmospheric dynamics "interesting" for weather forecasting, or difficult, depending on your disposition. However, in uniform flow where the velocity spatial derivatives are zero, equations can become linear.

**Box 4.1** Understanding Advective Terms

(1) Suppose we have a temperature field $T(x, y, z, t)$ that is constant in time ($\partial T/\partial t = 0$) but spatially varying, as shown in contours below. As an observer moves from place to place at velocity $\mathbf{v}$ the rate of change of temperature $T$ is

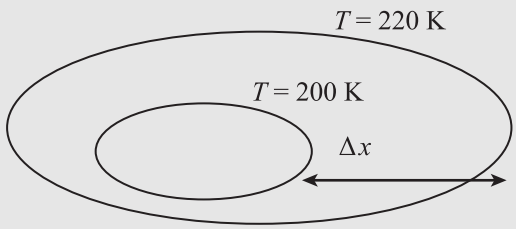


$$\frac{dT}{dt} = \mathbf{v}\cdot\nabla T$$

$$\text{e.g., } \frac{\Delta T}{\Delta t} = \left(\frac{\Delta x}{\Delta t}\right)\left(\frac{\Delta T}{\Delta x}\right) = \frac{20\text{ K}}{\Delta t}$$


(2) Now suppose contours change position with a velocity $\mathbf{v}$ but not value. An observer traveling at the same velocity sees no change in $T$ with time, so $dT/dt = 0$ because $\partial T/\partial t$ is balanced by the *advection* of temperature, $\mathbf{v}\cdot\nabla T$.

## 4.1.2 Characteristic Force Balance Regimes in Atmospheres

To provide physical insight, the $x$–$y$–$z$ equations of motion, (4.11)–(4.13), can be simplified further when different forces dominate and, in particular, they can then provide an intuitive understanding of the effect of planetary rotation on atmospheric circulation. We consider cases that apply according to whether a planet rotates rapidly or slowly. We then look at how a balance between heating and cooling leads to large-scale ascent and descent, which provides our starting point for discussing how heat is transported in large circulation cells on Earth, Mars, Venus, Titan, and Earth-like exoplanets (Sec. 4.2).

### 4.1.2.1 *Geostrophic Balance: Fast Rotating Planets*

If a planet rotates rapidly enough, the Coriolis terms in $f$ in eqs. (4.12) and (4.13) balance the pressure gradient in so-called *geostrophic balance*, at least in the extratropics. This balance is an excellent approximation when two interrelated conditions hold,

$$\frac{d(u,v)}{dt} \ll f, \quad \frac{u\tan\phi}{a} \ll f \qquad (4.15)$$

so that we can eliminate the $d/dt$ and metric terms in eqs. (4.12) and (4.13). The first condition applies when a dimensionless number, the *Rossby number*, is $\ll 1$:

$$\text{Rossby number}, Ro = \frac{\text{relative acceleration}}{\text{Coriolis acceleration}} = \frac{U^2/L}{fU} = \frac{U}{fL} \tag{4.16}$$

Here, $U$ and $L$ are characteristic horizontal velocity and length scales of the motions. Horizontal acceleration in eq. (4.15) has scale $d(u, v/dt) \sim U/t \sim U^2/L$. Since the maximum possible length scale is planetary radius $a$, the second condition in eq. (4.15) should be valid if the first holds, which we find on rapidly rotating planets: Earth, Mars, and the giant planets of the Solar System.

We can consider the Rossby number on various planets. On Earth, $U \approx 10$ m s$^{-1}$ and $L \approx 1000$ km $= 10^6$ m in mid-latitudes, while $f = 10^{-4}$ s$^{-1}$ at 45° N from eq. (4.8). Hence $Ro \approx 0.1$, and winds should be nearly geostrophic. Mars has a similar rotation rate and Rossby number to Earth, so geostrophy applies to Mars too. Jupiter has peaks winds ~100 m s$^{-1}$ at the boundaries of its bright zones and dark belts and a characteristic wind speed somewhat slower as $U \approx 50$ m s$^{-1}$, $L \approx 10\,000$ km $= 10^7$ m, and $f \approx 1.8 \times 10^{-4}$ s$^{-1}$. Thus, $Ro \approx 0.03$, so geostrophy again is reasonable. Saturn, with faster winds, has $Ro \approx 0.1$.

When both of the conditions in eq. (4.15) are satisfied, the horizontal flow described by eqns. (4.12) and (4.13) simplifies to geostrophic flow, as follows:

$$u_g = -\frac{1}{f\rho}\left(\frac{\partial p}{\partial y}\right)_z, \quad v_g = \frac{1}{f\rho}\left(\frac{\partial p}{\partial x}\right)_z \quad ; \text{ or } \quad u_g = -\frac{1}{f}\left(\frac{\partial \Phi}{\partial y}\right)_p, \quad v_g = \frac{1}{f}\left(\frac{\partial \Phi}{\partial x}\right)_p \tag{4.17}$$

Here, the "$g$" subscript indicates geostrophic winds (i.e., the approximation assumes $Ro$ = 0). Eq. (4.17) gives equivalent relations in two commonly used coordinate systems. In altitude coordinates on the left, the "$z$" subscript indicates that the partial derivative is evaluated along a surface of constant altitude $z$. In the other system, geopotential $\Phi$ (the gravitational potential energy per unit mass defined in eq. (1.13)) on a constant pressure surface is indicated by the "$p$" subscript. The second form is more compact because the pressure gradient force per unit mass in 3-D is simply $\nabla\Phi$, i.e., the geopotential variation along a constant pressure surface for a system in hydrostatic equilibrium.

The geostrophic wind has four properties.

(1) It flows tangential to the pressure gradient, i.e., parallel to isobars. Equivalently, it's parallel to geopotential contours on a constant pressure surface.

(2) In any small latitude range, speed is proportional to the spacing of those contours.

(3) The low-pressure region is to the left of the wind vector in the northern hemisphere on Earth, giving rise to a "Low to the Left" mnemonic known as the *Buys-Ballot* law after an early Dutch meteorologist. The converse is true in the opposite hemisphere.

(4) The wind speed implied by a given geopotential contour spacing (or isobar spacing, approximately, in altitude coordinates) is inversely proportional to sine of latitude, i.e., increases at lower latitudes as $f \to 0$.

As a consequence of the first and third properties, winds blow along the isobars of terrestrial low-pressure-centered *cyclonic* systems in the sense shown in Fig. 4.3. The opposite sense occurs around *anticyclonic* systems. In reality, as depicted in Fig. 4.3, surface friction causes the winds to flow at a slight angle to the isobars near a planet's surface. This creates convergence and divergence, i.e., inward and outward airflow, on low- and high-pressure areas, respectively.

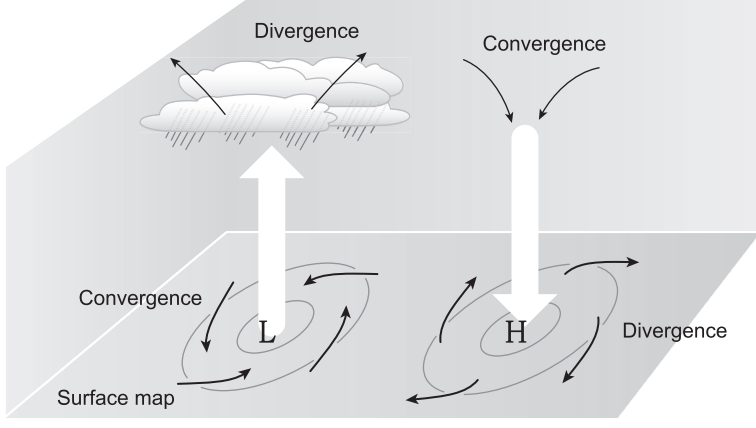


**Figure 4.3** Winds in cyclones (low-pressure systems) and anticyclones (high-pressure systems) in the northern hemisphere of the Earth. Divergent and convergent airflow near the surface and aloft are also shown.

It may seem odd that purely geostrophic air flows at right angles to the pressure gradient instead of down the gradient. However, air moving because of a pressure gradient will veer sideways in response to the Coriolis force on a rotating planet and *in time* reach the state of geostrophy. In eq. (4.16) for the Rossby number, $L/U$ is a timescale $\tau$ for a flow feature to move across its own diameter. We can estimate the timescale by writing the Rossby number as $Ro = 1/f\tau = 1/[(\Omega(2\sin\phi)\tau] = \tau_d/[(2\pi)(2\sin\phi)\tau]$, where $\tau_d$ is a sidereal day. At $\phi = 45^\circ$ latitude, $Ro \approx \tau_d/9\tau$, so if $Ro < 0.1$, which is required for geostrophy, $\tau$ must exceed a sidereal day. Thus, geostrophy is a balance developed by large-scale flow that takes longer than a sidereal day to cross a characteristic vortex dimension. The flow is therefore inevitably affected by rotation, which operates over that timescale.

### 4.1.2.2 *"Thermal Wind" (or "Thermal Windshear") Balance*

If there is a temperature gradient in the horizontal direction, a column of air (if isothermal) will shrink or grow relative to neighboring columns, setting up different horizontal pressure gradients at altitude and producing changing wind vectors with height. The *thermal wind* (or *thermal windshear*) equation relates *wind shear* – defined as the change of wind speed and direction with height – to horizontal temperature gradients. Differentiation of the geostrophic wind equation and substitution of the hydrostatic equation gives the thermal wind equation. For the meridional wind $v_g$, the algebra is as follows:

$$fv_g = \frac{1}{\rho}\left(\frac{\partial p}{\partial x}\right) = \frac{\overline{R}T}{P}\left(\frac{\partial p}{\partial x}\right),$$

differentiate w.r.t. $z$ and use the hydrostatic and ideal gas eqns:

$$f\frac{\partial v_g}{\partial z} = \overline{R}T\frac{\partial^2}{\partial z\partial x}(\ln p) \approx \overline{R}T\frac{\partial}{\partial x}\left(\frac{1}{p}\left(\frac{\partial p}{\partial z}\right)\right) = \cancel{\overline{R}T}\left(\frac{g}{\cancel{\overline{R}T^2}}\frac{\partial T}{\partial x}\right) \text{ with } \frac{\partial p}{\partial z} = -g\rho = -\frac{gP}{\overline{R}T}$$

Here, we ignored vertical variations in $T$ and $\overline{R}$, and so inserted an approximation sign. Manipulation of the zonal geostrophic wind equation is analogous, giving the results:

$$f\frac{\partial u_g}{\partial z} \approx -\frac{g}{T}\frac{\partial T}{\partial y}, \quad f\frac{\partial v_g}{\partial z} \approx \frac{g}{T}\frac{\partial T}{\partial x} \quad ;\text{or} \quad f\frac{\partial u_g}{\partial(\ln p)} = \left(\frac{\partial(\overline{R}T)}{\partial y}\right)_p, \quad f\frac{\partial v_g}{\partial(\ln p)} = -\left(\frac{\partial(\overline{R}T)}{\partial x}\right)_p \tag{4.18}$$

Here, we've retained possible variability of $\overline{R}$ in the log-pressure coordinate form on the right. These thermal wind equations show that winds as a function of latitude and height (or log pressure) can be deduced from the temperature distribution in a planetary atmosphere. Temperatures can be measured by remote sensing of emitted thermal radiation. Of course, we need a boundary condition to integrate eq. (4.18), which can be winds measured at a level such as cloud top on a giant planet or surface of a rocky planet. For the latter, we could alternatively use the distribution of surface pressures measured with barometers. For rocky planets where we use known winds at some level, often an assumption is made that the surface wind is negligible with the price of some inaccuracy.

The great insight is that the thermal wind equation links geostrophic flow to atmospheric thermodynamics. For example, in a common situation where the distribution of incoming solar radiation sets up a temperature decrease from equator to pole, the equation predicts that prograde zonal winds increase with altitude. We will find that it is also insightful to think about thermal windshear in a "backwards" way: If we detect prograde zonal winds increasing with altitude on a rapidly rotating planet (e.g., through cloud motion), there must be a corresponding meridional temperature gradient.

### 4.1.2.3 *Cyclostrophic Balance*

On Earth, we sometimes encounter *cyclostrophic balance* when a strong local pressure gradient force is balanced by centrifugal force. For example, when spinning air in a tornado moves with tangential speed $V$ around a radius $R$, this balance is as follows:

$$\underset{\text{centrifugal acceleration}}{\frac{V^2}{R}} = \underset{\text{pressure gradient acceleration}}{\frac{1}{\rho}\frac{\partial P}{dR}} \tag{4.19}$$

A tornado may have $V \sim 50$ m s$^{-1}$, $R \sim 100$ m, and a correspondingly strong pressure gradient. In such systems, planetary rotation is not "felt" by the much faster circulation.

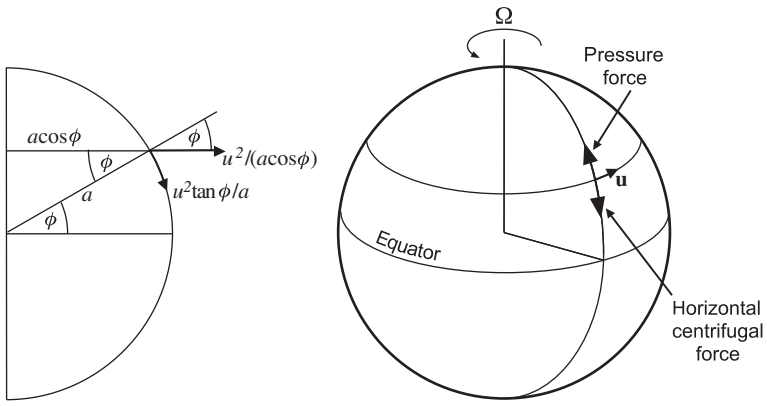


**Figure 4.4** The geometry of cyclostrophic balance at latitude $\phi$ on a slowly rotating planet, e.g. Venus. The zonal wind speed is $u$, the planetary radius is $a$, and $\Omega$ is the planet's angular rotation rate.

For planets or moons as a whole, we find cases such as Venus and Titan where there is little planetary rotation, so $\Omega \approx 0$, $f$ is small, and geostrophic balance does not apply. On Venus, a scale analysis at midlatitudes gives characteristic horizontal scale $L \approx 1000$ km $= 10^6$ m, characteristic wind speed $U \approx 10$ m s$^{-1}$, and $f = 2\Omega \sin\phi = 2(2.98\times 10^{-7}$ s$^{-1})(\sin 45^\circ) = 4.2\times 10^{-7}$ s$^{-1}$ at 45° N, so that the Rossby number, $Ro \approx 10$ from eq. (4.16). However, if the atmosphere itself rotates sufficiently rapidly over some altitude range, cyclostrophic balance prevails (Leovy, 1973). At latitude $\phi$, the centrifugal acceleration due to the zonal wind is $u^2/(a\cos\phi)$, because $a\cos\phi$ is the distance to the rotation axis (Fig. 4.4). This has a local component, parallel to the planet's surface, of $(u^2\tan\phi)/a$, giving

$$\frac{u^2\tan\phi}{a} = -\frac{1}{\rho}\frac{\partial p}{\partial y}; \qquad \text{or} \qquad \frac{u^2\tan\phi}{a} = -\frac{\partial \Phi}{\partial y} \tag{4.20}$$

We can also derive eq. (4.20) from eq. (4.13) by neglecting the Coriolis and substantial derivative terms. Physically, we have a picture where the centrifugal force balances an equator-to-pole pressure gradient (Fig. 4.4).

In evaluating the integral, we assumed an isothermal scale height $H = \overline{R}T/g$(eq. 1.12) and used $dz' = -H(dp/p)$ (eq. 1.10) and ignored vertical variations in $\overline{R}$.

Data show that the cyclostrophic approximation works for slowly rotating planets. Equations (4.20) and (4.21) are good approximations in the middle atmospheres of Venus and Titan given the observed increase of wind speed with altitude on Venus from *Pioneer Venus* probes (Seiff *et al.*, 1980) and on Titan from *Huygens* probe measurements (Bird *et al.*, 2005).

We can apply the theory to slowly rotating exoplanets. Consider the hot Jupiter HD209458b, which has a 3.5-day period and radius 1.35 $R_J$ where $R_J$ = Jupiter's radius of 69 911 km. Though not purely cyclostrophic, let's assume this approximation. We have some of the inputs to eq. (4.21) if we take $\overline{R} = 4160$ J K$^{-1}$ kg$^{-1}$ (Table 1.3), $\tan\phi = 1$ at 45° latitude, and a day–night contrast $\Delta T \sim 300$ K operating over a meridional scale of $\Delta y = 10^5$ km. We cannot solve eq. (4.21) without knowing $u^2$ at a reference level but we can assess the magnitude of $\Delta u^2$. Between pressure levels of 0.01 to 1 bar, we obtain:

$$\Delta u^2 = \left[(4160 \times 300 \times (1.35 \times 69\,911\,\text{km}) \times \ln(1/0.01))/\left(10^5\text{km}\right)\right] = 5.4 \times 10^6 \text{m}^2\text{s}^{-2}$$

We can also derive a *cyclostrophic thermal wind equation* that tells us how the zonal wind changes with altitude in response to a meridional temperature gradient. We use the same method as before: differentiation of the wind equation (4.20) w.r.t. $z$ and substitution of ideal gas and hydrostatic equations,

The peak winds on Jupiter are ~100 m s$^{-1}$, so a $\Delta u^2$ value of more than two orders larger on HD209458b indicates stronger thermal wind shear. If we assume a small zonal velocity at 1 bar then $\Delta u \sim 2$ km s$^{-1}$. Other scale analysis (eqs. (49) and (50) of Showman *et al.* (2010)) gives the same $\Delta u$ result. Thus, fast zonal winds are expected on

$$\frac{u^2\tan\phi}{a} = -\frac{\overline{R}T}{p}\frac{\partial p}{\partial y} \Rightarrow \frac{\tan\phi}{a}\frac{\partial(u^2)}{\partial z} \approx -\overline{R}T\frac{\partial}{\partial y}\left(\frac{1}{p}\frac{\partial p}{\partial z}\right) = -\frac{\cancel{\overline{R}}\,g}{\cancel{\overline{R}}\,T^{\cancel{2}}}\frac{\partial T}{\partial y}$$

$$u^2(z,\phi) = u^2(z_0,\phi) - \frac{\overline{R}a}{\tan\phi}\int_{z_0}^{z}\frac{1}{H}\frac{\partial T}{\partial y}\partial z' \approx u^2(z_0,\phi) - \frac{\overline{R}a}{\tan\phi}\frac{\Delta T}{\Delta y}\ln\left(\frac{p_0}{p}\right) \tag{4.21}$$

hot Jupiters, which is consistent with hotspots that are offset from a planets' substellar points by fast winds (Agol *et al.*, 2010; Knutson *et al.*, 2007) and detection of fast winds from Doppler-shifted absorption lines (Showman *et al.*, 2013a; Snellen *et al.*, 2010). In the future, similar dynamics may be detected on slowly rotating Earth-like exoplanets.

#### 4.1.2.4 *Thermodynamic Balance: Large-Scale Ascent and Subsidence of Air*

In Sec. 2.4.5, we assumed that that atmospheric structures are described well by 1-D radiative–convective equilibrium, but in fact large-scale motions disturb the temperature field through horizontal advection and also compression and expansion associated with ascent and subsidence. We can examine the latter using the associated thermodynamics.

The first law of thermodynamics expressed in terms of energy changes per unit mass, $dq$, was given in eq. (1.27) as $dq = c_p\, dT - \alpha\, dp$, where $\alpha$ =1/density = $1/\rho$ and $c_p$ is the specific heat capacity. Dividing by $\delta t$ and $c_p$, and taking the limit $\delta t \to 0$, we obtain:

$$\frac{dT}{dt} = \frac{\alpha}{c_p}\left(\frac{dp}{dt}\right) + \frac{Q}{c_p} \tag{4.22}$$

Here, $Q = dq/dt$ [J kg$^{-1}$ s$^{-1}$] is the *diabatic heating* per unit mass caused by radiation, convection, or molecular conduction. We expand $dT/dt$, according to eq. (4.14):

$$\frac{dT}{dt} = \left(\frac{\partial T}{\partial t} + u\frac{\partial T}{\partial x} + v\frac{\partial T}{\partial y}\right) + w\frac{\partial T}{\partial z} = \frac{dT'}{dt} + w\frac{\partial T_0}{\partial z} \tag{4.23}$$

In the last equality, $T'$ represents the horizontal and time variable component of temperature – shown in the brackets in the first equality, and $T_0$ is the horizontal and time average temperature, which is assumed a function of altitude only. Thus, using eq. (4.23) and the relation that $dp/dt \approx -g\rho w = -gw/\alpha$ , where $w$ is the vertical velocity, we can re-write eq. (4.22) as

$$\underbrace{\frac{dT'}{dt}}_{\text{time variable component}} + \underbrace{w\left(\frac{\partial T_0}{\partial z} + \frac{g}{c_p}\right)}_{\text{work done}} = \underbrace{\frac{Q}{c_p}}_{\text{heat gain}} \tag{4.24}$$

In atmospheric science, this form of the first law of thermodynamics is the *thermodynamic energy equation*, which describes how energy input or loss causes a rate of temperature change [K s$^{-1}$ or K day$^{-1}$] for a parcel of air that moves up or down. The term $dT'/dt$ is often smaller than the other two terms and its omission gives

$$\underbrace{w\left(\frac{\partial T_0}{\partial z} + \frac{g}{c_p}\right)}_{\text{static stability}} = \underbrace{\frac{Q}{c_p}}_{\text{heat gain}}, \quad \text{or} \quad w(\Gamma_a - \Gamma) = \frac{Q}{c_p} \tag{4.25}$$

Here, the term in brackets on the left-hand side is *static stability*, i.e., the difference between the adiabatic lapse rate $\Gamma_a = g/c_p$ (e.g., $\Gamma_a$ = 9.8 K km$^{-1}$ for Earth) and the observed lapse rate $\Gamma = -(dT/dz)$ (e.g., $\Gamma \approx 6$ K km$^{-1}$ in the global mean for Earth), which we met previously in eq. (1.35). Equation (4.25) expresses a balance between compressional heating (or expansional cooling) on the left-hand side and diabatic heating (or cooling) on the right.

To understand thermodynamic balance, it helps to replace the diabatic heating term with the *Newtonian cooling approximation*, in which temperature relaxes back to an equilibrium reference temperature field described by $T_{eq}$:

$$\text{substitute } \frac{Q}{c_p} \approx -\alpha_N\left(T - T_{eq}\right), \qquad \text{so that} \quad w(\Gamma_a - \Gamma) = -\alpha_N\left(T - T_{eq}\right) \tag{4.26}$$

Here, $\alpha_N$ is a Newtonian cooling coefficient [s$^{-1}$], where $\alpha_N = 1/\tau_{rad}$, where $\tau_{rad}$ is the radiative time constant (Sec. 2.3.2). The quantity $T_{eq}$ is the temperature of radiative–convective equilibrium when radiation and convection are the only major heat sources and sinks. Equation (4.26) simply says that that heating or cooling due to vertical motion is balanced by radiative relaxation of the temperature back to an equilibrium temperature.

The above theory suggests that the observed atmospheric temperature field $T$ can be used with theoretical expectations of $T_{eq}$ to infer large-scale vertical velocities. Note that static stability ($\Gamma_a - \Gamma$) is generally positive, e.g., typically a few K km$^{-1}$ for the atmospheres of the terrestrial planets (Sec. 1.1.3.1). Thus, if we measure $T < T_{eq}$, then eq. (4.26) requires that $w$ is positive and large-scale ascent is taking place to produce a temperature colder than equilibrium because of expansion and cooling. Where $T > T_{eq}$, it follows from eq. (4.26) that $w$ is negative and large-scale subsidence is producing compressional heating and a temperature that exceeds that of radiative–convective equilibrium. In fact, such regions can be seen in zonal mean meridional temperature cross-sections of real planetary atmospheres, such as Mars' atmosphere at equinox shown in Fig. 4.5. At pressures below ~0.5 mbar, the atmospheric temperature *increases* with latitude from the equator to high latitudes. The atmosphere cannot be in radiative equilibrium, which

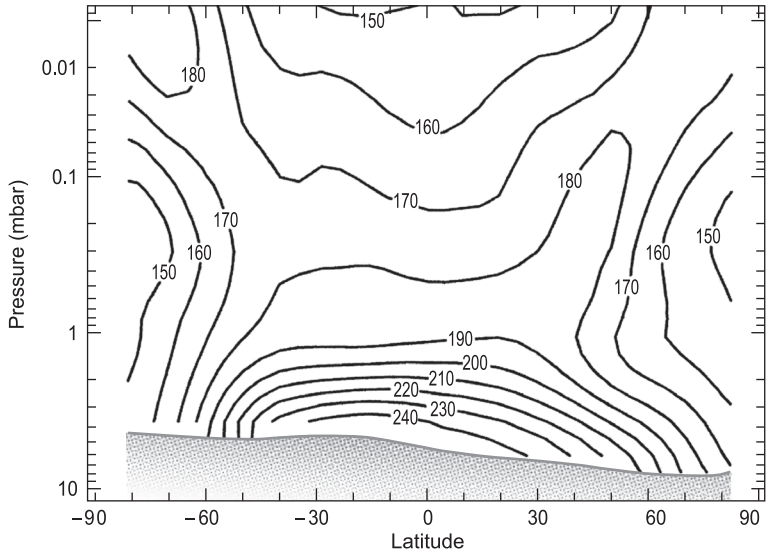


**Figure 4.5** Zonal mean meridional atmospheric temperatures at northern hemisphere autumnal equinox on Mars derived from measurements by the Thermal Emission Spectrometer (TES) instrument on NASA's *Mars Global Surveyor* spacecraft. The solid line at the lower boundary is the zonal mean atmospheric pressure at the surface. (Adapted from Smith *et al.* (2001). Reproduced with permission. Copyright 2001, John Wiley and Sons.)

implies dynamical effects. Large-scale meridional circulation in both hemispheres has ascent at low latitudes that causes cooling aloft and descent at mid to high latitudes that, at altitude, produces enough compressional heating to completely reverse one's expectation of a warm-to-cold equator-to-pole temperature gradient.

## 4.2 The Zonal-Mean Meridional Circulation and Thermally Driven Jet Streams

### 4.2.1 The Two Types of Jet Stream: Thermally Driven and Eddy Driven

One of the main features of atmospheric circulation on all planets is the jet stream structure – part of the arrangement of west–east wind systems over altitude and latitude. Because of planetary rotation, prograde winds tend to dominate (west-to-east for Earth), and usually they reach a maximum strength near the tropopause. Here, the term *jet stream* describes any wind maximum, whether it occurs in the prograde or retrograde direction.

Earth's atmosphere illustrates two types of jet stream. Seasonally and zonally averaged zonal winds are shown in Fig. 4.6(a). Below Earth's ~$10^2$ hPa tropopause, there are *subtropical tropospheric jet streams* at 30–40° latitude with a single such jet on average in each hemisphere. Of course, inhabitants of mid-latitudes know that a *polar front jet stream* is commonly present. But unlike the subtropical jet, the polar front jet stream is narrow, only partly continuous, and very mobile, so that it does not show up in the annual-average latitude-height section of Fig. 4.6(a). The subtropical jet arises from the temperature gradient between equator and higher latitudes combined with planetary rotation. This thermal gradient produces a large overturning of the atmosphere – the "Hadley circulation" discussed below. In contrast, the polar front jet stream is driven by eddies, i.e., the turbulent wind currents around low- and high-pressure disturbances in mid to high latitudes. We think of these two types of jets as *thermally driven* and *eddy driven*, respectively (Lee and Kim, 2003; Showman *et al.*, 2013b). They exemplify two types of jet expected in planetary atmospheres that we discuss below (Sec. 4.2.2 and Sec. 4.3).

On different planets, jet streams may be single or multiple in each hemisphere (Fig. 4.7); and they can also be strong or weak. In addition, jets can meander in latitude, such as on Earth and probably on Mars and Venus also, or can appear relatively straight. Terrestrial jets wander from *trough* regions of equatorward displacement to *ridge* regions of poleward shift. Meanders are often associated with transient eddies or waves. We describe such waves with a *zonal wavenumber*, which is the number of full wavelengths around an entire circle of latitude (Fig. 4.8). Zonal wavenumbers vary greatly from one planet to another because of different dynamics and a planet's size. The typical wavenumber of the meanders on Earth is ~6, on Venus it is 1 or 2, while on Mars, *Viking Lander* and orbital data suggest that it is 2–4. On Jupiter, the wavenumber can be >40. Jets appear straight in low spatial resolution images of Jupiter or Saturn, but much turbulence is evident at high spatial resolution.

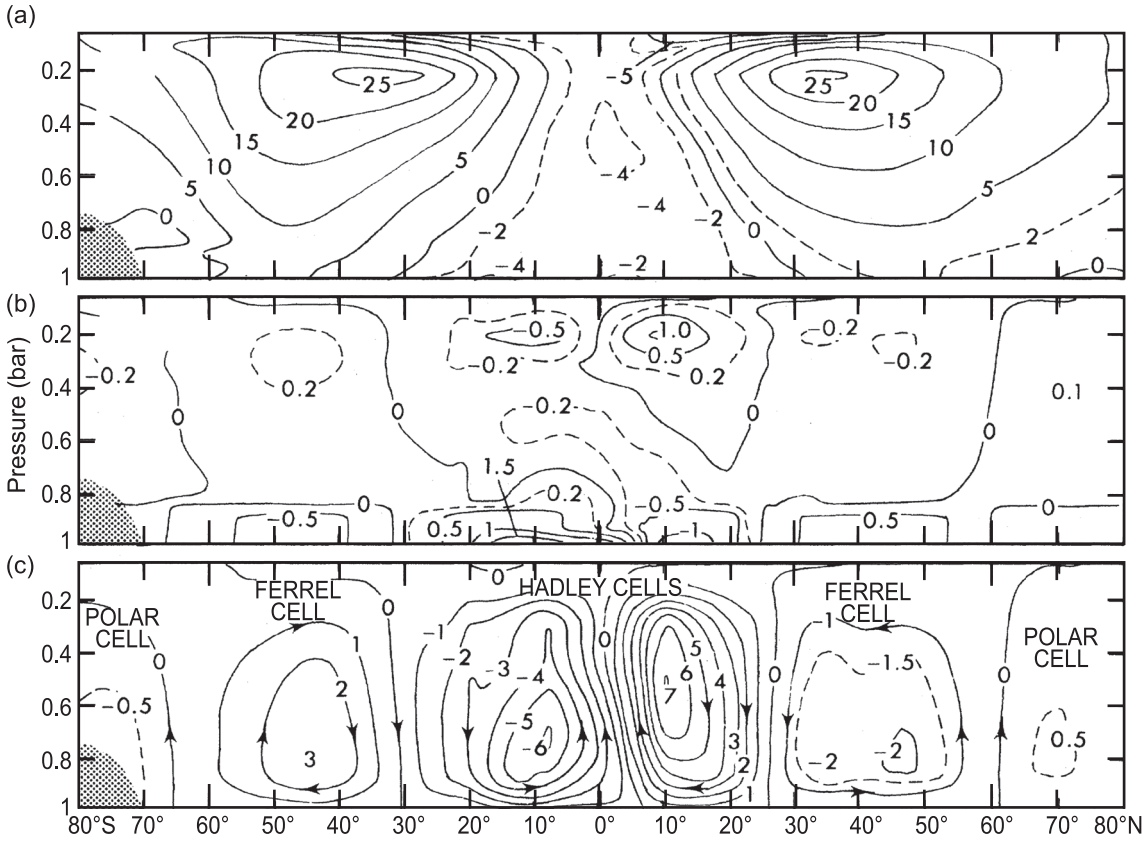


**Figure 4.6** (a) Earth's annual mean cross-section of the zonal wind (m $s^{-1}$). *Westerlies* (from the west, going eastward) are shown as solid contours, *easterlies* (from the east, going westward) are dashed contours. Below the tropopause (~0.1 bar) are *subtropical jet streams* at ~30–40° in each hemisphere. (b) The annual average meridional wind (m $s^{-1}$). Solid lines are northward, dashed lines are southward. (c) Inferred mass flow streamlines ($10^{10}$ kg $s^{-1}$) indicate Hadley cells, mid-latitude Ferrel cells, and weak polar cells in each hemisphere in the annual average. (Adapted from Peixoto and Oort (1984). Reproduced with permission. Copyright 1984, American Physical Society.)

### 4.2.2 The Hadley Circulation and Subtropical Jets

George Hadley (1685–1786) attempted to explain the winds in the Earth's tropics with a low latitude circulation (Hadley, 1735). The circulation that bears his name is often depicted as symmetric about the equator (Fig. 4.9 (a)), which is reasonable for the annual mean (Fig. 4.6) but actually atypical most of the time on planets with seasons, as discussed below. The same basic principles apply to a circulation that is not zonally symmetric provided zonal variations are small compared with meridional variations.

In a conceptual picture of the Hadley circulation, warm air rises near the equator (on Earth, primarily in convective cores of tall cloud systems) and spreads poleward from a level of maximum ascent near the tropopause. Air raised from near the surface at the equator has a greater angular momentum than that at higher latitudes by virtue of frictional coupling to planet's rotation. However, the flow aloft is less affected by friction. So, atmospheric parcels aloft tend to have eastward angular momentum relative to the surface as they move poleward, forming eastward winds and a subtropical jet stream. At upper levels, the poleward-moving air cools and sinks. On Earth, this occurs in the subtropics, where the resulting high-pressure zones of dry air create deserts such as the Sahara, Patagonian desert, and American southwest. The cycle is completed by return flow in low latitudes at low levels, on Earth in a boundary layer 1–2 km deep. In the return flow, conservation of angular momentum leads to the development of surface easterly (westward) winds. These equatorward, westward flows are the *trade winds*.

Hadley's original idea involved rising motion near the equator and symmetry about the equator, but Hadley

circulations on Earth and Mars are often highly asymmetric about the equator and also not uniform in longitude. Latitudinal asymmetry occurs because the rising branch is usually shifted well into one hemisphere and the descending branch shifted well into the other (Fig. 4.9(b)).

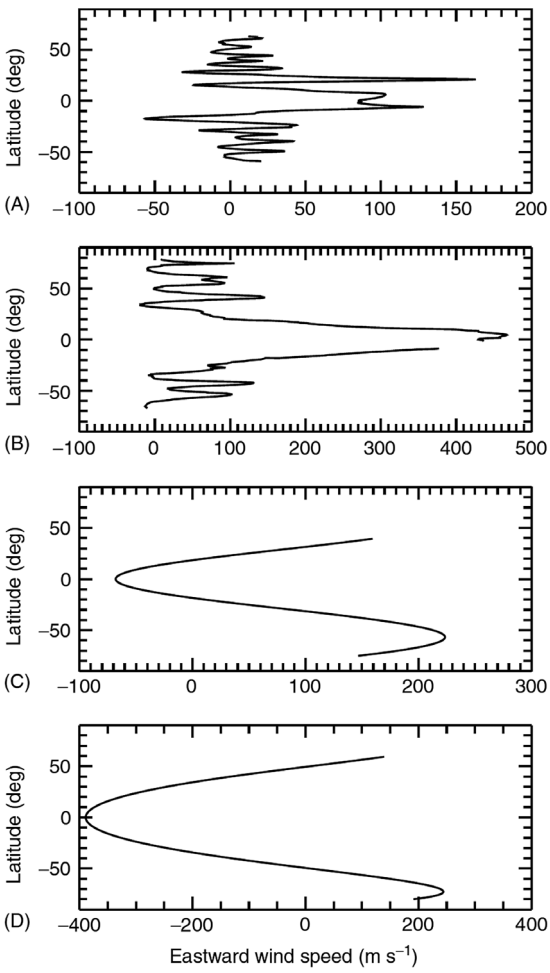


**Figure 4.7** Jet streams can be single or multiple on different planets. Zonal-mean zonal wind from cloud tracking for (A) Jupiter, (B) Saturn, (C) Uranus, and (D) Neptune show peaks that correspond to jets. Jupiter and Saturn have 20 east or west jets, while Uranus and Neptune appear to have three broad jets. (Source: Showman *et al.* (2010).)

On Earth, longitudinal asymmetry also results from continent–ocean contrasts, topography, and motion localized to small-scale convective cells that produce heavy rainfall in the *intertropical convergence zone* (ITCZ) where low-level trade winds converge. Earth's ITCZ is located close to, but not on the equator (Fig. 4.10). Descent also preferentially occurs in large-scale high-pressure areas of the subtopical Atlantic, Pacific, and Indian Oceans. Large-scale propagating waves also play a role in shaping the jet (Held and Phillips, 1990; Lee and Kim, 2003).

### 4.2.3 Symmetric Hadley Circulation Theory

Hadley did not attempt to answer two basic questions.

(1) What controls the most poleward latitude of the sinking motion?

(2) What sets the maximum zonal wind speed in the subtropical jet?

Two centuries later, Held and Hou (1980) provided a quantitative model of a zonally symmetric Hadley circulation based on three principles: (1) the tendency for parcels moving meridionally to conserve angular momentum, (2) geostrophic or cyclostrophic balance, and (3) a balance between energy gain by heating of the system and radiative loss to space. Although their model is a great conceptual model, it doesn't describe what happens in the real Hadley cells of the Earth, as discussed below. Nonetheless, it illustrated key concepts and moved the field forward. Below we follow its discussion similar to that in reviews by Showman *et al.* (2013b) and Schneider (2006).

In the Held–Hou model, the upper branch of the Hadley circulation conserves angular momentum per kg by assumption. If there is no relative zonal wind at the equator (latitude $\phi = 0$), the angular momentum per kg there is $\Omega a^2$. If angular momentum per kg is conserved in transport of air parcels from the equator to latitude $\phi$, then:

$$\Omega a^2 = (\Omega a \cos\phi + u) a \cos\phi \tag{4.27}$$

The terms on the right can be understood by examining Fig. 4.11. A point on the planet's surface at latitude $\phi$

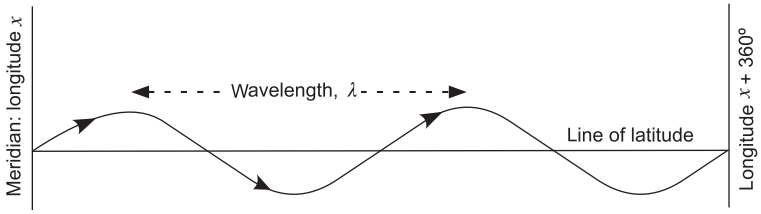


**Figure 4.8** The *zonal wavenumber* is the number of complete wavelengths around a circle of latitude. In this case, the zonal wavenumber is 2.

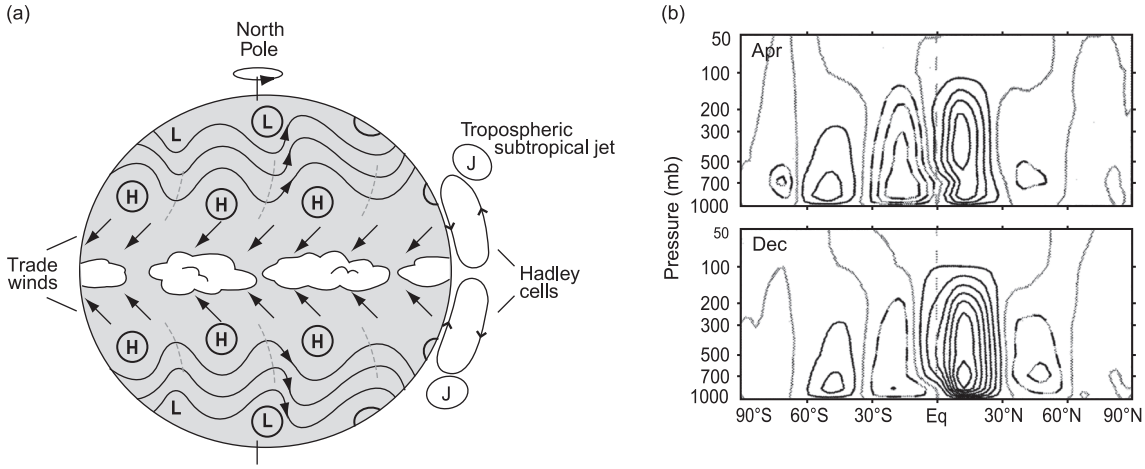


**Figure 4.9** (a) Idealized symmetric Hadley cells (Redrawn from Wallace and Hobbs (2006).) (b) A seasonally asymmetric Hadley circulation is revealed by reanalysis of observations in zonally averaged mass flow streamlines. Compare monthly averages for April (top), which is near the equinox, and December (bottom), which is near the southern summer solstice. Contours are $2 \times 10^{10}$ kg s$^{-1}$. (Source: Dima and Wallace (2003). Reproduced with permission. Copyright 2003, American Meteorological Society.)

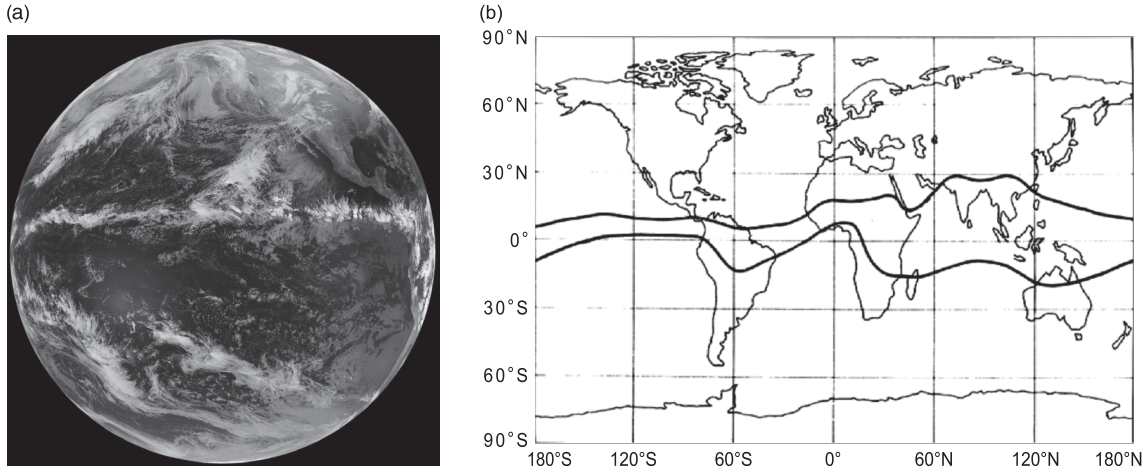


**Figure 4.10** (a) The Earth's intertropical convergence zone (ITCZ) is visible as a band of cloud across the eastern Pacific from west to east (courtesy: NOAA/NASA GOES project). (b) The latitude of the ITCZ changes seasonally and the annual average latitude of the ITCZ is north of the equator.

moves with tangential velocity $\Omega a\cos\phi$, to which we add the local zonal wind speed. However, the radius to the planetary rotation axis is $a\cos\phi$, so that the angular momentum per unit mass is given by the expression on the right of eq. (4.27). Solving for the zonal wind and using the identity $\sin^2\phi \equiv 1 - \cos^2\phi$, we have:

$$u\cos\phi = \Omega a\left(1 - \cos^2\phi\right) \quad \Rightarrow u = (\Omega a)\frac{\sin^2\phi}{\cos\phi} \qquad (4.28)$$

We remind ourselves that this equation applies for when the ITCZ is at the equator. For example, suppose that in the upper branch of Earth's Hadley circulation air is carried from the equator, where $u = 0$ and $\Omega a = (7.3\times10^{-5}$ rad s$^{-1})(6378\times10^3$ m) $\approx$ 465 m s$^{-1}$, to latitude 30°. Equation (4.28) gives the zonal wind speed at 30° as $u$ =134 m s$^{-1}$.

The zonal wind speed in the upper branch of Earth's Hadley circulation seasonally reaches ~30–70 m s$^{-1}$ in the core of the subtropical jet and is not as extreme as predicted by eq. (4.28) because friction and pressure forces reduce the angular momentum as a parcel travels. In detail, eddies associated with waves propagating from

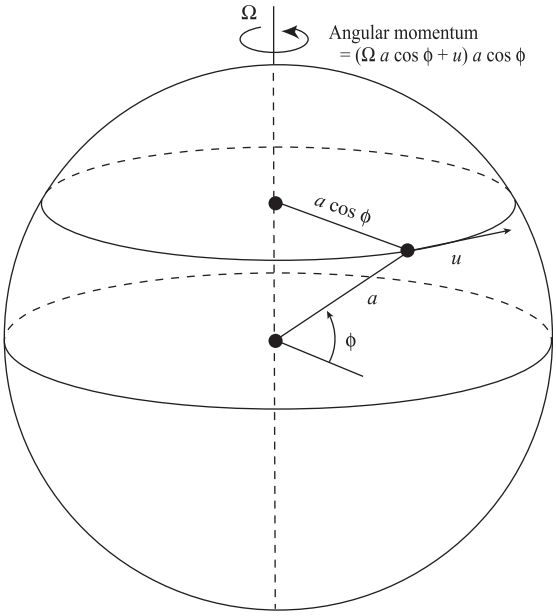


**Figure 4.11** Diagram illustrating the zonal angular momentum at latitude $\phi$, which can be compared to that at the equator to help understand the Hadley circulation. The zonal wind speed is $u$, the planetary radius is $a$, and the planet's angular rotation rate is $\Omega$.

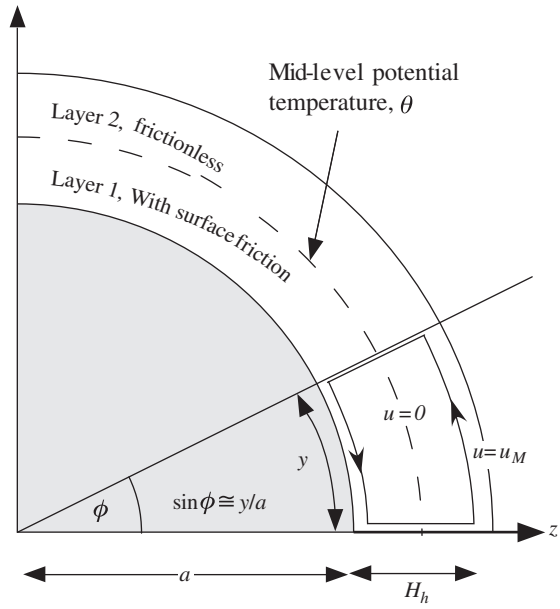


**Figure 4.12** The Held–Hou two-layer model of the symmetric Hadley circulation with equatorward flow at the surface and poleward flow at altitude $z = H_h$. The zonal wind speed, $u$, is assumed to be zero in the lower layer and $u_M$ in the upper layer.

the midlatitudes tend to provide westward angular momentum that decelerates the upper branch of the Hadley cell (Bordoni and Schneider, 2008, 2010; Randel and Held, 1991; Schneider and Bordoni, 2008). In any case, surface wind speeds must be far lower because of friction. Consequently, there must be a big increase of eastward wind speed with height near the jet. According to the thermal wind equation for the zonal wind (4.18), there needs to be a strong meridional temperature gradient $\partial T/\partial y$ at the jet latitude, with poleward temperature $T$ decreasing rapidly. The gradient in the radiative–convective equilibrium temperature $T_{\mathrm{eq}}$ should vary slowly and smoothly with latitude, but the actual temperature gradient is concentrated in the vicinity of the jet stream. On the equatorial side of the subtropical jet, $T < T_{\mathrm{eq}}$ implies large-scale ascent (Sec. 4.1.2.4)). Meanwhile on the polar side, $T > T_{\mathrm{eq}}$ implies large-scale descent.

Held and Hou's two-layer axisymmetric model for estimating the size of the Hadley circulation and its strength is shown in Fig. 4.12, and ignores variation of density with altitude. They assumed a latitudinal distribution of radiative–convective equilibrium potential temperature as $\theta_{eq} = \theta_0 - \Delta\theta_{eq}\sin^2\phi$, where $\theta_0$ is the equilibrium potential temperature at the equator and $\Delta\theta_{eq}$ is the equator-to-pole gradient of the equilibrium potential temperature. (Recall the definition of potential temperature (Sec. 1.1.3.2) and how it generally increases with altitude for real atmospheres that tend to be statically stable.) If near-equatorial latitude angles are small, then $\sin\phi \approx \phi \approx y/a$ and $\cos\phi \approx 1$ so,

$$\theta_{eq} = \theta_0 - \Delta\theta_{eq}\left(y^2/a^2\right) \tag{4.29}$$

Also, using $\sin\phi \approx y/a$ and $\cos\phi \approx 1$, eq. (4.28) simplifies to $u = \Omega y^2/a$.

The thermal wind equation can be used to predict the variation of temperature with latitude that we would expect if angular momentum conservation sets the zonal wind. In terms of potential temperature, the thermal wind is:

$$f\frac{\partial u}{\partial z} \approx -\frac{g}{\theta_0}\frac{\partial\theta}{\partial y} \quad \Rightarrow \left(\frac{2\Omega y}{a}\right)\frac{u_M}{H_h} = -\frac{g}{\theta_0}\frac{\partial\theta}{\partial y} \quad \Rightarrow \frac{\partial\theta}{\partial y} = \left(-\frac{\theta_0}{g}\right)\left(\frac{2\Omega y}{a}\right)\frac{\Omega y^2}{aH_h} \tag{4.30}$$

using $f = 2\Omega\sin\phi = 2\Omega y/a$ for the Coriolis parameter and assuming a height $H_h$ to the upper branch of the Hadley cell as shown in Fig. 4.12. Integration of eq. (4.30) in $\theta$ and $y$ then gives the variation of temperature with latitude as:

$$\theta = \theta_{M0} - \left(\frac{\Omega^2\theta_0}{2ga^2H_h}\right)y^4 \tag{4.31}$$

where $\theta_{M0}$ is the potential temperature at the equator (to be determined) and the "*M*" subscript reminds us that this temperature field derives from momentum conservation.

Lastly, two assumed constraints provide a solution. First, heating and cooling across the Hadley circulation are assumed to balance. With Newtonian cooling,

$$\int_0^Y \frac{d\theta}{dt}dy = 0, \quad \Rightarrow \int_0^Y -\alpha\left(\theta - \theta_{eq}\right)dy = 0, \quad \Rightarrow \int_0^Y \theta dy = \int_0^Y \theta_{eq}dy \tag{4.32}$$

where $Y$ is the maximum meridional extent of the Hadley cell. (Note that $Y = a\phi_H$ , where $\phi_H$ (radians) is the high latitude boundary of the cell.) The second constraint is that the temperature (4.31) is continuous with latitude at the subtropical edge of the Hadley cell and assumed equal to the radiative equilibrium temperature (4.29). These constraints produce two equations for the two unknowns, $Y$ and $\theta_{M0}$:

$$\theta_{M0}Y - \left(\frac{\Omega^2\theta_0}{10ga^2H_h}\right)Y^5 = \theta_0 Y - \left(\frac{\Delta\theta_{eq}}{3a^2}\right)Y^3; \quad \theta_{M0} - \left(\frac{\Omega^2\theta_0}{2ga^2H_h}\right)Y^4 = \theta_0 - \left(\frac{\Delta\theta_{eq}}{a^2}\right)Y^2 \tag{4.33}$$

These equations can be solved for the meridional extent of the Hadley cell, $Y$:

$$Y = \sqrt{\frac{5gH_h}{3\Omega^2}\left(\frac{\Delta\theta_{eq}}{\theta_0}\right)}, \qquad \text{or } \phi_H = \sqrt{\frac{5gH_h}{3\Omega^2a^2}\left(\frac{\Delta\theta_{eq}}{\theta_0}\right)} \tag{4.34}$$

With annual-mean values for the Earth of $\theta_0 \approx$ 260 K, $\Delta\theta_{eq} \approx$ 70 K and $H_h$ = 15 km, and with $a$ = 6380 km, $g$ = 9.8 m s$^{-2}$, and $\Omega = 7.2 \times 10^{-5}$ rad s$^{-1}$, we get $Y$ = 3570 km or $\phi_H \approx 30^\circ$, which is remarkably close to reality considering the simplicity of the model.

Equation (4.34) also implies that the latitudinal extent of the Hadley circulation should contract on a planet that rotates faster, i.e., with larger angular velocity Ω. Essentially, rapid rotation confines the Hadley circulation to low latitudes with the subtropical jet at the high latitude boundary. Earth-like GCM (general circulation model) simulations that vary planetary rotation rate support this inference (Del Genio and Suozzo, 1987; Kaspi and Showman, 2015; Navarra and Boccaletti, 2002; Showman *et al.*, 2013b). Conversely, as a planet's rotation rate slows, the Hadley circulation gets wider, heat is transported farther, and the equator-to-pole temperature contrast diminishes. If the Rossby number *Ro* exceeds ~10, the planet can be called an "all tropics" world in terms of its dynamics (Showman *et al.*, 2013b).

A limitation of the Held and Hou model is its neglect of turbulent eddies. In detail, the model predicts the strength of Earth's Hadley circulation as ~$10^{10}$ kg s$^{-1}$, which is an order of magnitude too small (cf. Fig. 4.6(c)); also, the exact dependence of Hadley cell width on rotation rate and other parameters is not supported in detail by GCMs. So alternative theories have been suggested. The leading idea is that midlatitude eddies confine the Hadley circulation (e.g., Bordoni and Schneider, 2010). Midlatitude eddies tend to generate eastward flow in the upper troposphere, so the application of the Coriolis force would imply an equatorward component of the flow in opposition to the poleward upper branch of Hadley cells. When the temperature changes rapidly in the horizontal and the wind changes strongly with height, the atmosphere is said to have a *baroclinic* structure. For example, lines of constant temperature tilt steeply downward in the midlatitudes of Mars' troposphere even at equinox (Fig. 4.5), and similar sloping isotherms occur in Earth's midlatitude troposphere, particularly in the winter hemisphere. In contrast, isotherms are relatively flat in the tropics. Midlatitude baroclinicity gives rise to *baroclinic instability*, which is when flow is driven by the extraction of potential energy from a latitudinal temperature gradient, giving rise to large-scale eddies.

Hadley cells perhaps extend to the latitude where the troposphere becomes baroclinically unstable (Held, 2000). Effectively, energy transported from the tropics by the Hadley circulation is passed on to baroclinic eddies at the subtropics, which transport energy to the poles. With a two-layer model of baroclinic instability and the latitudinal temperature gradient implied by angular momentum conservation (eq. (4.31)), Held (2000) derives a different latitudinal extent as follows:

$$\phi_H = \left(\frac{gH}{\Omega^2a^2}\left(\frac{\Delta\theta_{vert}}{\theta_0}\right)\right)^{1/4} \tag{4.35}$$

Here, $\Delta\theta_{vert}$ is the potential temperature difference going vertically from the surface to the top of the Hadley cell. Equation (4.35) has a much weaker power law

dependence on rotation rate and other variables compared to eq. (4.34) and provides a better fit to some GCM simulations (Frierson *et al.*, 2007; Lu *et al.*, 2009; Schneider, 2006). However, as mentioned above, winds in the real atmosphere do not obey simple angular-momentum conservation, so the model is simplistic. In fact, a theory that fully and clearly explains the strength and extent of Hadley cells remains elusive (Levine and Schneider, 2011).

The region of subsidence at subtopical latitudes on the Earth corresponds to descent on the equatorward flank of baroclinic waves, which forms part of the *Ferrel Cell*, a weak meridional circulation over midlatitudes (Fig. 4.6 (c)). The ascent of the Ferrel Cell occurs on the poleward flank of baroclinic waves and is driven by the mechanical energy of midlatitude storms. One should bear in mind that the Ferrel Cell is a temporal average and at any point in time, the circulation is dominated by very sporadic airflow associated with midlatitude storms and fronts.

### 4.2.4 Asymmetric Hadley Circulations on Earth and Mars, and Monsoons

As mentioned previously, the actual Hadley circulation on Earth is not symmetric about the equator but usually has the rising branch displaced toward one hemisphere or the other (Cook, 2004; Dima and Wallace, 2003; Lindzen and Hou, 1988). In general, a shift can be due to the tilt of the planet's rotation axis, which ensures that the sub-solar latitude is away from the equator for all but a very short part of the year. Or it can be due to other factors, as we next consider.

On average, Earth's Hadley circulation is stronger in the southern hemisphere because of the hemispheric difference in the distribution of oceans and continents. Earth's ITCZ lies at ~7° N in the annual average and is stronger at the solstices than near the equinoxes (Fig. 4.10). Because the ITCZ is offset from the equator, surface flow crosses the equator toward the opposite hemisphere. As it does so, it can curve from the Coriolis force from westward to eastward, and become a monsoon circulation. A *monsoon* is where there is a seasonal reversal of winds associated with latitudinal movement of the ITCZ. Monsoons are also effectively seasonal intensifications of the Hadley circulation in longitudinal bands because of land–sea temperature contrasts or a mountain range barrier. Such circulations are important in the continents of America, Africa, and Asia where summer heating shifts the rising branch of the Hadley circulation far from the equator.

Monsoon-like circulations also occur on Mars. Mars' orbit has relatively high eccentricity with more incoming solar radiation near the southern summer solstice when the Hadley circulation is stronger than during southern winter solstice (Fig. 4.13).

Absorption of solar radiation by dust is an important component of atmospheric heating on Mars that affects

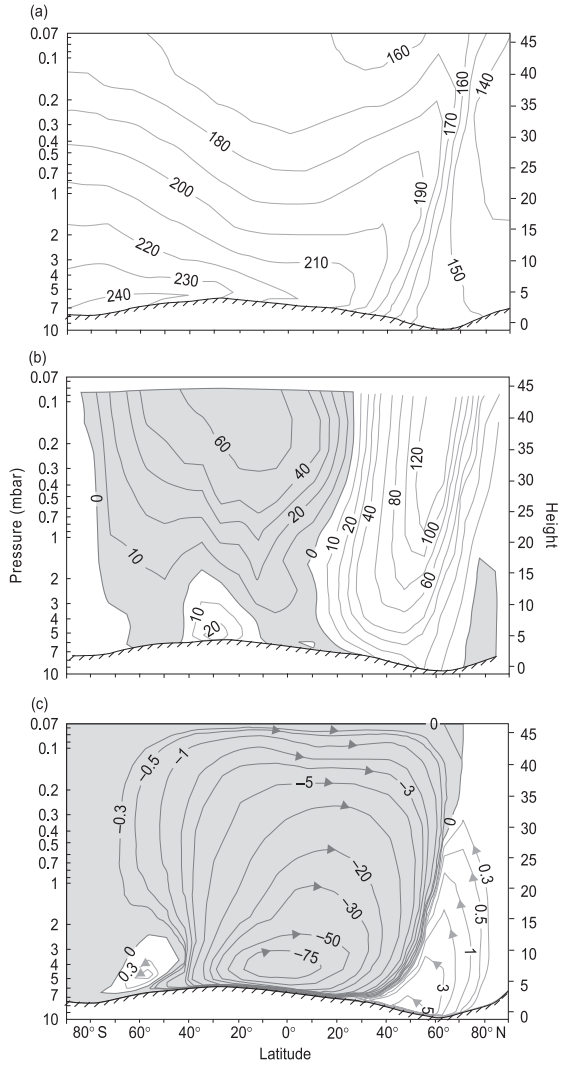


**Figure 4.13** Illustration of the Martian Hadley circulation at northern winter solstice, as calculated by the NASA Ames Mars general circulation model. The zonal mean temperature distribution (top panel) shows a temperature gradient maximum at 50–60° N in the winter hemisphere where there is a subsiding branch of the Hadley circulation. (b) Zonal mean winds, where shading corresponds to westward winds. Note the eastward jet stream at 60° N, 30 km altitude. Note also monsoon-like eastward winds near the surface in the southern subtropics. (c) Mass flow streamlines ($10^8$ kg $s^{-1}$) for the overturning thermally driven circulation. Clockwise flow is in the shaded plane. Note the large latitudinal extent of the zonally asymmetric Hadley circulation. (Source: Leovy (2001). Reprinted by permission from Macmillan Publishers Ltd: (C. Leovy, 412, 245–249) © 2001.)

the monsoon circulation. Local dust storms occur throughout the year, but during southern summer near perihelion, dust raised into the atmosphere can spread globally and greatly increase atmospheric heating on a planet-wide scale. In some years, planet-wide dust storms are associated with a big increase in the intensity of the latitudinally asymmetric Hadley circulation (Lewis *et al.*, 2007). Winds generated by the intensifying Hadley circulation contribute to widespread lifting of dust. The monsoon circulation becomes intense and dust is raised into the atmosphere throughout the monsoon latitude band, where it intensifies solar heating. The resulting positive feedback helps initiate and maintain these planet-wide storms. Not only does the dust spread to high latitudes (~55° N) in the expanding Hadley circulation, it is also lifted up to ~60 km altitude. Such dust storms mix constituents between the lower and middle atmosphere and presumably influence atmospheric chemistry.

### 4.2.5 Hadley Circulations on Venus and Titan

Much less is known about Hadley circulations on Venus and Titan. However, their study might tell us about circulations expected on slowly rotating exoplanets, which could be important for habitability, in some cases. Venus has a solar constant of 2614 W $m^{-2}$, but only a paltry ~30 W $m^{-2}$ is absorbed in the lower atmosphere and ~20 W $m^{-2}$ at the surface (Titov *et al.*, 2007). Meager heating in a dense atmospheric layer can drive only a very weak Hadley circulation. Because the constraining effect of rotation is small, this circulation probably extends to high latitude (cf. eqs. (4.34) and (4.35)). Surface wind markings measured by the *Magellan* spacecraft radar are spatially variable with an unknown time of emplacement, but a general equatorward direction at higher latitudes and an east–west direction nearer the equator suggests a possible Hadley circulation over a broad latitude range (Greeley *et al.*, 1997). Emitted infrared radiation as a function of latitude has a much flatter shape on Venus than on Earth, which is evidence for a smaller equator-to-pole temperature gradient and poleward transport of heat (Taylor *et al.*, 1983).

A second Hadley-like circulation appears to exist near Venus' cloud top level (~60–70 km) where ~100 W $m^{-2}$ is absorbed, which is most of the non-reflected, incoming solar radiation (Baker and Leovy, 1987). A strong temperature gradient and a weak maximum in the zonal wind speed relative to the background flow near 55° latitude suggest that this circulation extends to about this latitude in both hemispheres. Poleward of this latitude, the bottom of an approximately isothermal stratosphere drops in altitude and a tropopause minimum in the temperature profile becomes evident, unlike the absence of a temperature minimum in the equatorial regions (Tellmann *et al.*, 2009).

The situation on Titan is less clear. As on Venus, the heating per unit mass of the lower atmosphere is small so any thermally driven circulation must be weak. Evidence for prevailing winds in the lowest part of the Titan atmosphere comes from dunes in dark areas in low latitudes (Jaumann *et al.*, 2009). The dunes indicate eastward flow – exactly opposite to the direction expected for the trade winds of a Hadley circulation. Numerical simulations suggest that the dunes may form during brief periods when equatorial zonal winds reverse and are relatively strong (Tokano, 2009, 2010). In particular, occasional methane storms in low latitudes around equinox (because of strong updrafts then) may couple surface winds to fast superrotating eastward winds aloft (Charnay *et al.*, 2015).

### 4.2.6 Mean Meridional Circulation and Planetary Habitability

The zonal-mean meridional circulation discussed above is one of the most obvious areas where dynamics affects planetary climate. On Earth, the Hadley circulation creates dry, cloud-free conditions in its subtropical descending branch (Sec. 4.2.2). The *runaway greenhouse effect* sets the inner edge of the habitable zone around a star for Earth-like planets (Sec. 2.4.5.4 and Sec. 13.4). In 3-D models examining the runaway greenhouse, dry areas associated with the descending Hadley cell branch prove important for increasing the solar flux threshold at which an Earth-like planet goes into a runaway state (Leconte *et al.*, 2013). Another example concerning the dry descending branch of the Hadley circulation is a 3-D model of *Snowball Earth* (Sec. 11.10). This branch creates a latitudinal zone of bare ice rather than snow-covered ice, which lowers the albedo in that region, enabling a belt of water to persist in the tropics (Abbot *et al.*, 2011).

The ascending branch of Hadley-like circulation also has potentially important climatic effects. On tidally locked Earth-like exoplanets that have the same face towards their parent star, strong dayside convection can create a high albedo circular patch of sub-stellar water clouds that allows the inner edge of the habitable zone to be closer to the star than suggested by 1-D climate models (Yang *et al.*, 2013). Three-dimensional (3-D) models also show that atmospheric dynamical heat transport can warm the nightside of tidally locked Earth-like exoplanets and maintain their habitability by preventing the freeze-out of an atmosphere on the nightside (Joshi, 2003; Joshi *et al.*, 1997).

## 4.3 Eddy-Driven Jet Streams and Planetary Waves

Hadley's theory said nothing about Earth's atmospheric circulation in midlatitudes, where we find polar jet streams and a different circulation regime. As mentioned earlier, jets can also be forced by systematically structured eddies superimposed on the zonal mean flow. A familiar example of such eddies are terrestrial traveling cyclones and anticyclones. Another example is the stationary wave structure imposed on the zonal mean flow by lower boundary forcing and differential heating due to the distribution of continents and oceans on Earth.

Multiple jets in the atmospheres of Jupiter and Saturn, and the high latitude jets of Uranus and Neptune shown in Fig. 4.7 are probably eddy driven. Earth's atmosphere has two jets in the southern hemisphere much of the time. In northern hemisphere winter, there are also often two jets: the subtropical jet associated with the Hadley circulation and an eddy-driven jet at higher latitude that sometimes merges with the subtropical jet. Even on Mars and Venus, the single jet in each hemisphere – though primarily thermally driven – is modified by large-scale stationary and transient eddies.

### 4.3.1 Vorticity

To discuss eddy-driven jets, we need to introduce some concepts of fluid dynamics concerned with rotating air. The rotation at a point in a fluid could be specified in terms of radial distance from the center of rotation and the velocity field, but it is described more concisely through a single quantity, *vorticity*, which we now define.

*Relative vorticity* $\zeta$, is a measure of rotation about a vertical axis relative to the planet's surface, defined *positive if flow is counter-clockwise*, i.e., a right-hand rule: with fingers in the direction of curved flow, "thumb up" is positive. In solid body rotation, relative vorticity is equivalent to $2\omega$, where $\omega$ is the instantaneous angular velocity. For example, if tangential speed $V = 10$ m s$^{-1}$ in solid body rotation about radius $r = 300$ km, the relative vorticity $\zeta = 2(V/r) = 2(10\text{ m s}^{-1})/(300\times10^3\text{ m}) = 6.7\times10^{-5}\text{ s}^{-1}$. In a general flow field, *vorticity* at any point is the component of the curl of the wind about the local vertical. Thus, we take the **k** component of the expression in Box 4.2 to get the relative vorticity, i.e., the vorticity relative to the frame of reference of the planetary rotation:

$$\zeta = -\frac{\partial u}{\partial y} + \frac{\partial v}{\partial x} \tag{4.36}$$

We must also consider the effect of planetary spin. A fluid blob also possesses a component of planetary angular velocity of $\Omega \sin\phi$ about the local vertical (Fig. 4.2(b)). Doubling it gives *planetary vorticity* $2\Omega\sin\phi$, which is the Coriolis parameter, $f$ (eq. (4.8)). The *absolute vorticity* $\eta$ is the sum of relative and planetary vorticity:

$$\eta = \zeta + f = \left(-\frac{\partial u}{\partial y} + \frac{\partial v}{\partial x}\right) + f \tag{4.37}$$

Relative vorticity is expressed in atmospheres as a combination of horizontal shear (the change of velocity transverse to the flow, e.g., imagine eastward winds that weaken as you go north) and curvature (the rotation of the downstream flow direction). This explains why relative vorticity is $2\omega$ in solid body rotation: a shear contribution of the change in tangential velocity with radius, $\partial V/\partial r = \partial(\omega\ r)/\partial r = \omega$, is added to a curvature contribution of $\omega$ from the change in the tangential velocity with angle, $V(\partial(\text{angle})/\ \partial(\text{path})) = V(2\pi/2\pi r) = V/r = \omega$. In Earth's northern hemisphere, positive relative vorticity characterizes curvature in the counter-clockwise direction and/or sheared flow with decreasing flow speed toward the left of the flow direction. Positive relative vorticity occurs in cyclones, such as the surface low-pressure system in Fig. 4.3, and so is called *cyclonic vorticity*. Negative relative vorticity is expressed as curvature in the clockwise direction and/or as shear flow with speed increasing toward the left of the flow direction, which is referred to as *anticyclonic vorticity* (such as the surface high-pressure system on the right of Fig. 4.3). However, because an opposite relationship applies in the southern hemisphere where the sign of $f$ is opposite, we think of *cyclonic vorticity* as spin about a vertical axis in the same direction as the vertical component of the planetary rotation and

**Box. 4.2** Curl of a Vector Velocity Field Measures the Rotation of the Air

With a wind vector $\mathbf{v} = u\mathbf{i} + v\mathbf{j} + w\mathbf{k}$ (eq. (4.3)), the curl in Cartesian coordinates is:

$$\text{curl}\ \mathbf{v} = \nabla \times \mathbf{v} = \begin{vmatrix} \mathbf{i} & \mathbf{j} & \mathbf{k} \\ \frac{\partial}{dx} & \frac{\partial}{dy} & \frac{\partial}{dz} \\ u & v & w \end{vmatrix} = \mathbf{i}\left(\frac{\partial w}{\partial y} - \frac{\partial v}{\partial z}\right) + \mathbf{j}\left(\frac{\partial u}{\partial z} - \frac{\partial w}{\partial x}\right) + \mathbf{k}\left(\frac{\partial v}{\partial x} - \frac{\partial u}{\partial y}\right)$$

*anticyclonic vorticity* as the opposite. (To add complication for the uninitiated, dynamicists also talk about *curvature* of a flow, such as the flow of a wave circling round a planet. When a flux line is concave up, like a bowl, curvature is defined to be positive. Negative curvature applies to convex up, like a hill.)

The change of vorticity in time tells us how atmospheric circulations emerge and can be expressed in a *vorticity equation*. To derive it, we neglect the small term $u\tan\phi/a$ in the equations of motion, (4.12) and (4.13), add momentum forcing terms $F_x$ and $F_y$ to the left sides of (4.12) and (4.13), expand the substantial derivatives using (4.14), operate on the equations with $-\partial/\partial y$ and $+\partial/\partial x$, respectively, and add. This is somewhat tricky, so we show the full expansion and explain how it is simplified:

$$\underbrace{\frac{\partial}{\partial t}\left(\frac{\partial v}{\partial x}-\frac{\partial u}{\partial y}\right)}_{\zeta}+\overbrace{u\frac{\partial}{\partial x}\left(\frac{\partial v}{\partial x}\right)+\boxed{\frac{\partial u}{\partial x}\frac{\partial v}{\partial x}}}^{\text{column of }\partial/\partial x\text{ terms}}-\overbrace{u\frac{\partial}{\partial y}\left(\frac{\partial u}{\partial x}\right)-\boxed{\frac{\partial u}{\partial y}\frac{\partial u}{\partial x}}}^{\text{column of }\partial/\partial y\text{ terms}}+$$

$$v\frac{\partial}{\partial y}\left(\frac{\partial v}{\partial x}\right)+\boxed{\frac{\partial v}{\partial x}\frac{\partial v}{\partial x}}-v\frac{\partial}{\partial y}\left(\frac{\partial u}{\partial y}\right)-\boxed{\frac{\partial v}{\partial y}\frac{\partial u}{\partial x}}+$$

$$w\frac{\partial}{\partial z}\left(\frac{\partial v}{\partial x}\right)+\frac{\partial w}{\partial x}\frac{\partial v}{\partial z}-w\frac{\partial}{\partial z}\left(\frac{\partial u}{\partial y}\right)-\frac{\partial w}{\partial y}\frac{\partial u}{\partial z}+$$

$$\boxed{+f\frac{\partial u}{\partial x}}+\cancel{u\frac{\partial f}{\partial x}}+\qquad\boxed{f\frac{\partial v}{\partial y}}+v\frac{\partial f}{\partial y}=$$

$$\cancel{\frac{-1}{\rho}\left(\frac{\partial^2 p}{\partial x\partial y}\right)}+\cancel{\frac{1}{\rho}\left(\frac{\partial^2 p}{\partial x\partial y}\right)}+\frac{1}{\rho^2}\left(\frac{\partial p}{\partial y}\frac{\partial \rho}{\partial x}\right)-\frac{1}{\rho^2}\left(\frac{\partial p}{\partial x}\frac{\partial \rho}{\partial y}\right)+\frac{\partial F_y}{\partial x}-\frac{\partial F_x}{\partial x}$$

The double-underlined terms sum to the $d\zeta/dt$; also, the six terms in boxes sum to $(f+\zeta)(\partial u/\partial y+\partial v/\partial y)$. Using $\eta = f+\zeta$ (eq. (4.37)), and noting that $vdf/dy = df/dt$, the above simplifies to:

$$\frac{d\eta}{dt}+\eta\Delta-\left(\frac{\partial w}{\partial y}\frac{\partial u}{\partial z}-\frac{\partial w}{\partial x}\frac{\partial v}{\partial y}\right)+\frac{1}{\rho^2}\left(\frac{\partial \rho}{\partial x}\frac{\partial P}{\partial y}-\frac{\partial P}{\partial x}\frac{\partial \rho}{\partial y}\right)=-\frac{\partial F_x}{\partial y}+\frac{\partial F_y}{\partial x}=S_\eta \tag{4.38}$$

Here, $\Delta = \partial u/\partial x + \partial v/\partial y$ is the *divergence* of the horizontal wind, which is a tendency of outward flow from a point if positive or inward flow (*convergence*) if negative. Terms in $F_x$ and $F_y$ define a vorticity forcing term $S_\eta$, which can arise from friction or from stirring by eddies. The first bracketed term in eq. (4.38) corresponds to the inter-conversion between vorticity about axes, i.e., "twisting" of horizontal vorticity because of vertical wind shear. This twisting usually results from small-scale motions. The second term with brackets results from (baroclinic) horizontal shears of pressure and density.

To simplify, we neglect the vertical velocity and baroclinic terms. Also, if vertical velocity is negligible ($w = 0$), there is no horizontal divergence, i.e., no expansion or narrowing of columns of air resulting from vertical shrinking or stretching, so the divergence term ($\eta\Delta$) vanishes. Then eq. (4.38) becomes very simple:

$$\frac{d\eta}{dt} = S_\eta \tag{4.39}$$

Here, in purely horizontal flow, the substantial derivative is the horizontal form, $d/dt = \partial/\partial t + u\,\partial/\partial x + v\partial/\partial y$. Equation (4.39) shows that if there is no forcing by friction or stirring and $S_\eta = 0$, the absolute vorticity does not change in time and so is said to be conserved in horizontal flow. Because absolute vorticity ($\eta$) is the sum of relative ($\zeta$) and planetary vorticity ($f$), it means that as air shifts latitude and $f$ changes, the air must acquire relative vorticity and start spinning, which proves to be a useful concept, as we shall see.

### 4.3.2 Jet Forcing by Stirring or Friction

The vorticity equation can help us see how jets are forced by eddies and how this can account for multiple jets that

switch from eastward to westward on the giant planets at different latitudes and no doubt also in atmospheres of some large rapidly rotating exoplanets. Jet formation from eddies is also reviewed by Showman *et al.* (2013b) and in Ch. 12 of Vallis (2006).

To understand vorticity forcing by eddies and its relationship to jets, we can consider a case where there is a uniform zonal mean flow of speed $\overline{u}$ and an eddy fluctuation deviation from the average that is primed, e.g., $u = \overline{u} + u'$. We also assume a small meridional perturbation $v = v'$. Here, the zonal mean value of the fluctuation is zero, $\overline{u'} = 0$. These primed values arise from transient eddies that are associated with rapidly developing and decaying weather disturbances of the kind commonly experienced in terrestrial midlatitudes. The average of the product of fluctuation components, e.g., $\overline{u'v'}$, is called the *covariance* and is non-zero when $u'$ and $v'$are correlated.

Using the above theory, a term such as $u(\partial\eta/\partial x)$ within the vorticity equation (4.39) can be written:

$$u\frac{\partial \eta}{\partial x} = (\overline{u} + u')\frac{\partial(\overline{\eta} + \eta')}{\partial x} = \overline{u}\frac{\partial \eta'}{\partial x} + u'\frac{\partial \eta'}{\partial x} \approx \overline{u}\frac{\partial \eta'}{\partial x} \quad (4.40)$$

Here, we use the fact that $\overline{\eta}$ has no dependence on $t$ or $x$. With such "perturbation theory," we linearize the time-dependent vorticity equation (4.39) by expanding the substantial derivative and using eq. (4.40):

$$\left(\frac{\partial}{\partial t} + (\overline{u} + u')\frac{\partial}{\partial x} + v'\frac{\partial}{\partial y}\right)(\overline{\eta} + \eta') = S_\eta{}' \quad \Rightarrow \left(\frac{\partial}{\partial t} + \overline{u}\frac{\partial}{\partial x}\right)\eta' + v'\frac{\partial}{\partial y}\overline{\eta} = S_\eta{}' \quad (4.41)$$

To obtain an equation for the vorticity variance (also called *enstrophy*) in terms of the covariances between meridional velocity, vorticity, and vorticity forcing, we multiply eq. (4.41) by $\eta'$and take the zonal average (deleting terms with a zonal mean of zero):

$$\overline{\eta'\frac{\partial \eta'}{\partial t}} + \overline{u}\overline{\eta'\frac{\partial \eta'}{\partial x}} + \overline{v'\eta'}\frac{\partial \overline{\eta}}{\partial y} = \overline{S_\eta{}'\eta'} \Rightarrow \frac{1}{2}\frac{\partial \overline{(\eta\prime)^2}}{\partial t} + \frac{\overline{u}}{2}\frac{\partial \overline{(\eta\prime)^2}}{\partial x} + \overline{v'\eta'}\frac{\partial \overline{\eta}}{\partial y} = \overline{S_\eta{}'\eta'}$$

$$\Rightarrow \underbrace{\overline{v'\eta'}}_{\substack{\text{poleward vorticity} \\ \text{transport by eddies}}} = \underbrace{-\frac{\partial \overline{(\eta\prime)^2}/\partial t}{2\partial \overline{\eta}/\partial y}}_{\text{vorticity variance term}} + \underbrace{\frac{\overline{S_\eta{}'\eta'}}{\partial \overline{\eta}/\partial y}}_{\text{eddy forcing term}} \quad (4.42)$$

How does eq. (4.42) apply? Assume that eddies are generated at and cross latitude "1," $\phi_1$, as shown in Fig. 4.14. If the meridional gradient of absolute vorticity $\partial\overline{\eta}/\partial y$, exceeds 0 everywhere (because $f$ increases with latitude and $\partial f/\partial y$ is positive (Sec. 4.3.3)), eq. (4.42) shows that, in the time-mean horizontal flow, eddy stirring is associated with a poleward flux of vorticity across latitude circle $\phi_1$ by the eddies represented by $\overline{v'\eta'}$ at $\phi_1$. This increases vorticity in the area of the planet poleward of latitude $\phi_1$.

We next see how the increase of vorticity above latitude $\phi_1$ drives a prograde jet at $\phi_1$. Whereas vorticity measures rotation of a fluid at a point, *circulation* [unit $m^2$ $s^{-1}$] quantifies rotation over an area. The vorticity within an area is related to the circulation around a closed curve enclosing that area by *Stokes' theorem* (e.g., see Fleagle and Businger (1980), p. 407, for a derivation):

$$\Gamma_C = \oint V_s\, ds = \iint \eta dA \quad (4.43)$$

Here, $V_s$ is the component of velocity along the arc $ds$ (positive when in the sense of planetary rotation), $dA$ is an element of area, and $\Gamma_C$ is the circulation. Applying Stokes' theorem to the polar cap area bounded at its southern extent by latitude $\phi_1$, we have:

$$2\pi(a\cos\phi_1)\overline{u} = \int_{\lambda=0}^{2\pi}\int_{\phi=\phi_1}^{\pi/2} \eta a^2 \cos\phi\, d\phi\, d\lambda = 2\pi[\eta]a^2 \int_{\phi=\phi_1}^{\pi/2} \cos\phi\, d\phi \quad (4.44)$$

where $\lambda$ is longitudinal angle and $a$ is planetary radius. On the left, we evaluated the line integral by averaging around latitude $\phi_1$ of circumference $2\pi(a\cos\phi_1)$, and on the right, we inserted an element of area in latitude–longitude coordinates, $a^2\cos\phi\, d\phi\, d\lambda$ (see Fig. 2.9(a)), and wrote the average vorticity over the polar cap region as $[\eta]$. Equation (4.44) shows that a poleward vorticity

flux by eddies that increases the average vorticity $[\eta]$ in the cap region poleward of $\phi_1$ also increases the mean zonal wind $\overline{u}$ at latitude $\phi_1$ (Fig. 4.14).

Now suppose that stirring generates eddies along $\phi_1$, forcing a prograde jet at that latitude, and eddies propagate poleward to a second latitude $\phi_2$ where there is dissipation and hence negative covariance between eddy vorticity forcing and eddy vorticity itself, i.e., $\overline{S_\eta{}'\eta'}$ is negative. According to eq. (4.42), along latitude $\phi_2$, the eddy vorticity flux $\overline{v'\eta'}$ will be equatorward (negative), which means that a retrograde jet will be forced. Thus, if eddies can propagate north and south, both prograde and retrograde jets can be generated. This argument provides an explanation for how multiple jets can arise from eddies on giant planets or in atmospheres on rapidly rotating planets in general.

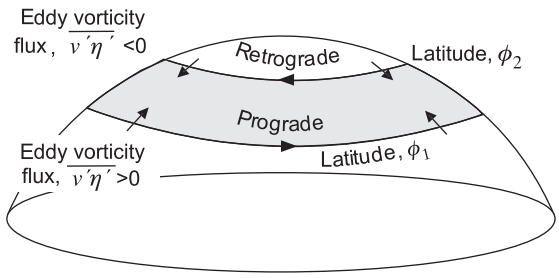


**Figure 4.14** Illustration of the connection between vorticity flux across latitude circles and zonal flow acceleration. Vorticity flux due to eddy stirring $\overline{v'\eta'}$ is northward across latitude $\phi_1$ and southward across latitude $\phi_2$ because of dissipation (small arrows). This flux accelerates zonal flow in the prograde direction along $\phi_1$ and in the retrograde direction along $\phi_2$ (bigger arrowheads). The shaded zone is the zone around which circulation is increasing according to Stokes' theorem (see text).

Another view of eddy forcing of jets in horizontal flows follows from considering zonal angular momentum, which turns out to be mathematically equivalent to considering vorticity transport. The poleward flux of zonal angular momentum per unit mass is $\overline{u'v'}$ $[(\mathrm{m}^2\ \mathrm{s}^{-1})/\mathrm{s}]$, which is the covariance between zonal and meridional components of the eddy wind velocity. Positive $\overline{u'v'}$ corresponds to a northward flux of zonal momentum and negative $\overline{u'v'}$ corresponds to a southward flux. Eddy wind component covariance corresponds to a tendency for systematic tilt of eddies. Where $\overline{u'v'} > 0$ (positive $v'$ and $u'$), vector addition of $u'$ and $v'$ implies that eddies have a southwest to northeast tilt. Conversely, $\overline{u'v'} < 0$ produces a northwest to southeast tilt (Fig. 4.15). Idealized GCM simulation even show those tilts as precipitation patterns (Frierson *et al.*, 2006). On the Earth, warm subtropical air is rotating faster than cold polar air and tilted waves associated with eddies in northern midlatitudes will transfer eastward momentum and heat northwards, while cold air is carried southwards (Fig. 4.15(b)).

The equivalence of a northward flux of eddy vorticity $\overline{v'\eta'}$ with the convergence of zonal mean momentum flux (expressed through its meridional gradient, $-\partial\left(\overline{u'v'}\right)/\partial y$) means that zonal angular momentum flows into the source region for eddies from both north and south and feeds an eastward jet there. This flux of zonal momentum to a region of already high zonal momentum is said to be "up-gradient." The equivalence with vorticity transport can be shown by using the fact that non-divergent flow can be fully described by a *stream function*, $\psi$, which is a scalar field for a fluid flow with contour lines that are streamlines of the flow. An advantage of working with a stream function rather than a velocity field is that we need

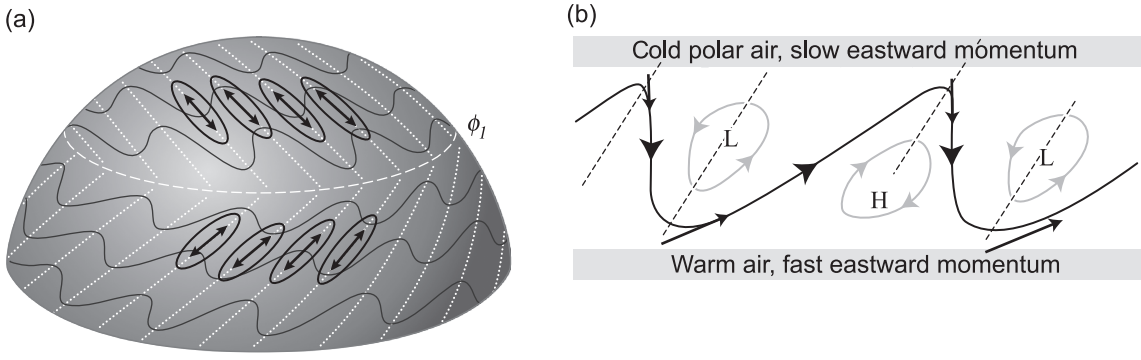


**Figure 4.15** (a) Streamlines of an eastward zonal flow with superimposed wave (heavy solid lines with arrowheads). Momentum flux converges at latitude $\phi_1$ where it drives an eastward jet. Thin ovals with thin slanting double-headed arrows represent the eddy perturbations north and south of $\phi_1$. Such a repeating pattern could drive prograde and retrograde jets on giant planets. (b) Titled eddies in the midlatitudes of the Earth transport eastward angular momentum from the subtropics to the poles, along with heat.

only find one function rather than two ($u$ and $v$) because the stream function $\psi$ is defined as:

$$u = -\frac{\partial \psi}{\partial y}, \quad v = \frac{\partial \psi}{\partial x} \tag{4.45}$$

Relative vorticity, defined by eq. (4.36), can be written in terms of $\psi$, as follows,

$$\zeta = -\frac{\partial u}{\partial y} + \frac{\partial v}{\partial x} \Rightarrow \zeta = \frac{\partial^2 \psi}{\partial x^2} + \frac{\partial^2 \psi}{\partial y^2} = \nabla^2 \psi \tag{4.46}$$

where $\nabla$ is the horizontal Laplace operator. By introducing perturbation forms of eq. (4.45), i.e., $u' = -d\psi'/\partial y$ and $v' = d\psi'/\partial x$ into eq. (4.46), we get $\zeta'$. Thus, the poleward vorticity flux in terms of $\psi'$is as follows (eliminating the $x$ derivative of zonal mean quantities that are zero):

$$\overline{v'\eta'} = \overline{v'\zeta'} = \overline{\frac{\partial \psi'}{\partial x}\left(\cancel{\frac{\partial^2 \psi'}{\partial x^2}} + \frac{\partial^2 \psi'}{\partial y^2}\right)} = \frac{\partial}{\partial y}\overline{\left(\frac{\partial \psi'}{\partial x}\frac{\partial \psi'}{\partial y}\right)} \Rightarrow \quad \overline{v'\eta'} = -\frac{\partial(\overline{u'v'})}{\partial y} \tag{4.47}$$

Equation (4.47) says that meridional vorticity transport (left) and the meridional flux of zonal mean angular momentum (right) by eddies are equivalent; they are just alternative ways ways to think about eddy forcing of jets.

### 4.3.3 Planetary Waves

Jets can meander back and forth in latitude because of waves in the circulation, including some comparable in size to the planet itself. Oscillations and propagating waves can occur in any medium in which perturbations from equilibrium are resisted by a restoring effect. In planetary atmospheres, the meridional gradient of absolute vorticity (arising from planetary rotation) provides a restoring effect that produces waves. To understand how such waves arise, we assume a zonal mean zonal wind $\overline{u}$ and differentiate absolute vorticity $\eta$ (eq. (4.37)) w.r.t. $y$:

$$\frac{\partial \eta}{\partial y} = \beta - \frac{\partial^2 \overline{u}}{\partial y^2}, \qquad \text{where } \beta \equiv \frac{\partial f}{\partial y} = \frac{\partial(2\Omega \sin\phi)}{\partial y} = \frac{1}{a}\frac{df}{d\phi} = \frac{2\Omega \cos\phi}{a} \tag{4.48}$$

In differentiating $f$, we have used $\delta y = a\delta\phi$, from spherical geometry. The meridional planetary vorticity gradient $\beta$, is normally much larger in magnitude than the second term, the vorticity gradient due to the mean zonal flow $-\partial^2\overline{u}/\partial y^2$, so that $\beta$ dominates the expression for $\partial\eta/\partial y$. For this reason, we were safe to assume earlier that $\partial\eta/\partial y > 0$ in eq. (4.42). The restoring effect due to the planetary vorticity gradient is called the *beta effect*.

The beta effect can be appreciated by considering a gas parcel blowing from west to east with zero relative vorticity that drifts across latitude $\phi_1$ because of some perturbation, such as flow over mountains. As the parcel moves poleward, planetary vorticity $f$ increases but absolute vorticity ($\eta = \zeta + f$) is conserved so relative vorticity $\zeta$ must decrease. This decrease is expressed in part by an increase in anticyclonic curvature (clockwise in Earth's northern hemisphere), so the parcel trajectory curves equatorward and crosses latitude $\phi_1$ with zero relative vorticity. Equatorward of $\phi_1$, relative vorticity increases, cyclonic curvature develops and the trajectory returns again toward latitude $\phi_1$. In this way, in the absence of dissipation or stirring, the gas parcel sinusoidally oscillates about $\phi_1$ as it moves downstream. This is the mechanism of *Rossby waves*, which are members of a larger class of planetary waves influenced by the restoring effect of the planetary vorticity gradient (Fig. 4.16). Typical meanders in Earth's midlatitude jet stream with wavenumbers of 4 to 6 are guided by Rossby waves.

We can derive a wave equation for Rossby waves in horizontal flow by considering the vorticity equation linearized with a perturbation about the mean zonal flow $\overline{u}$, eq. (4.41). Neglecting the vorticity forcing term $S_\eta$, we have:

$$\left(\frac{\partial}{\partial t} + \overline{u}\frac{\partial}{\partial x}\right)\eta' + v'\frac{\partial \overline{\eta}}{\partial y} = 0 \quad \Rightarrow \frac{\partial(\nabla^2\psi')}{\partial t} + \overline{u}\frac{\partial(\nabla^2\psi')}{\partial x} + \beta\frac{\partial(\psi')}{\partial x} = 0 \tag{4.49}$$

where we have substituted for the following:

$$\eta' = \frac{\partial^2 \psi'}{\partial x^2} + \frac{\partial^2 \psi'}{\partial y^2} = \nabla^2\psi' \quad \text{and} \qquad \frac{\partial \overline{\eta}}{\partial y} = \beta \qquad \text{and} \quad v' = \frac{\partial \psi'}{\partial x} \tag{4.50}$$

For simplicity, we assume that the approximately spherical geometry of the planet can be neglected so that we can

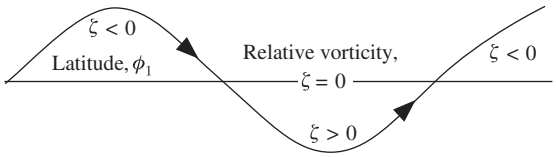


**Figure 4.16** Illustration of the Rossby wave mechanism. A fluid parcel in the northern hemisphere moves through the wave pattern from west to east. Starting from the left, as the parcel crosses its equilibrium latitude $\phi_1$, the relative vorticity $\zeta = 0$. North of $\phi_1$, conservation of absolute vorticity requires $\zeta < 0$ and so the trajectory curves southward anticyclonically. South of $\phi_1$, the trajectory curves northward cyclonically and $\zeta > 0$.

work with horizontal flow in a local Cartesian coordinate system in order to examine mechanisms and gain intuitive understanding.

With the additional assumption that the zonal mean zonal wind $\overline{u}$ is constant in the vicinity of latitude $\phi_1$, we guess wave-like solution to (4.49), sinusoidal in $x$ and $y$:

$$\psi'(x,y,t) = \Psi e^{i(\omega t - kx - ny)} = \Psi e^{i\xi} = \Psi(\cos\xi + i\sin\xi) \tag{4.51}$$

Here, the expression includes a wave amplitude factor $\Psi$, an angular frequency $\omega$, and zonal and meridional wavenumbers $k = 2\pi/\lambda_x$ and $n = 2\pi/\lambda_y$, where $\lambda_x$ and $\lambda_y$ are zonal and meridional wavelengths, respectively. (We remind ourselves that, in physical space, $\psi'$, is identified with the real part of the complex function). Substituting eq. (4.51) in eq. (4.49), allows us to derive a *dispersion relation*, meaning how the eastward phase speed $c$, of the Rossby wave varies with wavelength:

$$(-\not{\iota}\omega + \not{\iota}\overline{u}k)\left(k^2+n^2\right) - \not{\iota}k\beta = 0 \;\Rightarrow \omega = k\overline{u} - \frac{k\beta}{\left(k^2+n^2\right)}$$

$$c = \frac{\omega}{k} = \overline{u} - \frac{\beta}{\left(k^2+n^2\right)} \tag{4.52}$$

Equation (4.52) gives the phase speed relative to the planet's surface. If we take $n = 0$, we see that Rossby waves propagate westward relative to the zonal wind at phase speeds that increase with increasing wavelength or smaller wavenumber, given $\lambda_x = 2\pi/k$. Stationary Rossby waves when $c = 0$ occur only in eastward zonal flows since $\beta^2/\left(k^2+n^2\right)$ is positive. If we set $n = 0$ and $c = 0$, eq. (4.52) gives $k^2 = \beta/\overline{u}$ and we see that stationary waves have a west–east wavelength of $\lambda_x = 2\pi(\overline{u}/\beta)^{0.5}$. Taking $\overline{u}$ = 20 m s$^{-1}$ in Earth's middle troposphere at 45° latitude where $\beta \sim 1.6 \times 10^{-11}$ m$^{-1}$ s$^{-1}$, the stationary wavelength is ~7000 km. Four of these waves would girdle the Earth. Even longer Rossby waves would propagate westward relative to the Earth's surface.

Rossby waves can steer and affect the amplitude of smaller, faster-moving baroclinic waves (see below) such that low-pressure cyclones tend to form in the troughs of the waves, and high-pressure anticyclones tend to form in the crests of the waves. To see Earth's Rossby waves in data, the faster-moving baroclinic waves need to be smoothed out by averaging over several days. Then, the height of 500 mbar surfaces, for example, reveal Rossby waves, usually moving slowly eastward a few degrees longitude per day. Similar Rossby waves have been observed on Mars in midlatitudes in spring and winter with wavenumber 1–2 (Hollingsworth and Barnes, 1996; Wilson *et al.*, 2002).

If we relax the constraint of constant $\overline{u}$, the stream function amplitude will vary with meridional distance. An appropriate form of $\Psi(y)$ is then

$$\frac{\partial^2\Psi}{\partial y^2} + n^2(y)\Psi = 0 \tag{4.53}$$

where substitution of eq. (4.53) and eq. (4.51) into eq. (4.49) gives $n$ as

$$n^2(y) = \frac{\beta}{(\overline{u} - c_x)} - k^2 \tag{4.54}$$

where $c_x$ is the eastward phase speed of the wave. Equation (4.53) has the form of a 1-D wave equation that is common in acoustics and optics so we can use concepts from those fields to discuss what it means.

The factor $n^2(y)$ is the square of the 1-D *refractive index* – analogous to the refractive index in optics. The analogy includes the concepts of *wave activity* – a wave property that depends on the square of the amplitude of the wave that is approximately conserved in propagation through a variable medium (e.g., Vallis, 2006, pp. 299–302), *wave packets* or *groups*, which are bounded disturbances consisting of closely spaced Fourier components, and *group velocity* ($d\omega/dk$), which is an approximate velocity of wave packet propagation. Waves can propagate in the $y$ direction when $n^2(y) > 0$ but not when $n^2(y) < 0$, so latitudes at which $n^2(y)$ changes sign are of special importance.

Under two circumstances, $n^2(y)$ changes sign. In the first, $n^2(y) = 0$ when $[\,\beta/(\overline{u} - c_x)] - k^2 = 0$ in eq. (4.54), and the eastward phase speed $c_x$, of the wave matches that of the freely propagating Rossby wave discussed previously. These are *turning point latitudes*. When a wave with specified frequency and zonal wave number $\omega$ and $k$ propagating in the $+y$ direction (northward) encounters a turning point at $y = y_{\text{turn}}$, it is refracted back toward its origin. The wave cannot propagate beyond $y_{\text{turn}}$. Pairs of turning points can form a waveguide such that waves generated between the turning points are trapped. For example, prograde jets may have turning points for waves

with the appropriate values of $\omega$ and $k$ on both sides of the jet core. Waves generated by stirring or other processes near the jet core with $\omega$ and $k$ that have turning points on the edges of the jet will be trapped in the waveguide. Only waves with $c_x < \overline{u}_{\min} - \beta/k^2$ can escape the wave-guide, where $\overline{u}_{\min}$ is the minimum mean zonal flow speed on either side of the eastward jet. Usually these will be waves with small values of $k$ (long wave-lengths) and rapid westward phase speed. All other waves are blocked by the mean zonal flow.

The second condition under which $n^2(y)$ changes sign is $(\overline{u} - c_x) = 0$, which occurs at *critical latitudes*, denoted $y_{\text{crit}}$. As a critical latitude is approached through regions with allowed wave propagation, $n^2(y)$ tends to infinity through positive values by inspection of eq. (4.54). On the opposite (non-propagating) side of $y_{\text{crit}}$, $n^2(y)$ approaches infinity at $y_{\text{crit}}$ through negative values. Oscillation behavior near $y_{\text{crit}}$ is very different at critical latitudes than at turning point latitudes. As $y_{\text{crit}}$ is approached through positive values, energy of waves with the values of $\omega$ and $k$ appropriate to that value of $y_{\text{crit}}$ is absorbed. Wave oscillation rate increases to infinity, but wave amplitude diminishes to zero. No propagation of waves past $y_{\text{crit}}$ is allowed.

This can be illustrated by considering waves in eastward flow on the poleward side of a prograde jet (Fig. 4.17). Assume they are generated at latitude $y_{\text{gen}}$. Outside of the generation region, planetary wave packets, consisting of disturbances with a narrow range of $\omega$ and $k$ propagate poleward. But as these packets encounter critical latitudes for the specified values of $\omega$ and $k$ in the packets, wave energy will be absorbed. In this way, wave packets generated in the vicinity of a particular latitude, $y_{\text{gen}}$, where the resulting eddy vorticity generation drives eastward mean zonal flow, can propagate poleward or equatorward to a distant latitude $y_{\text{crit}}$. At latitude $y_{\text{crit}}$, the waves are absorbed and the resulting eddy vorticity dissipation drives westward acceleration. This combination of generation, propagation, and dissipation can increase jets going in both directions and strengthen the zonal mean wind shear between jets.

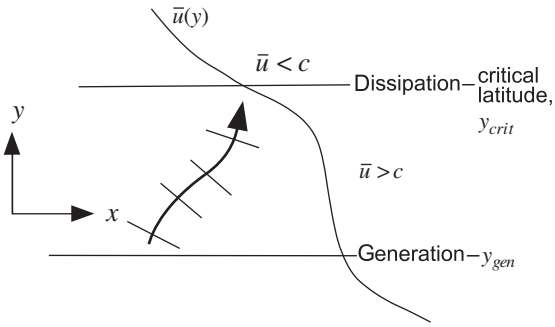


**Figure 4.17** A schematic diagram of mean zonal wind $\overline{u}$ as a function of meridional distance $y$ showing regions of planetary wave generation and dissipation. Waves of phase speed $c$ are generated at latitude $y_{\text{gen}}$ where $\overline{u} > c$ and propagate to the critical latitude $y_{\text{crit}}$ where $\overline{u} = c$. Wave energy is absorbed near $y_{\text{crit}}$. The wave packet trajectories are depicted by the curved heavy line, and wave phase surfaces are shown as the thin lines crossing the trajectories. Eastward flow is accelerated near latitude $y_{\text{gen}}$ and decelerated near latitude $y_{\text{crit}}$.

Near critical latitudes, meridional wavelengths become short and the parcel trajectories begin to stretch so that parcels from distant origins are brought close together. This allows small scale eddies to efficiently mix properties and dissipate variations. Rossby waves are reversible distortions of contours of absolute vorticity (Fig. 4.16), but at a critical latitude the strong distortion of these contours is irreversible (Fig. 4.18). The process bears a rough analogy to ocean waves propagating shoreward from deep water. As waves approach a beach, the waves overturn, break, and dissipate. Because of this analogy, the atmospheric process of dissipation near critical latitudes is also referred to as *wave breaking*. Critical latitudes for planetary waves are more complex than waves on the beach because under certain conditions critical latitudes can reflect certain discrete Fourier solutions of the wave equation called *normal modes*. Nevertheless their most important role is absorption of planetary waves (Randel and Held, 1991).

### 4.3.4 Effects of Vertical Variation

In contrast to our consideration of waves in Sec. 4.3.3, real atmospheric flows are obviously not strictly horizontal. Vertical variations of wind and corresponding horizontal variations of temperature are of great importance. Strictly horizontal flows with no temperature variations on isobars are termed *barotropic*, while more general flows with vertical wind variations, non-zero vertical velocity, and horizontal temperature gradients are termed *baroclinic*, as we met earlier.

For baroclinic flow, the concept of vorticity remains useful but must be generalized to include vertical variations of wind and temperature. An analogous quantity, *potential vorticity* is conserved for a fluid element in the absence of forcing, i.e., mixing, friction, or heat transfer. Potential vorticity allows for the generation of absolute vorticity through vertical stretching or shrinking of fluid columns. Mass conservation means that vertical stretching of a column corresponds to horizontal narrowing.

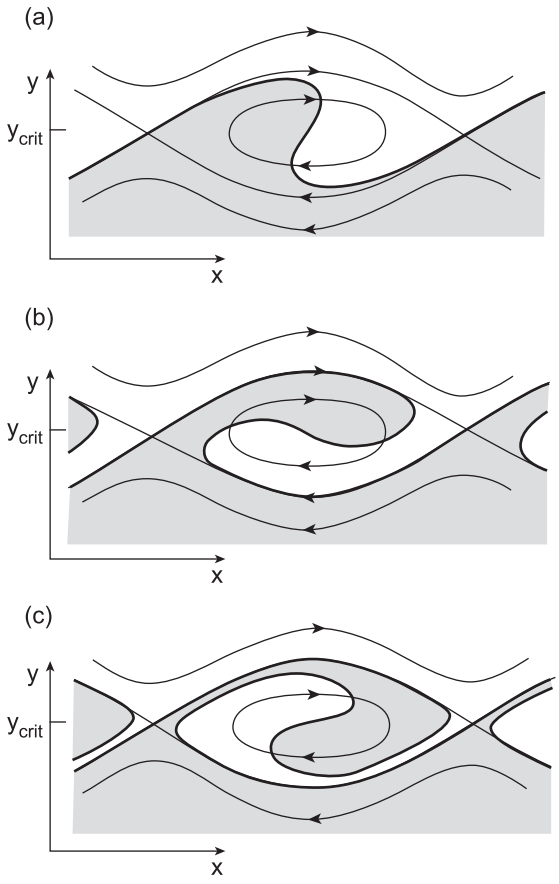


**Figure 4.18** Depiction of three phases (a)–(c) in the evolution of a breaking planetary wave in zonal ($x$) and meridional ($y$) space. The critical latitude is $y_{crit}$ and the $y$ scale is highly exaggerated. Thin lines indicate streamlines and the center, where streamlines are closed, is known as a "Kelvin's cats eye." The thick line is a contour of absolute vorticity, where the shaded region has less absolute vorticity than this contour value. As the wave breaks, vorticity contours curl up tighter and tighter. (Redrawn from Andrews *et al.* (1987), p. 256.)

Horizontal shrinking of columns of spinning fluid increases the spin rate, just as the spin rate of an ice skater increases as she draws her arms in toward her body (Fig. 4.19). Spin is virtually always present and cyclonic because of the dominant cyclonic planetary vorticity.

In a constant density fluid, the potential vorticity $P_V$ [$m^{-1}$ $s^{-1}$] is

$$P_V = \frac{\eta}{h} = \frac{(f+\zeta)}{h} \tag{4.55}$$

where $h$ is the incompressible (volume-conserving) height of a fluid column (e.g., Wallace and Hobbs, 2006, p. 289). When density $\rho$ varies with height, an illuminating quantity

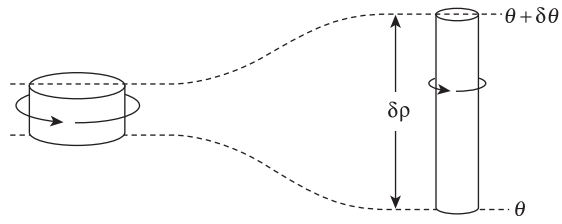


**Figure 4.19** Illustration of Ertel's potential vorticity. A fluid column moves isentropically, i.e., within contours of potential temperature as shown. As it stretches vertically, it shrinks horizontally, increasing its spin rate.

that links the concept of vorticity to thermodynamic constraints is called *Ertel's potential vorticity*, $Q_P$,

$$Q_P = \frac{\eta}{\rho}\frac{\partial\theta}{\partial z} \tag{4.56}$$

where $\theta$ is potential temperature and $\partial\theta/\partial z = -(g\rho)(\partial\theta/\partial p)$ measures static stability, as discussed in Sec. 1.1.3.2. Here, $\eta$ is evaluated on surfaces of constant $\theta$. Quantity $Q_P$ is often expressed in potential vorticity units, PVUs, of $10^{-6}$ K $kg^{-1}$ $m^2$ $s^{-1}$. In adiabatic flow, an increase in static stability $\partial\theta/\partial z$ corresponds to vertical shrinking and horizontal expansion of fluid columns so that, if $Q_P$ is conserved, the absolute vorticity $\eta$ must decrease according to eq. (4.56). Correspondingly, decreasing static stability in adiabatic flow corresponds to vertical stretching, horizontal shrinking, and increasing $\eta$. Equation (4.56) shows that potential vorticity involves potential temperature variations and so $Q_P$ can be generated and dissipated by diabatic heating as well as by stirring and friction.

A dramatic example of generation of vorticity by heating is a hurricane. Such a cyclonic storm with very low central pressure draws air near the surface inward toward a wall cloud surrounding the core, or "eye," of the storm. In the wall cloud, air rapidly ascends and because tropical storms are very moist at low levels, condensation, precipitation, and rapid release of latent heat energy take place. As a result, atmospheric columns in the eye wall stretch rapidly in the vertical, increasing or maintaining both the high rate of spin (vorticity) and the low level inflow to the eye wall cloud.

Ertel's potential vorticity is not easy to work with analytically. So an alternative is *quasi-geostrophic (QG) potential vorticity* $q_g$, an approximate form valid when the Rossby number ($Ro$) is small and flows are approximately geostrophic. QG equations are widely used in dynamics because they facilitate study of large-scale, relatively low-frequency motions characteristic of atmospheric circulations. Derivation of an equation for QG potential vorticity

requires detailed work. The form given here is derived in Satoh (2004), pp. 59–63 and pp. 113–114. See also Andrews *et al.* (1987) pp. 118–122. We skip straight to the result:

$$q_g + q_g{}' = \eta + \left(\frac{f_0}{\rho_0}\right)\frac{\partial}{\partial z}\left(\frac{\rho_0\theta'}{(\partial\theta_0/\partial z)}\right) = (f_0 + \beta y) + \zeta' + \left(\frac{f_0}{\rho_0}\right)\frac{\partial}{\partial z}\left(\frac{\rho_0\theta'}{(\partial\theta_0/\partial z)}\right) \tag{4.57}$$

$$\Rightarrow q_g + q_g{}' = \underbrace{(f_0 + \beta y)}_{\text{basic state}} + \underbrace{\nabla^2\psi' + \left(\frac{1}{\rho_0}\right)\frac{\partial}{\partial z}\left(\rho_0\frac{f_0^2}{N^2}\frac{\partial\psi'}{\partial z}\right)}_{\text{perturbation}} \tag{4.58}$$

Here, $f_0$ represents the value of the Coriolis parameter $f$ at a reference latitude ($f = f_0 + \beta y$), $N$ is the Brunt–Väisälä frequency defined in Sec. 1.1.3.3, $\rho_0$ and $\theta_0$ represent height-dependent zonal and time-mean values of density and potential temperature ($\rho_0 = \rho_s\exp(-z/H)$, where $H$ is density scale height and $\rho_s$ a reference density), and $\theta'$ represents horizontal and time-dependent departures from $\theta_o$. In eq. (4.58), the QG potential vorticity is written in terms of a QG perturbation stream function to obtain an equation in a single variable. Like the stream function for horizontal flow, the QG stream function satisfies eqs. (4.45) and (4.46) for geostrophic zonal and meridional winds, i.e., $u_g = -\partial\psi'/\partial y = (-1/f_0\rho_0)(\partial p'/\partial y)$ and $v_g = \partial\psi'/\partial x$. The vertical variation of $\psi'$ ($=p'/(f_0\rho_0)$) is found by differentiating it w.r.t. $z$:

$$\frac{\partial\psi'}{\partial z} = \frac{1}{f_0}\frac{\partial}{\partial z}\left(\frac{p'}{\rho_0}\right) = \frac{g}{f_0}\left(\frac{\rho'}{\rho_0}\right) \Rightarrow \frac{\partial\psi'}{\partial z} = \left(\frac{N^2}{f_0}\right)\left(\frac{\theta'}{(\partial\theta_0/\partial z)}\right) \tag{4.59}$$

Here, we used $N^2 = (g/\theta_0)(\partial\theta_0/\partial z)$(eq. 1.40) and a perturbed hydrostatic equation $\partial p'/\partial z = -\rho' g$. Equation (4.59) explains the last term in brackets in eq. (4.57) vs. eq. (4.58).

It turns out that that there's a "free lunch": absolute vorticity $\eta$ can be formally replaced by QG potential vorticity $q_g$. So, after linearization about the zonal mean flow $\overline{u}(y,z)$, the vorticity equation (4.41) can be replaced by its exact QG analog:

$$\left(\frac{\partial}{\partial t} + \overline{u}\frac{\partial}{\partial x}\right)q_g{}' + v'\frac{\partial\overline{q_g}}{\partial y} = S_q{}' \tag{4.60}$$

Then, after multiplying by the basic state density $\rho_0$, eq. (4.42) is similarly replaced by

$$\underbrace{\rho_0\overline{v'q_g{}'}}_{\substack{\text{poleward potential}\\ \text{vorticity transport}\\ \text{by eddies}}} = \underbrace{-\frac{\partial\rho_0\overline{(q_g{}')^2}/\partial t}{2\partial\overline{q_g}/\partial y}}_{\substack{\text{potential vorticity}\\ \text{variance term}}} + \underbrace{\frac{\overline{\rho_0 S_q{}' q_g{}'}}{\partial\overline{q_g}/\partial y}}_{\text{eddy forcing term}} \tag{4.61}$$

Here, the zonal mean QG potential vorticity gradient is

$$\frac{\partial q_g}{\partial y} = \beta - \frac{\partial^2\overline{u}}{\partial y^2} + \left(\frac{1}{\rho_0}\right)\frac{\partial}{\partial z}\left[\left(\rho_0\frac{f_0^2}{N^2}\right)\frac{\partial\overline{u}}{\partial z}\right] \tag{4.62}$$

One key physical change is that the eddy vorticity forcing term $S_q{}'$ in eq. (4.61) now includes contributions from eddy potential vorticity generation by heating.

In addition, the relationship between zonal momentum flux and absolute vorticity fluxes (eq. (4.47)) is replaced by its analog for QG potential vorticity,

$$\overline{v'q_g{}'} = -\frac{\partial\left(\overline{u'v'}\right)}{\partial y} + \left(\frac{f_0}{\rho_0}\right)\frac{\partial}{\partial z}\left(\frac{\rho_0\overline{v'\theta'}}{(\partial\theta_0/\partial z)}\right) \tag{4.63}$$

We see that the meridional potential vorticity flux has a contribution from the meridional flux of zonal mean momentum $\overline{u'v'}$, as with absolute vorticity, but there is now also a contribution from the zonal mean meridional heat flux represented by $\overline{v'\theta'}$.

Analogous to the way we looked for wave solutions of (4.49), it is possible to look for wave solutions of eq. (4.60), setting $S_q{}' = 0$, as follows,

$$\psi' = e^{(z/2H)}\Psi(y,z)e^{i(\omega t - kx)} \tag{4.64}$$

where $H$ is the density scale height, $\omega$ an angular frequency, and $k$ is the zonal wavenumber. Mak (2011), pp. 166–172, provides a detailed discussion of such wave solutions to eq. (4.60). We note that the wave propagates in the $x$-direction with amplitude that depends on height. The factor $\exp(z/2H)$ anticipates that the amplitude of the wave perturbation should grow as altitude increases with the inverse square root of the background density $\rho_0$. In the absence of dissipation, the wave kinetic energy density $E \sim \rho_0\psi'^2$ is independent of height (cf. ½(mass) × (velocity)$^2$). So, if this energy $E$ remains constant with altitude, the amplitude of the perturbation grows as $\psi' \sim \rho_0^{-0.5}$. Since density $\rho_0$ varies with altitude in the barometric law as $\sim\exp(-z/H)$, the amplitude variation goes as $(\exp(-z/H))^{-0.5}$, which is $\exp(z/2H)$. Such a relationship has consequences for atmospheric chemistry because eddy diffusion (at least to certain altitudes) is often parameterized in photochemical models of planetary atmospheres proportional to $\rho_0^{-0.5}$. The same $\rho_0^{-0.5}$ relationship

also applies to the vertical amplitude growth of buoyancy (gravity) waves (Sec. 4.4.2).

The 1-D wave equation for the stream function complex amplitude in barotropic flow (eq. (4.53)) with a 1-D refractive index can also be replaced by a 2-D analog for the amplitude of the quasi-geostrophic stream function $\Psi(y, z)$ that incorporates a 2-D squared refractive index. The result is analogous to the results with horizontal flow. But instead of turning latitudes and critical latitudes, there are *turning surfaces* where refraction occurs for specified $\omega$, $k$ where $(\overline{u} - c)$ is large, and *critical surfaces* where $(\overline{u} - c)$ approaches zero, the wave oscillation rate is large, and waves are absorbed (Fig. 4.20). Andrews *et al.* (1987), pp. 183–186 provides more discussion on this topic.

Unfortunately, the analogy between absolute vorticity and potential vorticity expressed in eqs. (4.42) and (4.61) is imperfect (there is no totally free lunch) because absolute vorticity and potential vorticity are not the same quantities and their fluxes correspond to different responses of the zonal mean flow. In the QG-limit, acceleration of the zonal-mean zonal wind depends on the poleward potential vorticity flux (see Ch. 7 of Vallis (2006) for discussion). But the 3-D case is more complicated than the 2-D case because potential vorticity is proportional both to absolute vorticity and static stability (eq. (4.56)), so its poleward flux corresponds to some combination of increase of the mean absolute vorticity and the mean static stability of the background flow in the region poleward of the latitude of the flux. Nevertheless, the general tendency is for prograde jets to be forced in regions in which eddies are generated and retrograde jets to be forced in regions in which eddies are dissipated (Held, 1975; Thompson, 1971).

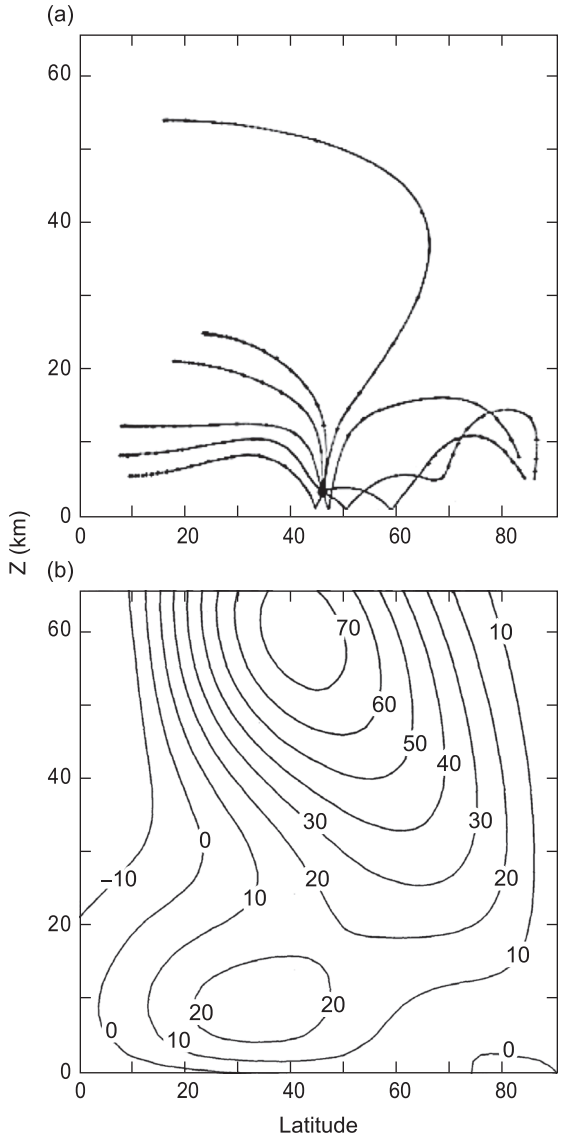


**Figure 4.20** Calculated meridional cross-section of rays (wave packet trajectories) for stationary Rossby waves, i.e, where phase speed $c$, relative to the surface is $c = 0$. The diagram depicts Earth's wintertime middle atmosphere. Crosses mark daily time intervals. (a) Rays refract away from the zonal mean ($\overline{u}$) wind maxima shown in (b) and toward zonal mean wind minima (the $\overline{u} = 0$ contours) where $\overline{u} - c$ approaches zero. (b) Zonal mean wind distribution. Because zonal wind is the major factor in refractive index, most rays are refracted toward weak zonal mean winds and away from strong zonal mean winds. (Redrawn from Andrews *et al.* (1987), p. 186.)

### 4.3.5 Planetary Wave Instability

When the restoring effect of the potential vorticity gradient vanishes, gas parcels do not undergo stable wave-like motions in the meridional plane, but can drift away from their initial latitude and altitude. Such motions are said to be unstable. *Instability* of planetary waves can occur where $\partial\overline{q}_g/\partial y$ as expressed in eq. (4.61) changes sign. Sign changes of $\partial\overline{q}_g/\partial y$ (given by eq. (4.62)) occur with some combination of large positive horizontal curvature of the zonal mean flow $\partial^2\overline{u}/\partial y^2$ or large negative curvature or large positive vertical shear of the mean zonal wind, $(1/\rho_0)\partial/\partial z(\rho_0 B\partial\overline{u}/\partial z)$, where $B = f_0^2/N^2$. Through the thermal wind (eq. (4.18)), $\partial\overline{u}/\partial z$ is linked to the horizontal gradient of zonal mean temperature. When $\partial^2\overline{u}/\partial y^2$ is the dominant factor in eq. (4.62), the growing unstable eddies derive their energy from the kinetic energy of the zonal mean flow and the instability is referred to as *barotropic instability* or *Rayleigh-Kuo instability*. When $(1/\rho_0)\partial/\partial z(\rho_0 B\partial\overline{u}/\partial z)$ is the dominant factor, unstable eddies draw their energy from the mean

meridional gradient of temperature and the instability is referred to as *baroclinic instability*, as mentioned earlier.

The effect of planetary wave instabilities on the mean zonal flow depends on the statistical properties of the life cycles of unstable eddies as they grow, propagate, and dissipate. Eddy growth corresponds to vorticity that generates stirring and prograde acceleration of zonal mean flow. Propagation carries eddy wave packets to altitudes and latitudes separated from the altitude and latitude of origin, while eddy dissipation corresponds to vorticity dissipation and retrograde zonal mean flow acceleration.

Barotropic instability accelerates prograde flow in the latitude–altitude region in which the instability is centered. Large positive values of $\partial^2\overline{u}/\partial y^2$often occur in the negative shear zones (i.e., where the zonal wind decreases to the right of the flow) on the flanks of prograde jets where the vorticity due to the shear is anticyclonic. Barotropic instability tends to reduce the positive curvature in shear zones, noting that if a jet stream follows the trough of the wave, there is positive (cyclonic) vorticity due to curvature on both the north and south side of the jet. As unstable eddies develop, they propagate to latitudes where they decay and accelerate retrograde zonal mean flow. The scale of the most unstable eddies, which will be close to the scale of the dominant planetary waves produced by the instability, depends on the strength of the zonal mean wind and the $\beta$ effect, corresponding to the condition $\partial^2\overline{u}/\partial y^2 > \beta$ . There is a meridional length scale associated with this instability, called the *Rhines radius*, $r_{\mathrm{Rh}} \sim (2U/\beta)^{1/2}$, where $U$ is the typical speed of the jet (Rhines, 1975). In fact, the number of bands on the face of a gas giant is roughly given by a semi-circle circumference divided by the Rhines radius, $\sim(\pi a)/r_{\mathrm{Rh}}$ (Cho and Polvani, 1996; Menou *et al.*, 2003). This scaling for banding applies if the flow is highly turbulent and forced at small scales by baroclinic instabilities or convection but can be violated on bodies such as hot Jupiters where flow is forced at more global scales.

For baroclinic flows in the case where vertical curvature of the mean zonal wind (i.e., $\partial^2\overline{u}/\partial z^2$) and vertical variations of the factor $B = f_0^2/N^2$ are small, the baroclinic term in eq. (4.62) reduces to:

$$\left(\frac{1}{\rho_0}\right)\frac{\partial}{\partial z}\left[(\rho_0 B)\frac{\partial \overline{u}}{\partial z}\right] \approx \left(\frac{B}{\rho_0}\right)\left(-\left(\frac{\rho_0}{H}\right)\frac{\partial \overline{u}}{\partial z} + \rho_0 \cancel{\frac{\partial^2 \overline{u}}{\partial z^2}}\right) \propto -\left(\frac{1}{H}\right)\frac{\partial \overline{u}}{\partial z} \tag{4.65}$$

Here, we have used the barometric law $\rho_0 = \rho_s \exp(-z/H)$ and differentiated w.r.t. $z$ using the product rule. Thus, instability occurs with sufficiently large positive vertical shear of the mean wind, $\partial\overline{u}/\partial z$, e.g., when $\partial\overline{u}/\partial z$ exceeds ~1 m s$^{-1}$ km$^{-1}$ in terrestrial midlatitudes. The thermal wind eq. (4.18) indicates that this vertical shear corresponds to a horizontal gradient of ~5 °C over 20° latitude, which is much less than the temperature gradient expected from solar heating. Consequently, the production of turbulent eddies from baroclinic instability is inevitable in the midlatitudes of Earth-like planets.

Baroclinic instability (e.g., Pierrehumbert and Swanson, 1995) is fostered by the constraint of the lower boundary where the vertical velocity vanishes, and it is most commonly found near a lower solid boundary of an atmosphere in regions of strong vertical shear of the mean zonal wind. The horizontal scale of the most unstable eddies in this instability is proportional to the *Rossby radius of deformation*,

$$r_{\mathrm{Ro}} = \frac{NH}{f_0} \tag{4.66}$$

where $H$ is the scale height, $N$ is the Brunt–Väisälä frequency, and $f_0$ is a reference Coriolis parameter. Equation (4.66) indicates that eddies decrease in size with increasing planetary rotation rate, which should be relevant for interpreting exoplanet atmospheres.

We can estimate Rossby radii. In Earth's midlatitude troposphere, $r_{\mathrm{Ro}}$ ~ 700 km, using $f_0 \sim 10^{-4}$ s$^{-1}$, $H$ ~ 7 km, and $N \sim 10^{-2}$ s$^{-1}$ (see Sec. 1.1.3.3). With a typical mean zonal wind of $\overline{u}$ ~10 m s$^{-1}$, the time for a disturbance to grow is ~700 km/10 m s$^{-1}$ ~ 1 day, which agrees with observations of weather systems. Since $r_{\mathrm{Ro}} \sim 10^3$ km, only one eddy-driven jet can fit within Earth's baroclinic midlatitudes. On Jupiter, $r_{\mathrm{Ro}} \sim \left[(0.003 \text{ to } 0.02) \times 27)\right] / \left[2 \times (2\pi \,/\, 35730) \times \sin(45^\circ)\right] \approx$ 325–2200 km, which is far smaller than the planetary size and allows for multiple jets. Here, we have used Jupiter's rotation period of 35 730 s, a scale height of $H$ ~27 km at the 1 bar level, and a range of $N$ from ~0.003 s$^{-1}$ measured by the *Galileo* probe in an unusual cloudless spot (Magalhaes *et al.*, 2002) to ~0.02 s$^{-1}$, which might be more typical (Shetty and Marcus, 2010).

The Rossby radius of deformation has the following interpretation. Suppose that an eddy develops and generates vorticity by vertical stretching and corresponding horizontal divergence that spreads the eddy laterally. Initially, when the eddy is small, it is constrained primarily by the static stability factor $N$, but as it continues to grow, it "feels" the constraining effect of the planetary vorticity $f$, which limits further lateral extent as the eddy begins to spin. The distance from the origin of the eddy at which planetary vorticity limits the spread is ~$r_{\mathrm{Ro}}$.

### 4.3.6 Eddy-Driven Jets on the Outer Planets: Shallow Layer Atmospheres

The jet structure on Jupiter and Saturn with strong eastward equatorial jets and alternating eastward and westward jets at higher latitudes (mapped from cloud motions, Fig. 4.7) is a puzzle that historically has provoked two classes of explanations. The first is based on winds in shallow layers overlying horizontally uniform, convective interiors; the second concerns winds that are surface manifestations of atmospheric dynamics that extend deeply (Del Genio *et al.*, 2009; Dowling, 1995; Ingersoll *et al.*, 2004; Vasavada and Showman, 2005).

The giant planet atmospheres are difficult to model because of their large horizontal extent, great depth, uncertainty about properties and processes in the deep atmospheres, and relatively small Rossby radius. Explicit models must use horizontal scales well below the Rossby radius, which requires huge computing power. Consequently, simpler models are often used. One of these is a barotropic *shallow layer atmosphere* in which the layer depth $D_L$, satisfies $D_L \ll r_{\mathrm{Ro}}$ and $D_L \ll r_{\mathrm{Rh}}$. According to one view, the winds are shallow and they are weak below a "weather layer" extending to a depth where the pressure is ~10 bar (Ingersoll and Cuzzi, 1969).

A shallow barotropic atmospheric layer can be stirred by forcing from below. We have discussed the role of stirring by baroclinically unstable eddies in accelerating prograde and retrograde jets but another stirring process may be applicable to the outer planets. Forcing can be imposed by convective elements driven by convective instability in the deep atmosphere impinging on the statically stable upper layer and spreading laterally. The spread will continue until its predominantly divergent motion is converted to rotational motion through the influence of planetary rotation (the term $\eta\Delta$ in eq. (4.38)). This will occur at a radial distance from a convective core of ~$r_{\mathrm{Ro}}$.

There is direct evidence that convection impinges from below on Jupiter's statically stable layer where we observe the winds. Patches of rapidly growing and evolving cloud are observed. Some patches correspond to lightning flashes, indicative of convective energy release (Little *et al.*, 1999), which is consistent with deep, moist (water) convection. Terrestrial lightning requires both liquid water droplets and frozen particles to undergo collisions that generate charge, followed by the gravitational separation of unlike charges on small and large particles, which creates an electric field. By analogy, Jupiter's lightning suggests that convection extends below the liquid water condensation level at ~5 bars. This is not to say that water vapor is the only condensable gas that can release latent heat energy on Jupiter. Ammonia and sulfur-containing gases condense too. Molecular hydrogen also comes in *ortho* and *para* states, corresponding to parallel and antiparallel spins of the hydrogen nuclei, respectively, and latent heat release can arise from the conversion between these two states. But water vapor has much larger possible latent heat release and so potential to generate eddies and jets (Lian and Showman, 2010). It follows that the most intense Jovian convective storms are likely to be ~90 km deep, in contrast to Earth where the depth of convection does not exceed ~10 km. There is also evidence for deep convection in the form of rapidly evolving small-scale cloud systems and lightning on Saturn (Dyudina *et al.*, 2010).

If this type of convection is responsible for driving the large-scale jets on Jupiter and Saturn, it must migrate around the planet to cause features spread over longitude. In a possible scenario, slow convection throughout the deep interior of the planet reaches the layer in which water condensation can take place. Convection imposes strong static stability upon its surroundings because of stabilizing downward motion outside of the convective clouds. Thus, most of the atmosphere will present a stable barrier near the base of the condensation layer. Over time, the build up of energy from below will break the barrier allowing localized deep convection to occur. Gradually changing conditions near the barrier or in the atmosphere above might allow regions of convection to migrate.

### 4.3.7 Eddy-Driven Jets on the Outer Planets: Deep Atmospheres

In contrast to shallow layer models, another category of simulations for giant planets are *deep models*. The huge amount of energy from planetary accretion causes heat to be lost from within giant planets and the high interior opacities lead to convection and thus temperature and density profiles that should be very nearly adiabatic (Guillot *et al.*, 2004). Atmospheres are not shallow and circulation systems must extend deep into the quasi-adiabatic interiors. Since an adiabatic atmosphere cannot support significant horizontal density variations, deep atmospheric regions must also be barotropic so jet stream structures in these atmospheres can extend to great depth. Direct evidence for strong, deep winds of 180 m $s^{-1}$ at 20 bar and 420 K comes from the *Galileo* probe that descended into a Jupiter at an entry point of 6.5° N (Atkinson *et al.*, 1997).

In a deep atmosphere, convection currents combined with the effects of planetary rotation organizes the internal winds into geostrophic flow on cylindrical

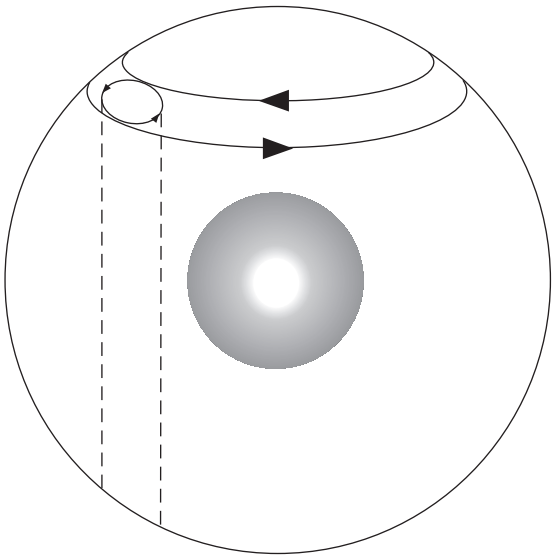

**Figure 4.21** Schematic diagram of Bussé's model of winds on Jupiter. Models and lab experiments show that the combination of convection and rapid rotation could organize fluids into differentially rotating cylinders that are concentric with the planet's rotation axis. The fluid would move in columns (dashed). The surface manifestation of the rotating columns (small arrows) would be a series of zonal winds that reverse in direction (large arrows).

surfaces parallel to the planetary rotation axis, extending throughout the whole molecular hydrogen layer (Busse, 1976, 1983). The jet stream structure in the upper troposphere will be the upper manifestation of these cylindrical structures (Fig. 4.21). Prograde and retrograde upper tropospheric jets will occur where the cylindrical flow that intercepts the upper troposphere is prograde and retrograde respectively. Cylindrical structures can penetrate through the entire planet at low latitudes where they do not intercept a solid or liquid deep interior. At higher latitudes, they can penetrate only to the solid or liquid interior. The flow in these models is driven by the convective heat flux from the deep interior.

Some models of this interior circulation produce realistic looking results for Jupiter's upper tropospheric jet stream structure, e.g., Heimpel *et al.* (2005), Heimpel and Aurnou (2007). But one fundamental difficulty with these models is that they require larger energy input rates than are available from the Jupiter's combined internal and solar heat fluxes. So they cannot be considered a realistic solution to the problem of explaining the jet stream structures of Jupiter and Saturn. Moreover, the Jupiter-like jet patterns depend on the existence of an impermeable lower boundary condition in these models. So a second basic problem is that giant planets lack the internal boundary that is crucial in these models for getting a Jupiter-like flow.

### 4.3.8 A Shallow Atmosphere Model Coupled to the Deep Interior of Outer Planets

A third class of models includes shallow atmospheres driven by baroclinic instability, which produce realistic looking simulations of the upper tropospheric jet stream structure (Williams, 1979, 2003); however, the relationships of the upper tropospheric circulation to the circulation in the deep troposphere and the global energy budget of the Jovian atmosphere are not addressed.

Detailed modeling of the complete system including the upper tropospheric circulation and deep atmosphere circulation is still precluded, but Schneider and Liu (2009) have used a hybrid model that may incorporate important effects of both the upper and lower troposphere on the jet stream structure. Their model couples a shallow upper troposphere to the deep atmosphere via large scale overturning circulations generated by eddy forcing in the upper troposphere. They hypothesize that deep meridional circulations transfer momentum downward from the upper troposphere to the partially ionized deep atmosphere at ~$10^5$ bar where circulation is damped by *ohmic dissipation*, i.e., when electrical energy turns into heat as electric currents flow through a resistance. Such magnetohydrodynamic (MHD) drag affects the zonal flow only off the equator. The shallow atmosphere eddy-driven jets modeled in the upper troposphere are presumed to extend downward to the dissipation region but the model goes down to only ~3 bar, so an artificial drag is imposed to represent the effect of the MHD drag in the outer atmosphere.

Results from an extended run of the Schneider and Liu model that uses the appropriate solar and internal energy input fluxes show stable jet structure resembling Jupiter's at both high and low latitudes (Fig. 4.22). In this model, middle and high latitude jets are forced by baroclinically unstable eddies whose instability arises from the meridional gradient of incoming solar radiation and temperature. Near the equator, strong prograde jet structure is produced by convection associated with the planetary internal heat flux. Convection arising from a uniformly distributed internal heat flux is not strong enough to drive jets at high latitudes, and low-latitude temperature gradients and baroclinic instability are not strong enough to drive the equatorial jet. Both solar heating and internal heat flux are required to produce the low and high latitude jet structure. This hybrid model shows promise for Saturn as well as Jupiter; however, its depth to only 3 bar and dry convective adjustment does not deal with latent heating, which is likely critical for generating horizontal temperature contrasts. Neglect of vertical momentum transport also means that realistic convective plumes are not captured.

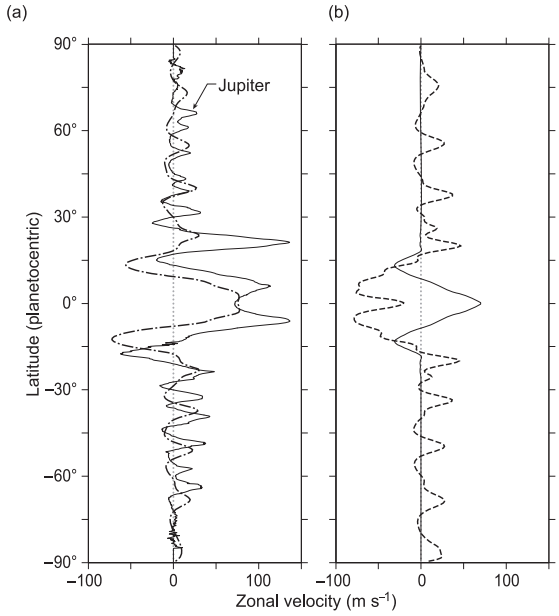


**Figure 4.22** (a) Observed Jupiter zonal winds (dash-dot line) at 0.65 bar compared with zonal winds from the model of Schneider and Liu (2009) (solid line) including both convective forcing and forcing by baroclinically unstable waves. (b) Calculation of Schneider and Liu without baroclinic instability (dashed line) and without internal convection (solid line). (From Schneider and Liu (2009) Reproduced with permission. Copyright 2009, American Meteorological Society.)

### 4.3.9 Ice Giants: Uranus and Neptune

Given the multiple jet structures and strong low latitude prograde winds found on Jupiter and Saturn, the upper tropospheric winds measured from cloud drifts on the ice giants, Uranus and Neptune, are surprising (Fig. 4.7). On both planets, there is a broad band of strong retrograde winds at low latitudes and a high latitude prograde jet. In fact, the retrograde jet on Neptune reaches ~600 m $s^{-1}$, the fastest in Solar System atmospheres.

The reasons for the marked differences in circulation between the ice giants and gas giants are unclear. Why is there only one prograde jet at high latitudes on the two outer planets? Why are low latitudes filled with a broad smooth band of retrograde zonal winds? One observation is that heat flux from the interior is much weaker on the ice giants than gas giants (Sec. 2.2.6). There are also physical differences at depth. Water changes into ions ($OH^-$ and $H_3O^+$) and ammonia changes into $NH_4^+$ at much shallower depths (>0.1 Mbar) on the ice giants than the >3 Mbar pressure required for the sea of hydrogen ions and electrons inside the gas giants. Thus, the neutral molecular atmospheres of Jupiter, Saturn, Uranus, and Neptune extend to different depths: 0.8, 0.5, 0.8, and 0.85 planetary radii or depths of 15 000 km, 30 000 km, 5500 km, and 3500 km, respectively.

One possibility for the dynamical disparities is that the upward heat fluxes in the upper tropospheres of the two ice giants are too weak to drive convection or generate baroclinic instabilities almost everywhere. Convective forcing may only occur where the static stability in the upper layer is sufficiently weak. On Neptune that could happen at high latitudes where the annual average incoming solar radiation flux is weak, but this idea leaves unanswered the question of why Uranus, whose rotation axis lies close to the ecliptic (98° obliquity), would exhibit zonal winds so closely resembling Neptune's (30° obliquity). Nevertheless, if vertical heat fluxes were confined to high latitudes for whatever reason, prograde jets forced by eddies would be confined to high latitudes as well. Across the tropics and subtropics, retrograde winds could be maintained by persistent vorticity mixing. This picture of the mechanism of the Uranus and Neptune circulations is consistent with the general conclusions of Schneider and Liu (2009) for Jupiter.

## 4.4 Buoyancy Waves and Thermal Tides

There is another class of waves besides planetary waves that influences the structure of planetary atmospheres. Such waves are central for understanding motions and temperatures in the terrestrial mesosphere of the Earth, for example. In their simplest form, these waves are confined to the vertical and one horizontal coordinate. Buoyancy acts as a restoring force that causes a vertically displaced gas parcel to oscillate about its equilibrium position in a statically stable atmosphere. Such waves are often called *gravity waves*, but because buoyancy is the restoring force, we refer to them as *buoyancy waves*. If the wave is vertically *propagating*, it is said to be *internal*, and if it decays with height and is "trapped" and *evanescent*, it is called *external*. Nappo (2012) proposes using the descriptive terms "propagating" and "evanescent" and refraining from the obscurity of "internal" and "external." We follow this suggestion.

Like planetary waves, buoyancy waves can transport momentum from one region of the atmosphere to another and accelerate or decelerate the atmospheric mean flow far from the point of wave origin. Even though the mechanisms and geometries are different, some key concepts developed for planetary waves apply to the mechanisms by which buoyancy waves affect the mean zonal flow.

### 4.4.1 Mechanism and Properties of Buoyancy Waves

In Sec. 1.1.3.3, we saw that a gas parcel oscillating in the vertical and subject to the restoring force of buoyancy in a

statically stable atmosphere will oscillate at angular frequency $\omega = N$ where $N$, the buoyancy frequency, is given by eqs. (1.39) and (1.41) as

$$N^2 = \frac{g}{T}\left(\frac{dT}{dz} + \frac{g}{c_p}\right) = \frac{g}{\theta}\frac{d\theta}{dz} \tag{4.67}$$

Here, $\theta$ is potential temperature. Purely vertical oscillations are idealized and in real atmospheres, the simplest approximation for buoyancy waves is an oscillation at some angle to the vertical in an $x$–$z$ plane. For such waves, Fig. 4.23 shows what is meant by the terminology of a *wave front* of constant phase, which is perpendicular to a *wave vector* for a wave that propagates.

Consider a buoyancy wave oscillation tipped at an angle $\beta$ with respect to the vertical in the $x$–$z$ plane, as shown in Fig. 4.24(a). We imagine a parcel of air of unit mass displaced vertical distance $\delta z$ from A to B up a slope distance of $\delta s = \delta z/\cos\beta$. The parcel will oscillate about point A as part of a propagating transverse wave with a wave vector $\boldsymbol{\kappa}$ as shown in the inset of Fig. 4.24(a). The oscillation's angular frequency, $\omega$, is the projection of $N$ on the slope, $\omega = N\cos\beta$. Earlier, we saw that the downward buoyancy force was $N^2\delta z$ for a purely vertically displaced parcel (Sec 1.1.3.3). This force has a component *up* slope A–B of $-(N^2\delta z)\cos\beta$. The acceleration up the slope can also be written $d^2(\delta s)/dt^2 = d^2(\delta z/\cos\beta)/dt^2$. Hence, Newton's second law is:

$$\frac{d^2}{dt^2}\left(\frac{\delta z}{\cos\beta}\right) + N^2\delta z\cos\beta = 0 \;\Rightarrow \frac{d^2(\delta z)}{dt^2} + \left(N^2\cos^2\beta\right)\delta z = 0 \tag{4.68}$$

In eq. (4.68), we recognize simple harmonic motion of the standard form "$\ddot{X}+\omega^2 X = 0$". Consequently, the parcel will oscillate at an angular frequency,

$$\omega = N\cos\beta = \frac{Nk}{\left(k^2+n^2\right)^{1/2}} \tag{4.69}$$

This equation relates angular frequency to the wave structure, i.e., it is a dispersion relation. In eq. (4.69), we used the wave vector geometry of the Fig. 4.24(a) inset where $\cos\beta = k/|\kappa|$ and $|\kappa| = \left(k^2+n^2\right)^{1/2}$. According to eq. (4.69), as the oscillation tips into the vertical ($\beta = 0^\circ$, $\cos\beta = 1$) the frequency approaches $N$, fluid particles oscillate vertically, and waves propagate horizontally. If tipped towards the horizontal ($\beta = 90^\circ$, $\cos\beta = 0$), the angular frequency becomes very low and approaches

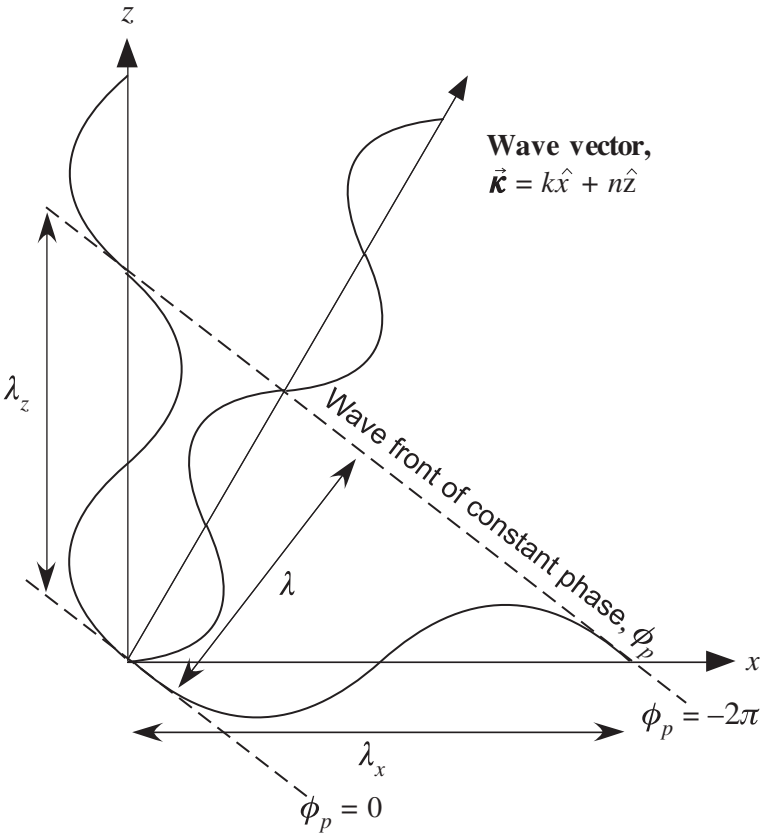


**Figure 4.23** Wave vector $\boldsymbol{\kappa}$ and associated wave fronts and wavenumbers $k$ and $n$ for a 2-D wave of wavelength $\lambda$ in an $x$–$z$ plane. Negative values of phase angle $\phi_p$ indicate where the wave front passed a stationary observer at (0,0) earlier than the subsequent wave fronts. (Adapted from Nappo (2013), p.16.)

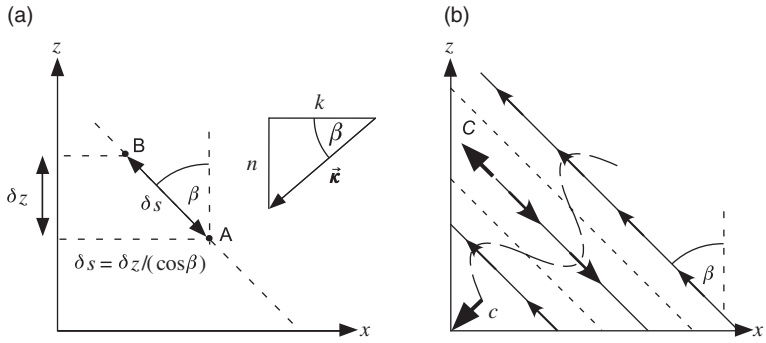


**Figure 4.24** (a) A fluid parcel is displaced from point A to B along a slope inclined at angle $\beta$ from the local vertical. The vertical displacement is $\delta z$, while the slope distance is $\delta s$. The resulting oscillation has a wave vector $\vec{\kappa}$ with horizontal wavenumber $k$ and vertical wavenumber $n$, shown in the inset. (b) An $x$–$z$ plane representation of buoyancy wave phase surfaces. Propagating waves are tipped at the angle $\beta$ to the local vertical. Gas parcel trajectories relative to the background flow go parallel the phase surfaces. The directions of phase velocity $c$ and group velocity $C$ are indicated by the heavy arrows. Curiously, the vertical components of $c$ and $C$ are in opposite directions: i.e., the phase velocity component is downward when the group velocity component is upward.

zero. This is equivalent to a situation of very strong stratification, i.e., small $\omega / N$. Towards this limit, the fluid particles oscillate almost horizontally and waves propagate almost vertically.

We can derive from eq. (4.69) expressions for the vertical components of the phase velocity $c_z$ and group velocity $C_z$ . The latter is important because the flux of wave energy is in the direction of group velocity:

$$c_z = \frac{\omega}{n} = \frac{Nk}{n\left(k^2+n^2\right)^{1/2}}, \quad C_z = \frac{\partial \omega}{\partial n} = -\frac{Nnk}{\left(k^2+n^2\right)^{3/2}} \tag{4.70}$$

Equation (4.70) shows that $C_z$ and vertical propagation of wave activity vanishes when either $n$ or $k$ is zero, i.e., when the oscillation tips into the vertical or horizontal. It also indicates the peculiar property that the vertical component of the group velocity $C_z$ is opposite in sign to the vertical component of phase velocity $c_z$. Buoyancy waves propagating wave energy upward will be propagating phase downward, as shown in Fig. 4.24(b).

It is possible to derive a wave equation for buoyancy waves called the *Taylor–Goldstein* equation, analogous to eq. (4.53) for planetary waves using the linearized equations of motion, continuity, and thermodynamic energy in the $x$-$z$ plane, including a zonal mean wind. The method is to assume small variations from basic state variables of density, vertical velocity, pressure and potential temperature. The interested reader can find the algebra in many textbooks (e.g., Holton, 2004, pp. 196–201); a comprehensive treatment is given in the book by Nappo (2012) devoted to buoyancy waves. Suffice it to say that perturbations in the state variables follow a waveform with an amplitude that varies as $\sim e^{\left(z/2H_\rho\right)} e^{i(kx-\omega t)}$, where the factor $\exp(z/2H_\rho)$ accounts for the vertical variation of atmospheric density, where $H_\rho$ is the density scale height.

An approximate dispersion relation derived from detailed analysis is the same as eq. (4.69) except that the zonal mean wind Doppler shifts the angular frequency:

$$\omega_r = (\omega - k\overline{u}) \approx \frac{Nk}{\left(k^2+n^2\right)^{1/2}} \tag{4.71}$$

$$\Rightarrow n^2(z) \approx \frac{k^2 N^2(z)}{\omega_r^2(z)} - k^2 \tag{4.72}$$

Here, $\omega_r$ is the relative angular frequency in coordinates moving with the background zonal flow, $\overline{u}$.

Equation (4.72), like its analog for planetary waves, tells us about the propagation of buoyancy wave packets. Variation of $n^2(z)$ determines the wave behavior. Heights called *turning point levels* are where $n^2(z)$ approaches zero when $\omega_r{}^2 / k^2 = (c - \overline{u})^2$ becomes large and/or when $N^2$ (representing static stability) becomes small. *Critical levels* are where the local oscillation rate approaches infinity when $\omega_r{}^2 = (c - \overline{u})^2$approaches zero. At a critical level where $c = \overline{u}$, the mean flow absorbs the buoyancy wave and the wave cannot propagate any higher.

### 4.4.2 Wave Generation, Breaking, and Impact on the Zonal Mean Flow

The two main mechanisms for generating buoyancy waves are flow over topography and interaction of large-scale flow with convective cells. In Fig. 4.25, an

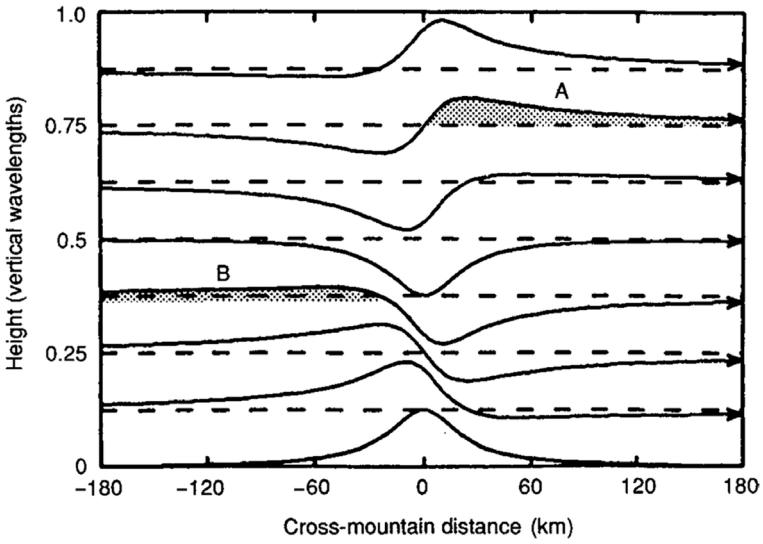


**Figure 4.25** A vertically propagating buoyancy wave produced by flow over an isolated ridge line. Phase tilts westward (upstream or to the left) with height if you consider a line going through troughs. Wave perturbation pressure is a maximum on the west-facing slope and minimum on the east-facing slope. Shaded areas A and B are where streamlines are displaced upward from the dashed equilibrium lines are places where clouds may form. (Source: Holton and Hakim (2013), p. 297.)

eastward wind blows across a north–south oriented ridge projecting into the page, producing a *mountain wave*, which is a buoyancy wave generated when stable air passes over a mountain. On the west-facing slopes, pressure, and upward vertical ($w'$) and westward horizontal velocity ($u'$) perturbations are positive while on the eastward slopes, pressure, upward vertical and westward horizontal velocity perturbations are negative. The wave phase tilts backwards with altitude relative to the mean flow, indicating upward flux of westward momentum through the correlation $\overline{u'w'}$ of the wave. The westward momentum extracted from the solid surface acts as a drag on the surface eastward wind. Pressure pushes eastward on the hill and thereby on the solid planet, which is essentially unaffected, but the hill pushes back on the atmosphere, which is affected. The upward flux of westward wave momentum affects the atmosphere in the altitude range over which the wave is dissipated.

Topographically forced waves have phase speeds at or close to $c = 0$, i.e., they're stationary. Non-zero frequencies and horizontal phase speeds occur only because of transience: the initiation, change, or termination of the flow. Similarly, waves produced by interaction with convection generally have horizontal phase speeds close to zero because convective cells tend to move slowly compared to the background flow at the upper levels of the convective cells where buoyancy waves are generated. We therefore focus on the behavior of solutions in which $c$ is close to zero and $\omega_r^2/k^2 = \overline{u}^2$.

Near turning point levels, buoyancy waves will be refracted toward their level of origin. Thus, turning points can trap buoyancy waves in a waveguide. Such waves can be easily identified because they persist as wave trains far downstream from the source, usually a topographic obstacle to the flow. Such *lee waves* are often rendered visible by a series of parallel clouds trains on Earth and Mars (Fig. 4.26). Trapped buoyancy waves are typically found beneath jet streams because the rapid increase of background flow $\overline{u}$ with height produces the conditions for trapping.

Buoyancy wave packets of relatively small initial amplitude that escape being trapped in the troposphere propagate upward toward the stratosphere and mesosphere, and there they significantly affect the atmospheric circulation. In Earth's lower mesosphere, there are westward and eastward jets around 50–70 km altitude in the summer and winter hemisphere, respectively (Fig. 4.27). Why do winds diminish and reverse in their direction above 70 km? The answer involves buoyancy waves.

In the winter hemisphere, vertically propagating buoyancy waves with eastward phase speeds will be absorbed at critical levels where $c = \overline{u}$. Small amplitude waves whose phase speed is westward or near zero (the speed of the underlying surface) can penetrate through the tropospheric zonal winds and will break in the lower mesosphere (above 85 km altitude) where their amplitudes increase because of density decrease. These effects are illustrated schematically in Fig. 4.28. The wave breaking causes the winter hemisphere eastward zonal wind speed to decrease with height in the mesosphere and this decrease further enhances wave breaking. Conversely, in the summer hemisphere, tropospheric winds are usually eastward (westerly), but relatively weak so

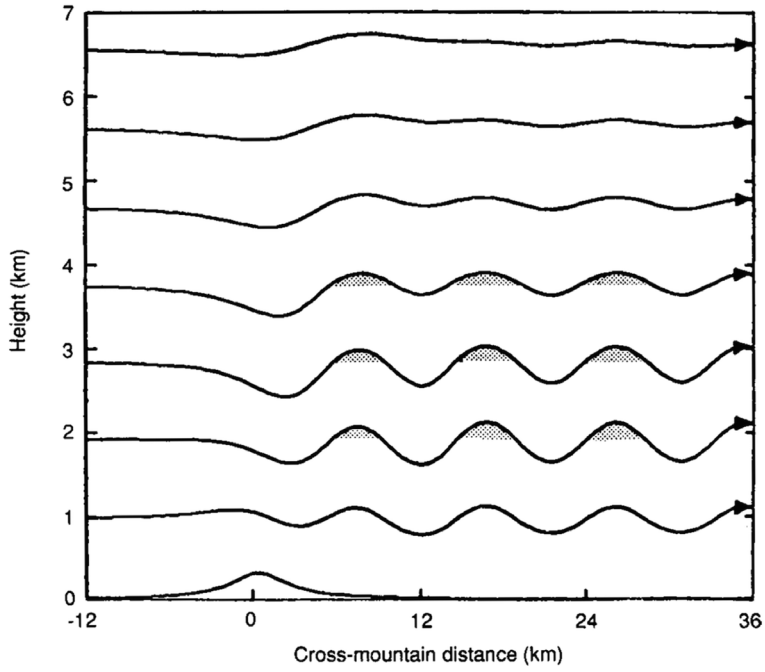


**Figure 4.26** Topographically forced buoyancy wave trapped by upward increase in wind and/or upward decrease in static stability. Shaded regions are where so-called lee wave clouds may form. (Source: Holton and Hakim (2013), p. 299.)

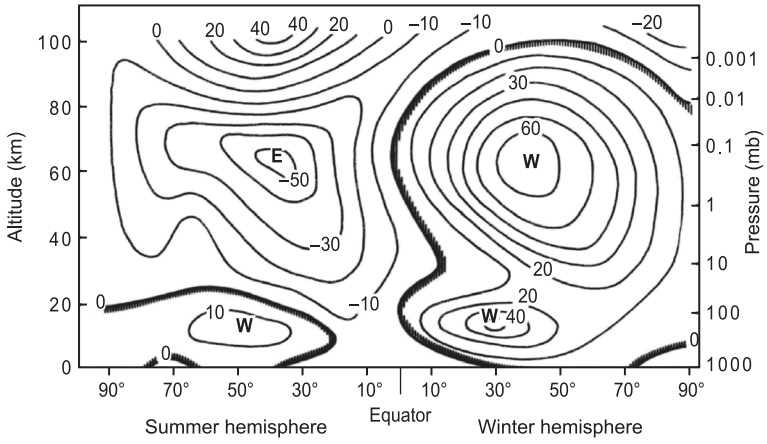


**Figure 4.27** Earth's zonal mean winds for winter and summer. E = easterly (westward) wind. W = westerly (eastward) wind. (Redrawn from Andrews *et al.* (1987), p. 8.)

buoyancy waves generated by flow over topography can propagate through the troposphere. But they encounter a critical layer in the stratosphere and break, modifying the stratospheric temperature and wind structure. Waves whose phase speeds are outside of the range of the background zonal winds penetrate to the mesosphere. In practice, in the summer hemisphere, these waves are those with moderate eastward phase speeds that tend to be produced on the eastward phase speed tail of the convectively generated wave spectrum. Since their initial amplitudes are very low, they break and dump eastward momentum in the upper mesosphere. Consequently, westward winds in Earth's summer mesosphere peak in a jet the lower mesosphere and decrease with height in the upper mesosphere.

The net effect of upward propagating buoyancy waves on the stratosphere and mesosphere is described as *closing off* all jets: the tropospheric jet, and the eastward and westward jets of the winter and summer mesosphere. The buoyancy waves act as a powerful drag on the background zonal flow and make the upper atmosphere "feel" the rotation speed of the underlying planet.

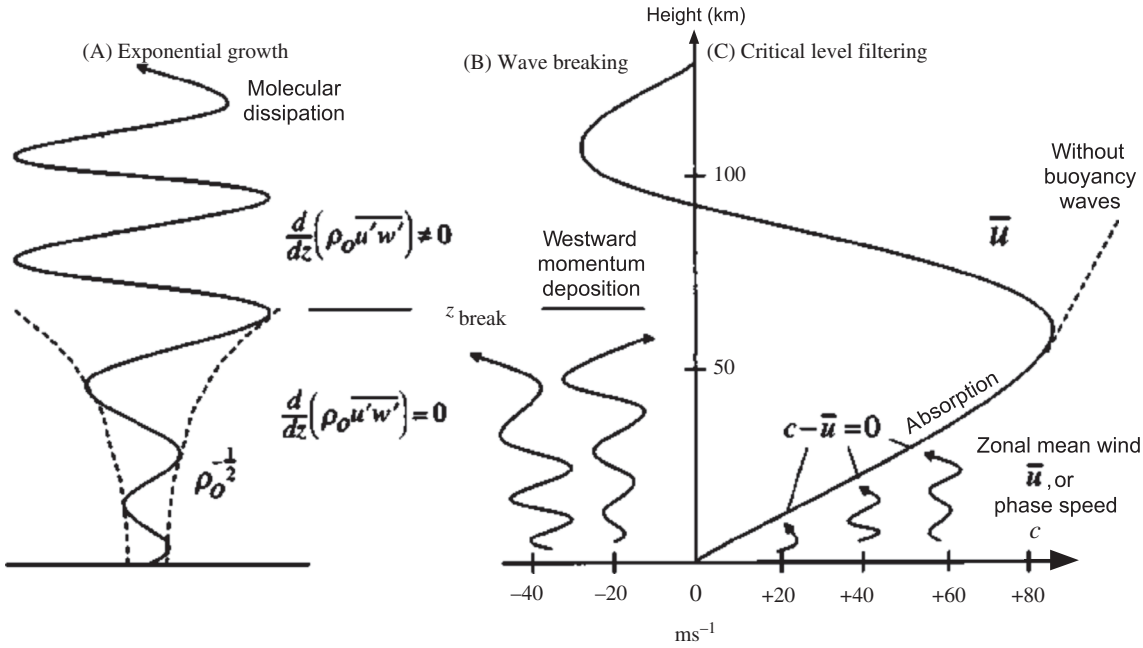


**Figure 4.28** A schematic diagram illustrating the effects of buoyancy waves on the Earth's upper atmosphere. (A) Without dissipation, the amplitude of vertically propagating buoyancy waves grows in height as $\rho_0^{-1/2}$. (B) Waves with westward phase speeds carry westward momentum upwards until they break in the upper atmosphere because their amplitudes grow large. This transfers westward momentum to the zonal mean zonal wind, which "closes" a mesospheric jet and reserves the wind speed. (C) Buoyancy waves with eastward phase speeds cannot penetrate beyond critical levels where $c = \overline{u}$. The effect of (B) and (C) is to close an eastward (westerly) mesospheric jet such as that shown in the winter hemisphere of Fig. 4.27. (Adapted from Forbes (2002). Reproduced with permission. Copyright 2002, John Wiley and Sons.)

Buoyancy waves affect the global circulation of the mesosphere. The vertical gradient of the upward flux of horizontal momentum ($\rho_0\overline{u'w'}$) is a force on the atmosphere that is approximately balanced in the steady-state zonal momentum equation by meridional flow:

$$\underbrace{-f\overline{v}}_{\text{Coriolis acceleration}} \approx -\underbrace{\frac{1}{\rho_0}\frac{d}{dz}\left(\rho_0\overline{u'w'}\right)}_{\text{force per kg}} = F_x \qquad (4.73)$$

Here, $\overline{v}$ is the zonal mean meridional wind. The air flows southward, i.e., $\overline{v}$ is negative, both in the northern hemisphere summer where $F_x > 0$ and $f > 0$ and in the southern hemisphere winter where $F_x < 0$ and $f < 0$. Because of this net summer-to-winter meridional flow, to conserve mass, air ascends at the summer pole and subsides on the winter pole. Because ascent causes adiabatic cooling and subsidence produces warming (Sec. 4.1.2.4), Earth's mesopause at ~90 km altitude is 130–160 K in the summer mid to high latitudes compared to 200–220 K at winter mid to high latitudes. Such a gradient is the opposite of that expected from purely radiative equilibrium and shows the importance of waves.

## 4.4.3 Atmospheric Tides

### 4.4.3.1 *Principles of Thermal Tides*

*All* externally heated rotating planetary atmospheres are subject to gravitational and thermal tides. Atmospheric gravitational tides are generated in the same way as ocean and solid planet tides and they exert torques on underlying solid or liquid layers. Acting over long periods of time, tidal torques can profoundly affect the rotation of a planet. Earth's rotation rate has slowed substantially over the past few billion years as a consequence of the lunar gravitational tide acting on the ocean (Sec. 6.8.2) with potential consequences for atmospheric dynamics and climate. The same side of Venus faces the Earth every time the Earth and Venus are aligned with the Sun in so-called inferior conjunction. It is possible that this Earth-locked rotation of Venus has resulted from the action of the gravitational tides of the Sun and Earth producing surface torque that ultimately slowed the solid planet Venus to its present resonance state (Dobrovolskis, 1980; Dobrovolskis and Ingersoll, 1980; Gold and Soter, 1969; Ingersoll and Dobrovolskis, 1978; Yoder, 1997). Here, we initially examine how thermal tides modify

atmospheric structure on relatively short timescales, and then discuss the issue of effects of thermal tides on rotation rate and climate in Sec. 4.4.3.2.

*Thermal tides* are global oscillations in the atmospheric pressure and wind fields caused by the heating and cooling associated with the apparent motion of the Sun over the surface of a planet. They are very large-scale waves with periods that are some fraction of a solar day, i.e., the noon-to-noon interval. The Fourier component with a solar daylength is the *diurnal tide*, while that with half a daylength is the *semi-diurnal* tide. Tides are classified as *migrating* or *non-migrating*. Migrating tides migrate with the Sun's apparent motion and so have constant phase with respect to solar heating as it moves around the planet once per solar day. Non-migrating tides are generated by interactions between migrating tides and non-uniform topography, such as the planetary scale topographic variations of Earth and Mars. Migrating tidal propagation can only be retrograde because the planet's surface moves underneath in a prograde sense away from the subsolar point of heating. However, non-migrating tides can propagate in either prograde or retrograde longitudinal directions. Because migrating tides are the dominant tides on Earth and Venus, we focus on them.

The theory of thermal tides involves considering buoyancy waves in a spherical geometry that includes planetary rotation. When one develops the linearized wave perturbation equations in this way, a key result is that the global-scale waves can only propagate vertically if their angular frequency $\omega$ is greater than the Coriolis parameter, i.e., $\omega > f$ (Lindzen, 1971). Since $f = 2\Omega \sin \phi$, where $\phi$ is latitude, it follows that the diurnal tide with $\omega = \Omega$ cannot propagate vertically beyond 30° latitude, because at that latitude $f = 2\Omega \sin(30°) = \Omega$. At latitudes outside ±30°, the diurnal tide acts like a Rossby wave and it does not propagate vertically away from its heat sources. In contrast, semi-diurnal tides can vertically propagate at all latitudes because $\omega > f$ for any $\phi$.

In a more complete treatment, one considers the daily solar heating variation $Q'$ as a function of latitude, longitude, altitude and time, i.e., $Q'(\phi, \lambda, z, t)$, relative to zonal mean heating. $Q'$ is decomposed into its Fourier components. In turn, these components are expanded as a series of *Hough functions* that depend only on latitude and describe horizontal structure, along with a heating function that depends on altitude (Chapman and Lindzen, 1970). Following Forbes (2002), the magnitude of the atmospheric tidal fields $X$ (where $X$ could be velocity, pressure or density, for example) in the horizontal structure of each tidal mode can be simplified to the following expression:

$$X(\phi, t) = A \cos(\omega t + s\lambda - \varphi) \tag{4.74}$$

Here, $s$ is the zonal wavenumber and $A$ and $\varphi$ are latitude-dependent amplitudes and phases. The dominant components are the $s = 1$ component, the diurnal migrating tide, and the $s = 2$ component, the semi-diurnal migrating tide. We can specify the time as a local time seen by an observer on the surface, $t_{LT} = t + \lambda/\Omega$. Substituting for $t$ and setting $s = 1$ or 2 corresponding to $\omega = \Omega$ or $2\Omega$, respectively, we obtain:

$$X_{\text{diurnal}}(\phi, t) = A_1 \cos(\Omega t_{LT} - \varphi_1) \tag{4.75}$$

$$X_{\text{semi-diurnal}}(\phi, t) = A_2 \cos(2\Omega t_{LT} - \varphi_2) \tag{4.76}$$

We see that both diurnal (4.75) and semi-diurnal (4.76) tidal fields are independent of longitude (at least on a uniform sphere). However, the diurnal and semi-diurnal tides have quite different properties over latitude and height. On both Earth and Mars, the semi-diurnal tide behaves as a global buoyancy wave from pole to pole with very large vertical wavelength, typically ~100 km. Its amplitude increases with height, and because it has large vertical wavelength, the response reflects little interference between heating in different layers of the atmosphere. The diurnal tide acts as a buoyancy wave only between latitudes ±30°. Within this latitude range, the diurnal migrating tide propagates vertically and its amplitude increases with height above the heat source. Because of its relatively short vertical wavelength (~30 km on Earth and Mars), there is significant interference between heating at different levels, and its amplitude is both smaller and less stable relative to its heat sources than the semi-diurnal tide.

### 4.4.3.2 *Observations and Implications of Atmospheric Tides for Planetary Climates*

Migrating and non-migrating tides have been observed on Earth (Fig. 4.29) and Mars, and migrating tides have been observed on Venus (Migliorini *et al.*, 2012; Pechmann and Ingersoll, 1984; Peralta *et al.*, 2012; Schofield and Taylor, 1983) (Fig. 4.30). Venus is an interesting case. With its 243-day rotation period and solar day of 117 Earth days, Venus hardly rotates with respect to the Sun, so why should it have thermal tides? Even though the equatorial surface rotates at a speed of only 4 m $s^{-1}$, the middle atmosphere near the cloud top level of ~65–70 km altitude rotates at ~110 m $s^{-1}$ with respect to both the planet and the Sun. The thermal tides in the middle atmospheric reflect this atmospheric rotation, *not* the rotation of the solid planet. The air rotates past the sub-solar point and migrating waves are established that

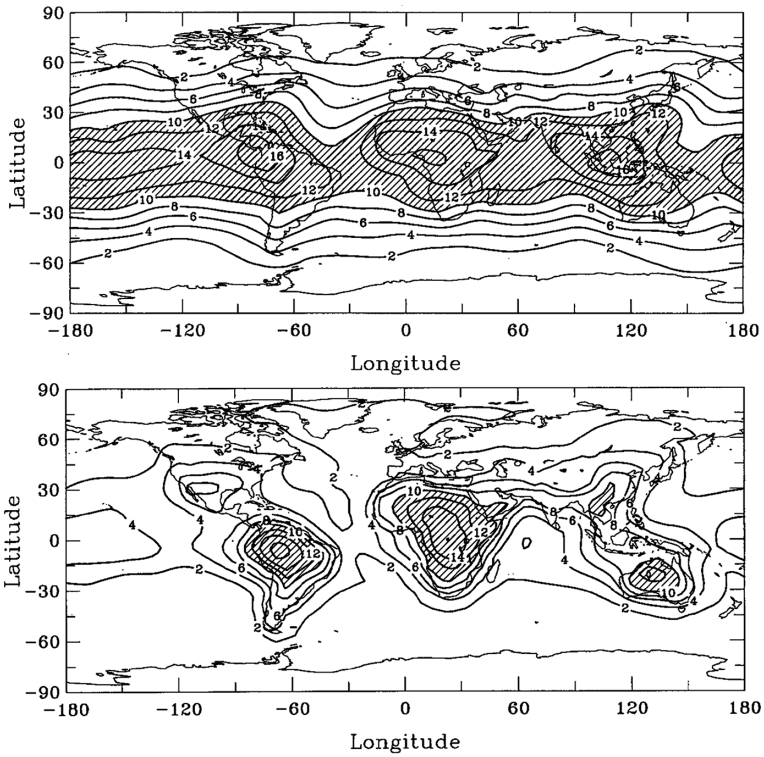


**Figure 4.29** The annual average amplitudes of semi-diurnal (top) and diurnal surface pressures on a latitude–longitude map in units of 0.1 mbar = 10 Pa. Each contour is separated by 20 Pa. Note the maxima in low latitudes and longitudinal variability of the diurnal tide due to differences in heating and non-uniform land mass distribution. (Source: Dai and Wang (1999). Reproduced with permission. Copyright 1999, American Meterological Society.)

are stationary with respect to the Sun but move opposite to the direction of the mean flow (Gierasch *et al.*, 1997). Titan's middle atmosphere also rotates at a significant rate, so thermal tides are expected in the middle and upper atmosphere of Titan.

The principal forcing factors for thermal tides depend on the properties of a planet's atmosphere. On Earth, forcing is by stratospheric heating due to absorption of solar radiation by ozone between ~20–60 km, heating in the troposphere by absorption of solar radiation by water vapor, and heating in the tropical troposphere by the diurnal cycle of deep convection. On Mars, the main tidal forcing is the daily cycle of radiative and convective heating of the lowest few km under clear conditions and heating of a deep layer due to absorption of solar radiation by dust when the atmosphere is moderately or very dusty. On Venus, the main forcing for the thermal tides in the middle atmosphere is heating by absorption of solar radiation in the cloud layer between 45 and 70 km (Fig. 4.30). Absorption of solar radiation by methane and other hydrocarbons in the middle atmosphere of Titan should be capable of generating significant thermal tides despite the large distance of Titan from the Sun.

Thermal tides have significant influence on the atmosphere of Mars. Feedback between tidal surface winds and lifting of dust high in Mars' atmosphere may contribute to the generation of planet encircling dust storms (Leovy *et al.*, 1973). Large amplitude tides may break and also contribute to vertical mixing in the Martian middle atmosphere.

Atmospheric thermal tides are characterized by an asymmetric mass distribution with respect to the substellar point (caused by thermal inertia), which can affect the rotation rate of a planet that's close to its host star (Cunha *et al.*, 2015; Laskar and Correia, 2004; Leconte *et al.*, 2015). The gravitational pull from a star on the asymmetric planetary atmosphere accelerates or decelerates rotation in the atmosphere, and the atmospheric angular momentum can be transferred to the solid planet by frictional coupling (Fig. 4.31). Such an effect probably accounts for the slow retrograde rotation of Venus (Correia and Laskar, 2001, 2003; Correia *et al.*, 2003; Dobrovolskis and Ingersoll, 1980; Ingersoll and Dobrovolskis, 1978) but the same physics could also drive rocky planets away from tidal synchronicity, even for planets with 1 bar atmospheres (Leconte *et al.*, 2015). Since synchronous rotation is assumed for some models of planetary habitability (e.g., Yang *et al.*, 2013) then atmospheric tides potentially could influence habitability.

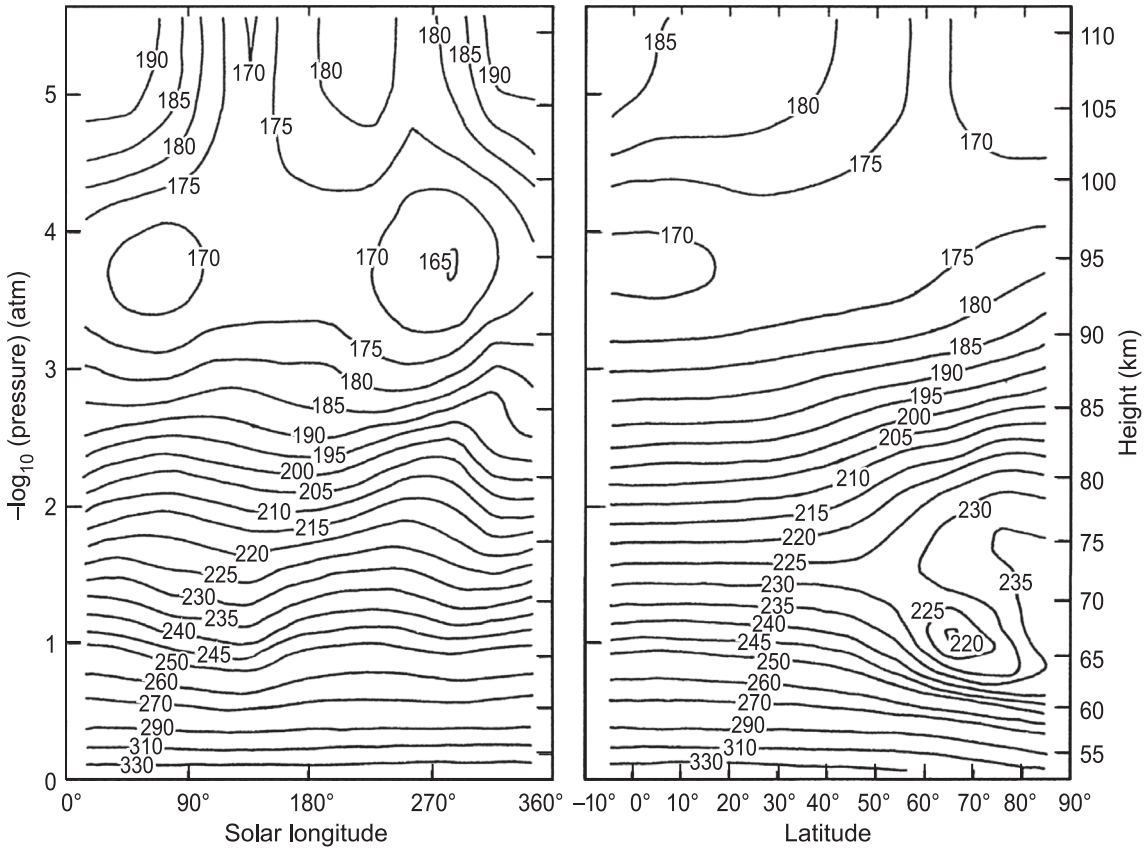


**Figure 4.30** Temperature (K) cross-sections of Venus' atmosphere above 55 km altitude averaged between 0–30° N. The field is shown in Sun-following coordinates where zero longitude is noon (left) and in zonal mean cross-section (right). From above the cloud-tops (70 km) to 100 km, a clear semi-diurnal variation is revealed. The phase in the solar longitude plot suggests a Sun-following eastward-propagating oscillation forced at lower altitudes. (Redrawn from Gierasch *et al.* (1997), p. 463.)

## 4.5 Superrotation

Superrotation is prograde atmospheric rotation at equatorial latitudes. (More specifically, superrotation is a region where the angular momentum per unit mass of the atmosphere about the rotation axis is a local maximum in the latitude–height cross-section and exceeds the surface angular momentum at the equator.) Because the angular momentum of a planet's surface is maximal at the equator, zonal mean torques cannot drive equatorial superrotation (Hide, 1969, 1970), so their generation and maintenance has been something of puzzle. We have already encountered superrotation on Jupiter and Saturn. Superrotation on slowly rotating planets such as Venus and Titan where the equatorial atmosphere rotates much faster than the solid planet is particularly perplexing.

A variety of data indicate superrotation on Venus. Cloud tracking shows superrotating winds (Belton *et al.*, 1991; Peralta *et al.*, 2007). The temperature distribution for Venus in the right panel of Fig. 4.30 can also be used to infer fast winds in the middle atmosphere. A meridional temperature gradient from warm equator to ~50° latitude occurs at 60–80 km altitude. The zonal wind in cyclostrophic balance (eq. (4.21)) with this meridional temperature distribution increases with height at low latitudes to ~110 m $s^{-1}$ at 65–70 km altitude, which is 2.5 times faster than terrestrial jet streams and 60 times faster than the solid planet below. The wind is sometimes called the "four-day rotation."

Evidence also exists for Titan's superrotation. Prior to the *Cassini–Huygens* mission, *Voyager* infrared data (Flasar *et al.*, 1981) and stellar occultation data (Hubbard *et al.*, 1993) implied superrotating zonal winds. Tracking of the *Huygens* probe indicated speeds ~100 m $s^{-1}$ at 130 km height (Bird *et al.*, 2005) while Earth-based

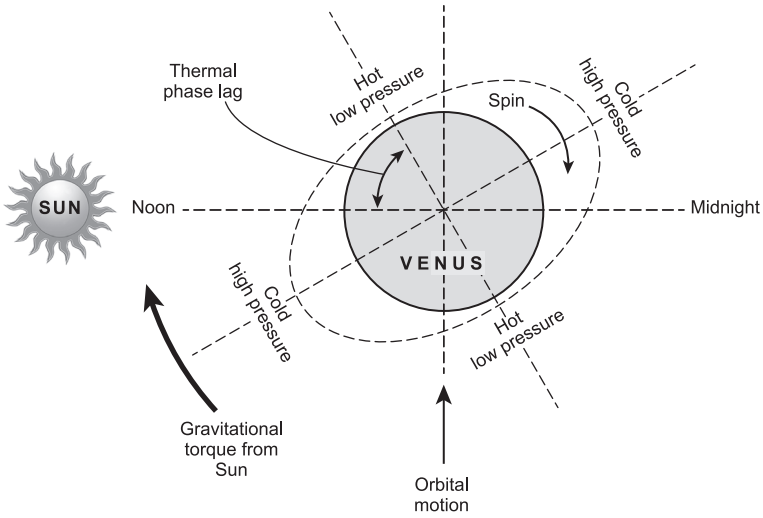


**Figure 4.31** Schematic diagram illustrating the principle of how atmospheric tides can affect the long-term rotation rate of a planet. Venus is our example, but the same principle should apply to exoplanets with sufficiently thick atmospheres. Thermal tides redistribute mass between warm and cold parts of the atmosphere. There is a low pressure (i.e., low mass) where the atmosphere is warm and high pressure where the atmosphere is cold. Thermal inertia means that the hottest time is not local noon but later in the afternoon. By symmetry, a maximum of cold, high atmospheric mass occurs before local noon. Because the atmospheric mass wave of the semi-diurnal tide (indicated with the dashed-line oval) has a maximum before noon, the Sun's gravity exerts a torque on this atmospheric mass. When the torque is transmitted via friction to the solid planet below, it accelerates the rotation in the prograde sense shown. Solid body tides raised on Venus by the Sun produce a solid bulge, which the spin of Venus tends to move ahead of the line connecting the Sun and Venus. The Sun, acting on this solid body bulge, tends to cause a torque in the opposite (retrograde) direction to that produced by the atmospheric tidal torque. The solar torque due to solid body tides, on its own, would tend to cause Sun-synchronous rotation. But the solar torque due to thermal atmospheric tides can impart net rotation and prevent synchronous rotation. (Adapted from a diagram by Schubert (1983), p. 720. Reproduced with permission from University of Arizona Press. Copyright 1983, The Arizona Board of Regents.)

spectroscopic measurements suggest ~200 m $s^{-1}$ (with large error bar) at 200 km (Kostiuk *et al.*, 2006). Infrared measurements from *Cassini* in 2004 (soon after northern winter solstice in October 2002) indicate a jet near 0.1 mbar with a core of 190 m $s^{-1}$ spanning 30–60° N (Achterberg *et al.*, 2008).

Net torque is required to maintain the angular momentum of superrotation against frictional loss to the surface. A general proposal is that eddies could provide the necessary torque (e.g., Gierasch, 1975), although gravitational torque acting on the atmosphere is an alternative (Gold and Soter, 1971). Eddies may act primarily in the horizontal plane as planetary or Rossby waves, or they can act largely in the vertical plane as buoyancy waves. In either case, they must provide a net convergence of angular momentum on the equator at the jet level (Del Genio and Zhou, 1996; Mitchell and Vallis, 2010; Showman and Polvani, 2011). In the case of Jupiter and Saturn, the required equatorward momentum fluxes may be primarily due to convectively driven large-scale eddies acting in the horizontal (Lian and Showman, 2010; Schneider and Liu, 2009).

The mechanism on Venus is unclear. Some models produce strong superrotation due to horizontal eddy torques while others generate little or no superrotation (e.g., Del Genio and Zhou, 1996; Hollingsworth *et al.*, 2007; Lebonnois *et al.*, 2010; Yamamoto and Takahashi, 2009). None of the models is able to simulate the entire Venus atmosphere at the scale of buoyancy waves and convection, and numerical studies generally have to assume a background superrotation at the cloud base. Superrotation also reduces the effective gravity causing a equatorial bulge, which should require a quasi-hydrostatic treatment (Tokano, 2013).

While some models may suggest that horizontal eddies can drive Venus' superrotation, the coincidence between the level of the equatorial wind maximum and the level of maximum solar heating implies that thermal tides play a role at least in determining the location and magnitude of the superrotation maximum (Gierasch *et al.*,

1997; Leovy, 1987; Pechmann and Ingersoll, 1984). A further indication of the role of thermal tides is the direct observation of the semi-diurnal tide in the atmosphere above the 65–70 km level of the superrotation maximum (Fig. 4.30, left panel). Upward propagation of wave activity related to this tidal component is associated with downward flux of prograde momentum toward the cloud top level. Below that level, observations do not reveal the presence of a tide, but it is likely that the semi-diurnal tide transports prograde angular momentum upward as well as downward toward the level of maximum solar heating near the cloud tops. It is possible that both horizontal and vertical eddies contribute with horizontal eddies forcing the background superrotation (~40 m $s^{-1}$) below the jet and thermal tides shaping the jet level winds.

Some models have succeeded in producing superrotation on Titan. However, the mechanism can be unclear (Crespin *et al.*, 2008; Rannou *et al.*, 2004), or the superrotation occurs only under special conditions (Lebonnois *et al.*, 2012; Newman *et al.*, 2011), or the magnitude of the superrotating zonal winds is too low (Friedson *et al.*, 2009; Lora *et al.*, 2015). The coincidence between the levels of maximum solar heating and maximum superrotation suggests that thermal tides again may play a role in determining the location and magnitude of the superrotation peak.

Finally, because two slowly rotating Solar System bodies exhibit superrotation in the middle atmosphere, we pose the following conjecture: Is atmospheric superrotation an inherent property of slowly rotating exoplanets subject to zonal mean and tidal heating? The idea may be testable through Doppler-shifted lines. Also, in extreme cases, superrotation may be detectable as prograde displacement of the temperature field in infrared spectra, like those predicted originally for hot Jupiters (Showman and Guillot, 2002). Shifted hot spots are detected on various hot Jupiters: HD 189733b (Knutson *et al.*, 2007; Showman *et al.*, 2013a), HD 209458b (Zellem *et al.*, 2014), and WASP-43b (Stevenson *et al.*, 2014).

## 4.6 Transport by Eddy-Driven Circulations

### 4.6.1 The Brewer–Dobson Circulation and Mesospheric Circulation

The generation or modification of jet stream structure changes the thermal structure according to the thermal wind equation (4.18), and so generates temperature fields that are not in radiative-convective equilibrium. These disequilibrium temperature fields are balanced by compressional heating and expansional cooling due to large-scale subsidence and rising motion (eqs. (4.25) and (4.26)) along with horizontal advection.

In the lower stratosphere of Earth where the subtropical jet stream decreases in amplitude with height as a result of wave driving, temperature decreases from high latitudes to the equator so that there is a temperature minimum, or *cold trap*, at the tropopause on the equator (Fig. 4.32(a)). Since this minimum corresponds to temperatures cooler than radiative-convective equilibrium, in the zonal mean, air rises in the tropical lower stratosphere with compensating stratospheric subsidence on the poleward side of the jet (Fig. 4.32(b)). These rising and sinking motions are not zonally uniform and, particularly in the sinking region, take place in large part in eddies. Nevertheless, the net effect is the *Brewer–Dobson Circulation*: a mean meridional overturning circulation that carries air through the tropical tropopause, poleward in the lower stratosphere at subtropical and middle latitudes, and downward at mid and high latitudes (Brewer, 1949; Dobson, 1956). This circulation maintains a distribution of stratospheric ozone in which the highest ozone concentrations are found at high latitudes despite the fact that ozone is produced photochemically in the tropical stratosphere where sunlight is most intense. Because water vapor or ice particles transported upward in the Brewer–Dobson Circulation must pass through the cold trap, the Brewer–Dobson Circulation also accounts for Earth's very dry stratosphere with only 3–4 ppmv $H_2O$.

Earlier, we encountered Earth's mesospheric meridional circulation, which is associated with a meridional temperature gradient that is far from radiative equilibrium (Sec. 4.4.2). Similar to the Brewer–Dobson Circulation, wave breaking and eddy dissipation drive this circulation and close off mesospheric jets above the level of the jet maxima.

Temperature distributions on Venus, Mars, and Titan also indicate eddy driven meridional circulations in their middle atmospheres. In Venus' middle atmosphere, temperatures are warmer near the poles than the equator, indicative of subsidence at high latitudes and ascending motions at low latitude (Fig. 4.30, right panel between 70 and 100 km altitude and ~50° latitude and the pole). Such a circulation would rapidly mix constituents vertically through the mesosphere. Since thermal tides are strong on Venus, it is likely that breaking of the tides is primarily responsible for driving this circulation. Similar warm areas near the pole and relatively cool areas at low latitudes are found in high-resolution vertical temperature profiles of the Martian atmosphere (McCleese *et al.*, 2010). This circulation system may be driven by a

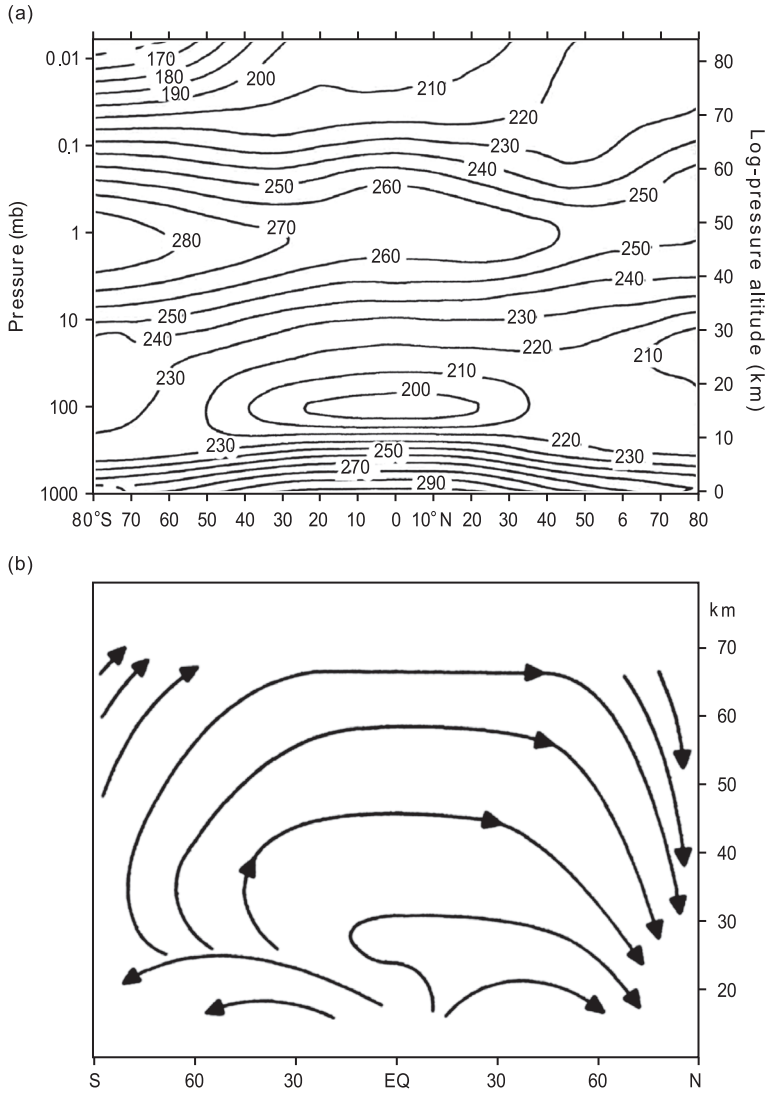


**Figure 4.32** (a) January temperature distribution in Earth's atmosphere. Temperature increases from equator to pole in the lower stratosphere and from summer pole to winter pole in the upper mesosphere. (Redrawn from Andrews *et al.* (1987), p. 222.) (b) Schematic streamlines of the circulation at the southern summer solstice deduced from eq. (4.25) and the equation of mass continuity. In the stratosphere, we see poleward motion of air, the Brewer–Dobson circulation, driven by planetary waves. Higher up is another circulation: air rises into the summer mesosphere and descends on the winter pole, which is driven mainly by buoyancy waves (Redrawn from Andrews *et al.* (1987), p. 304.)

combination of thermal tides and buoyancy waves. The mesosphere of Titan also has warmer temperatures near the poles than near the equator and the resulting circulation is responsible for downward transport of photochemically produced hydrocarbons in the polar regions (Fig. 4.33). Since forcing of buoyancy waves is likely to be weak, these circulations may also be driven largely by the thermal tides.

### 4.6.2 Implications of Large-Scale Overturning Circulations for Atmospheric Evolution

The transport of trace species through the middle and upper atmosphere and their ultimate escape to space can be strongly influenced by the dynamics of the middle atmosphere. For example, upward transport of water vapor and the subsequent escape of hydrogen on Earth are very sensitive to the temperature of the "cold trap" at the equatorial tropopause (Fig. 5.9). The temperature of this cold trap is controlled by the Brewer–Dobson Circulation, which ascends and cools near the equator. But where does the Brewer–Dobson Circulation come from? It is forced by planetary and buoyancy wave activity, as described above. Dynamically modulated cold trapping in the atmospheres of Venus and Mars also influences the upward flux of condensable trace species. Furthermore, the pressure level at the homopause influences the abundance of trace species at the escape level. This pressure level is determined by turbulence arising from the breaking of buoyancy waves and thermal tides (Leovy, 1982b),

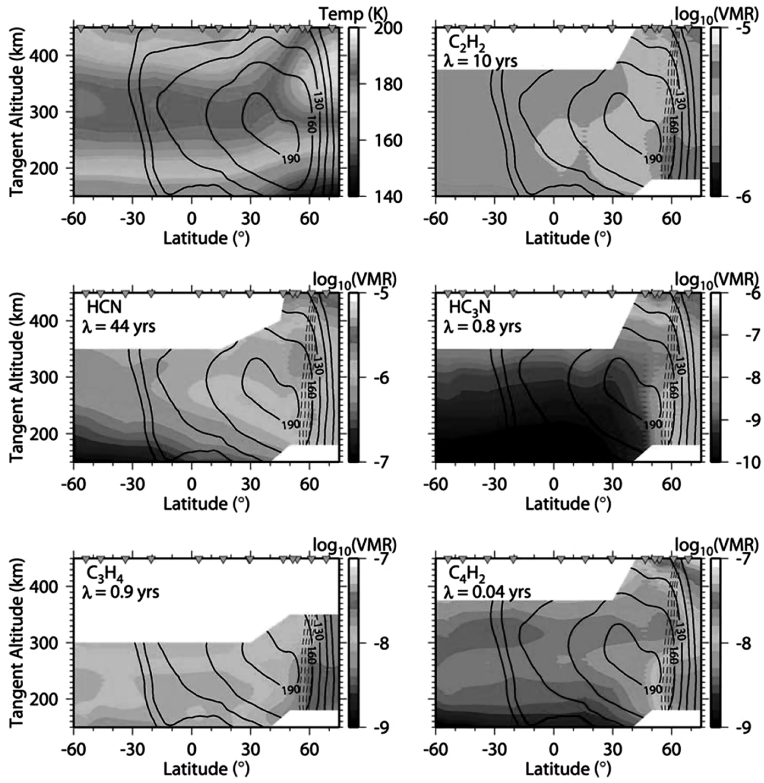


**Figure 4.33** Titan zonal mean temperatures (K), cyclostrophic zonal mean winds (m $s^{-1}$), and trace constituent concentrations (as $log_{10}$ volume mixing ratio (VMR)) above 150 km altitude. The photochemical lifetimes at 300 km are denoted by $\lambda$. The zonal mean winds exhibit strong equatorial superrotation as well as seasonal effects, and the constituents exhibit strong downward transport in the region of the temperature maximum near the winter pole. Blue dashed lines denote a dynamical mixing barrier (a region of steepest horizontal potential vorticity gradient) that confines a polar vortex. (Source: Teanby *et al.* (2008). Reproduced with permission. Copyright 2008, John Wiley and Sons.) (A black and white version of this figure will appear in some formats. For the color version, please refer to the plate section.)

so the dynamics of these waves can potentially affect the escape of trace gases through their influence.

One-dimensional (1-D) models of the composition of middle atmospheres generally employ an eddy diffusion scheme to account for vertical mixing (Appendix B), but the mechanism of vertical exchange is not well understood, so these schemes are usually *tuned* to give overall agreement with observations. Vertical transport in planetary middle atmospheres takes place largely through large-scale wave driven overturning circulations (Sec. 4.6.1). The role of these circulations has yet to be incorporated in a sophisticated way into 1-D photochemical models. Understanding their general behavior is important for attempting to model exoplanet photochemistry, including the formation of hazes that may be common features in some exoplanet atmospheres.

Large-scale wave-driven overturning circulations may even control the bulk composition of planetary atmospheres. For example, $CO_2$ on Mars is maintained against photodissociation by vertical transport that rapidly brings CO and O down from the mesosphere to the lower atmosphere where recombination to $CO_2$ is catalyzed (Sec. 3.4). The eddy diffusion approach requires an unreasonably large eddy diffusion coefficient to account for this transport, but transport by middle atmospheric circulations and episodic planetwide dust storms (which are likely associated with atmospheric tides (Sec. 4.4.3.2) can plausibly do the job.

## 4.7 Atmospheric Dynamics and Habitability: Future Prospects

We close this chapter by noting that atmospheric dynamics can affect atmospheric evolution and the habitability of planets in many ways. The various possibilities are yet to be fully explored and earlier we only identified a few cases. In general, the meridional transport system and the formation of jets (whether thermally forced or forced by planetary waves) influences cloud distribution, the surface climate, the transport of trace species through the atmosphere, and the movement of sand and dust near the surface, and hence even the geology in some cases. An example of geological influence is on Mars, where surface winds and meridional transport determine regions of long-term dust deposition and erosion (Haberle *et al.*, 2003). In this chapter, we have pointed out how the meridional circulation (Sec. 4.2.6), atmospheric tides (Sec. 4.4.3.2), and wave-driven overturning circulations

in the middle atmosphere can be important for atmospheric evolution or planetary habitability (Sec. 4.6.2). There are likely many more links between atmospheric dynamics and atmospheric evolution and habitability.

Ultimately, we would like to be able to use our dynamical understanding to infer properties of the general circulation and climate of exoplanets (Showman *et al.*, 2010; Showman *et al.*, 2013b). The principles outlined above are a starting point for predicting the distribution and character of jet streams, overturning circulation, and vertically and horizontally propagating waves, all of which may influence the habitability of a planet and the atmospheric evolution.